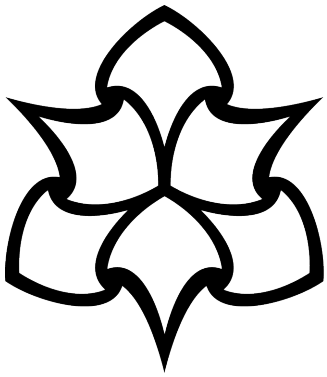

Investigation into Thermal and Acoustical Characteristics of Power Electronic Devices used for Photovoltaic Solar Systems

Adnan Badawood

A thesis submitted in partial fulfilment of the requirements of Manchester Metropolitan University for the degree of Doctor of Philosophy

Department of Engineering

Manchester Metropolitan University

2019

Abstract

Power electronic converters (PECs) play a vital role in the power industry, in particular, in solar photovoltaic energy systems. Damage to any single PEC component either reduces the efficiency of the entire system or causes it to malfunction. Thermal stress from switching devices used in PECs is a major contributor to failures in those systems. Most commonly used condition-monitoring techniques are based on intrusive electrical and thermal measurements. Therefore, there is a timely need for non-intrusive, non-contact and reliable monitoring techniques that can detect failures at an early stage.

The aim of this work is to assess the possibility of extracting useful condition-related information using thermal and acoustic characteristics of power electronic devices (PEDs) under different operation conditions.

First, a 3-D finite element model was developed to gain clear understanding of thermal and acoustical characteristics of PEC components. Second, the outcomes of the derived model were validated using experimental setups. The thermo-acoustic behaviour of this model was explained, by applying equations relating to heat and acoustic diffusion over the converter geometry through the semiconductor layers of the electrical contacts. Operational, environmental and loading effects on the generated acoustic signals were studied in detail both in time and frequency domains.

Results showed that the measured acoustic signals are observable and the accumulated signal is significantly visible and detectable even at high frequency (about 300 kHz). The peaks of the measured signals at the transition instance of the PWM proved to be an important element for predicting acoustic and thermal behaviour, which was validated by a referenced temperature sensor. Thus, the electro-thermal temperature can be relayed to an effective monitoring system, making future investigations in this area worth pursuing.

Declaration

I confirm that no part of this thesis has been presented in supporting an application for another degree or qualification at this, or any other university, or institute of learning.

Date:

Signed:

Acknowledgments

I would like to express my sincere thanks and gratitude to my supervisor for supporting my academic journey to the completion of a PhD. He has shown patience, encouragement and a high level of support, all of which has contributed to my continued academic development and enabled me to reach this stage of the project.

Additional recognition must also be given to my peers at Manchester Metropolitan University for the invaluable help and advice which they have offered in a friendly and positive manner. This has also been a significant factor contributing to my motivation and enthusiasm for completing these experiments and my thesis.

Finally, I would like to offer my sincere thanks and appreciation to my wife, Hanadi Elyas, my family and friends, all of whom have been an invaluable support during the completion of my studies.

Table of Contents

List of Figures

List of Tables

List of Abbreviations

AE	Acoustic emission/s
ARMA	Autoregressive moving average
CTE	Coefficient of thermal expansion
DER	Distributed energy resource
DFT	Discrete Fourier Transform
DOD	Depth of discharge
DUT	Device under test
IGBT	Insulated gate bipolar transistor
FFT	Fast Fourier Transform
kWp	Kilowatts peak
MARSE	Measured area under the rectified signal envelope
MOSFET	Metal oxide semiconductor field effect transistor
MPPT	Maximum power point tracking
NDT	Non-destructive testing
NDTE	Non-destructive testing and evaluation
PECs	Power electronic converters
PEDs	Power electronic devices
PV	Photovoltaic
PWM	Pulse width modulation
SOC	State of charge
STC	Standard testing conditions
STFT	Short Time Fourier Transform
TSA	Time synchronous average

1 Introduction

1.1 Background to the research

With rapidly increasing rates of population growth and economic development, the possibility of an imminent energy crisis and the need to mitigate the effects of global warming are both seen as pressing contemporary concerns. These dual threats of energy depletion and environmental pollution have placed the development of other methods for harvesting renewable energy resources at the centre of public interest and concern. One of those methods is the solar photovoltaic (PV) energy system. The solar PV systems generate DC electricity as a result of absorption of sun photons on the solar PV array without any emissions. A DC-DC converter is used in order to utilise this DC electricity to charge batteries. Moreover, an inverter can be optimised to convert DC power to AC, and this can be used to supply local loads or, alternatively, redirected back to the utility company (Chen, 2013).

In general, power electronic devices (PEDs) as shown in Figure 1-1 are widely used to convert and control electrical power and to switch devices. In the PV solar system, the power electronic interface performs two major duties. Firstly, conversion of the DC voltage produced into a proper AC current, which can be used for domestic purposes. The second is to regulate the terminal conditions for the PV modules, which helps to monitor the maximum power point to maximize the energy produced (Blaabjerg et al., 2004a). This needs to be achieved at the highest possible efficiency due to the variations between winter and summer, morning and noon. In addition, another of the main benefits of using PEDs is the high efficiency of the switching mode of the power conversion, which is about 96-99%, resulting in electricity savings. Furthermore, PEDs can be more easily cooled in comparison to analogue and digital electronic devices

(Shinde et al., 2009) and they also facilitate the interconnection of the DC output of the PV system to the load or grid, which incorporates DC-DC-AC and DC-AC-AC conversion.

When using the off-grid PV system batteries are needed to successfully manage the demand for energy at night time. Blocking diodes are utilised to protect the battery from short circuiting and to prevent the discharging of the batteries during the night.

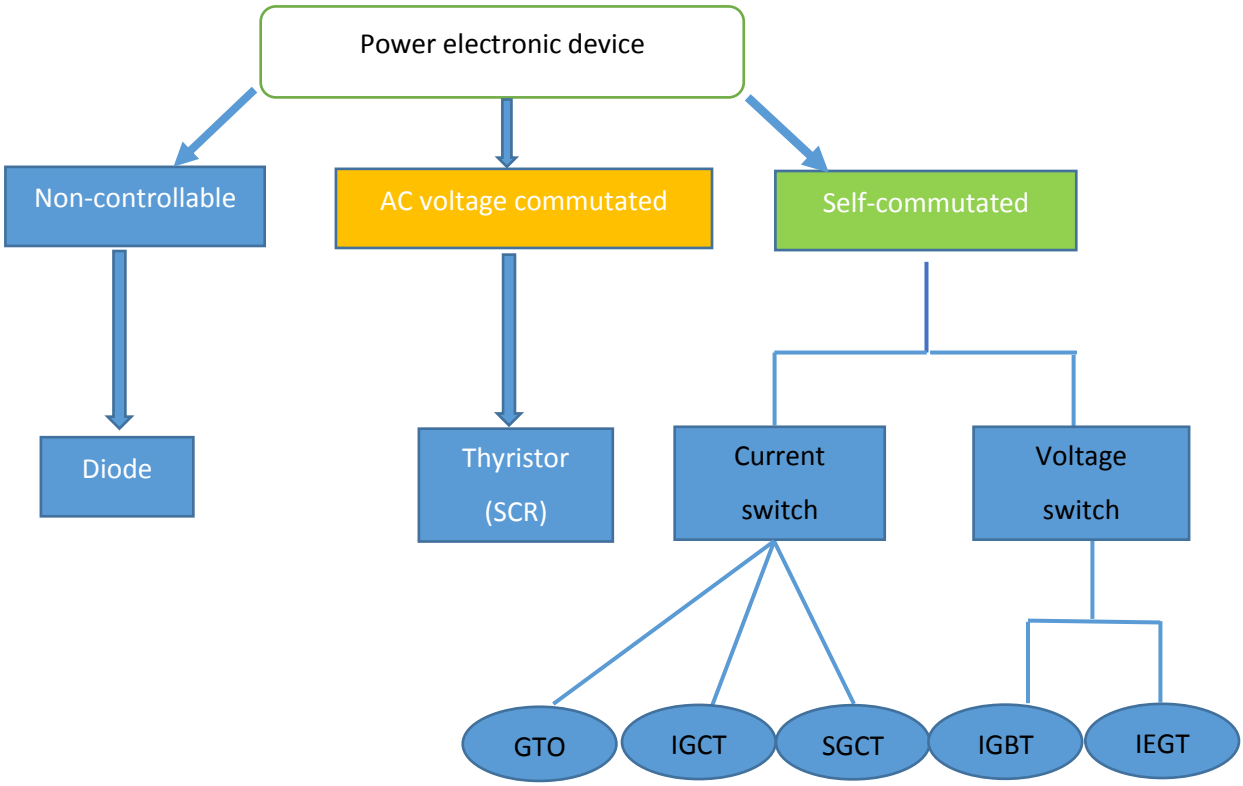

Figure 1-1 Classification of some medium- and high-power semiconductors (Chen, 2013)

Power electronic converters (PECs) play a vital role in power electronic systems and damage to any single component can either reduce the efficiency of the entire system or cause it to malfunction. DC-DC conversion has been used to cover the demands of obtaining stable characteristics for DC voltage and current without irradiance fluctuations. Several non-isolated DC-DC converters have been used to achieve this objective such as buck, buck-boost, boost and Cúk topologies with appropriate

modifications. These have been used to maintain the required voltage and current and also enhance the overall output power efficiency.

In particular, the performance of the PV system has been largely dependent on solar irradiance, temperature and conversion efficiency. Although there are many advantages to using these PV systems, their performance can be badly affected by external factors (in particular, adverse weather conditions) which results in the PV system breaking down, causing electricity supply outages and financial losses. The thermal behaviour and electrical stresses of switching devices used in PECs are major contributors to failures in those systems

Therefore, there is a high demand for non-intrusive, efficient and reliable monitoring techniques that can distinguish any potential failures at an early stage. Commonly used condition-monitoring techniques are based on intrusive measurements involving electrical and thermal variables. Hence, there is a need for more powerful, remote monitoring strategies.

This research examines the feasibility of extracting useful condition-related information using the measured acoustic signals generated by PECs. A warning system using this acoustic emission technique could be integrated into any existing circuit, automatically sending data online to notify the system operator that degraded power modules require servicing, before any other device within the power module fails.

This introductory chapter provides the background to this research. It examines the growing need for structures producing renewable energy, and then describes development of PV cells and of solar energy systems. It then briefly explains the important role that power electronics play in solar PV energy systems and how that

role is likely to expand with the growing trend towards distributed energy resource systems which will integrate renewable energy. Following this introduction, the aims and objectives of the research are presented. A chapter by chapter overview of the structural organization and contents of this thesis concludes this introductory chapter.

1.2 Renewable energy systems

Currently, the greatest part of the production of world energy continues to come from the use of fossil fuels, such as oil, coal, and natural gas. Data from the organisation Carbon Brief based on statistics on world energy provided by BP (see Figure 1-2) indicates that in 2014, fossil fuels (oil, coal and natural gas) accounted for a share of just over 86% of the world demand for energy (Evans, 2015). Renewable energy sources, including wind, hydro, solar and other renewable sources (i.e. geothermal, biomass, biofuels, wave and tidal energy) were responsible for providing 9.3% of global total energy needs.

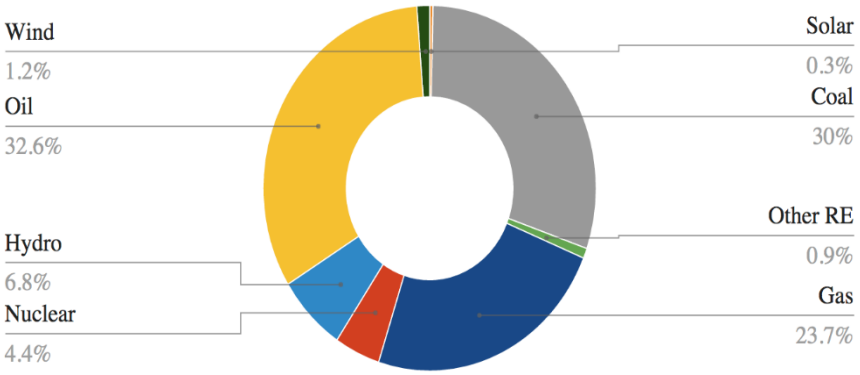

Figure 1-2 Percentage contributions of energy sources in 2014 (Source: Evans, 2015)

However, while world energy demands rise continuously, global resources of fossil fuels continue to decline, making them ever more difficult and more expensive to access. Moreover, since it has been estimated that they will be exhausted entirely by

the year 2030 if consumption patterns are not substantially changed, it is necessary to start searching for alternative sources to resolve this problem (Evans, 2015). Whilst some consider nuclear energy to be a viable alternative, in addition to the potential environmental and health risks this may pose, the initial financial investment required is beyond the reach of many developing countries and emerging economies.

The preferred solution for electricity generation would involve a source of energy that is renewable, low-cost, and also minimally polluting, given that environmental protection and the particularly the need to reduce CO_2 emissions is now also an issue of major global concern. For this reason, there has been growing interest in exploring the possibilities of decreasing dependency on fossil fuels by integrating alternative energy sources that rely on sun, wind or water, since these appear to offer the inexhaustible and easily exploitable energy which may serve as being a key component for the economic future of countries globally (EIA, 2016). To date, however, the penetration of solar energy into the renewable energy mix has made limited progress.

There are various reasons for this. The main disadvantage of solar energy is that it is affected by environmental conditions. The effectiveness of PV power systems depends on geographical location, weather conditions, and levels of solar irradiance (Assad, 2010). Microclimatic conditions vary considerably across the globe and when weather conditions are hostile, the amount of power that can be provided by the panels can be substantially reduced. However, as discussed later, this problem can be resolved by the installation of a battery-type storage device that is able to power the network during these periods, together with other systems such as sun and maximum power trackers. In addition, the orientation of the PV array and its tilt angle can also help improve total solar irradiance (Assad, 2010).

Solar energy could be increasingly valuable and central in the contemporary electric power energy mix. The incidence of radiation energy by the sun across global land masses has been estimated at 219,000,000 billion kWh per year, corresponding to 2500-fold of current world energy demands (TramStore21, 2012). Harrabin (2015) estimates that even in the UK with its variable levels of solar irradiance, solar energy would be capable of providing 4% of its electricity needs by 2020. It is interesting to note that even though Saudi Arabia still has vast reserves of oil, as part of its Saudi Arabia Vision 2030 policy paper, the Saudi government is now making major new investments in renewable energy, in particular PV systems, as part of its commitment to reduce global greenhouse emissions and to begin to address its economic dependency on hydrocarbons (Almasoud and Gandayh, 2015; Borgmann, 2016).

With their potential to provide clean energy, solar energy systems can play a vital role in helping governments to meet their targets to reduce greenhouse gases and reduce global CO_2 emissions. Solar energy has a number of major advantages when compared with fossil fuels or nuclear energy. Firstly, it is a renewable energy source that is non-polluting and does not produce waste or harmful gases. Secondly, it can be installed and used safely and comfortably anywhere as long as there is sunlight. The major advantages associated with PV power systems in comparison to wind turbines is that they do not produce noise and have few, if any, mechanical parts. In relative terms, they also require less maintenance and have a higher degree of reliability (Ravishankar et al., 2008; Assad, 2010).

1.3 Solar energy systems

Solar energy systems can be broadly divided into two categories: thermal and electrical energy. The latter system can be stand-alone or grid-connected but both are reliant on the use of PV technology.

1.3.1 Thermal solar energy systems

These systems rely on different kinds of collectors to gather the solar energy which in turn has a variety of potential uses. Typically, thermal solar energy systems are used to supply hot water or to provide heating in a domestic setting, often as a supplementary source.

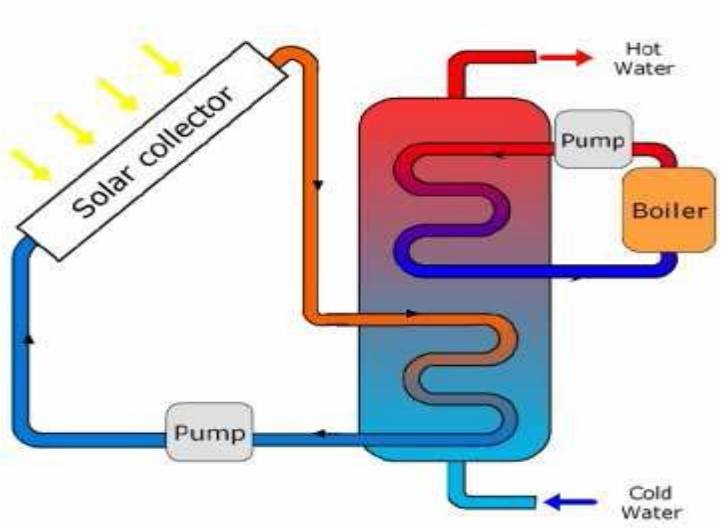

Figure 1-3: Solar Thermal System (source: Tramstore21, 2012)

As Figure 1-3 illustrates, a solar thermal energy system consists of three main components: the solar collector (fitted on the roof of the building), storage technology (such as a boiler) and a solar regulator system (such as a temperature difference control). The solar collector is the prime component in the solar thermal system since its function is linked to the conversion of sunlight into heat by absorbing solar radiation. Two principal kinds of collectors are utilised. The first of these is the evacuated-tube collector which has been created from parallel glass tubes, each of

which contains an outer and an inner glass tube. A vacuum exists between these two tubes to limit the amount of heat loss. Each glass tube contains a solar absorber. The second type, the flat-plate collector, comprises a box with a glass or plastic cover on top and a solar absorber made of copper piping located at the bottom. Both the bottom and the sides are insulated. The evacuated-tube collector is more expensive to manufacture but is also highly efficient and frequently used in colder climates (ESTIF, 2014).

The heat absorbed from the sun by the copper tubing in the solar collector is then transmitted to the water running through the collectors, as shown in Figure 1-3. When this water becomes warmer than that in the storage tank, the control unit triggers the pump, pumping it through the heat exchanger, keeping heat loss to a minimum. The exchanger then transfers this heat into the domestic hot water storage tank. The resulting circuit water, which has now been cooled, is pumped to the collector with the cycle repeated once more. To minimise heat loss, the space between the collector and the storage tank must be kept close. Where the solar thermal heat is deficient, the process is able to utilise a secondary heat exchanger within the boiler to heat more water. This is commonly required in colder climates (ESTIF, 2014). A so-called drain-back system can also be fitted to improve durability, safety and reliability and this protects the system against the boiler overheating or the collector freezing (ESTIF, 2014).

1.3.2 Electrical solar energy systems

Electrical solar energy systems can be used to provide electrical power by directly converting solar irradiance into electricity by employing selenium (Si) or other solar PV

cells that directly transfer solar energy into electricity. This type of system is known as PV or CPV when concentrated solar energy is used.

1.3.2.1 A brief overview of PV cell development

The first observation of the PV effect in solids can be dated to 1876, when two scientists, Adams and Day, discovered that when sunlight strikes selenium, a semi-conductor material, photo-generation of electrical current occurs. However, since this effect was so small in this element, having a conversion efficiency of approximately 1%, their discovery was not thought to have any practical applications, particularly since fossil fuels were relatively cheap and plentiful (Luque and Hegedus, 2011).

According to Dunlop (2009), contemporary photovoltaics began in 1954 when researchers working at Bell Laboratories in the United States discovered by chance that when the lighting in the room was on, p-n junction diodes generated a voltage. In less than twelve months, they succeeded in producing a selenium p-n junction solar cell that was 6% efficient. Other scientists at the Wright Patterson US Air Force Base published results of their own research in the same year, having produced a thin-film hetero-junction solar cell based on copper sulphide (CuS)/cadmium sulphide (CdS), with a similar efficiency level. The cell sets the foundations for the later thin-film solar cell. Five years later, Hoffman Electronics was able to raise efficacy of the selenium PV cells to 10%.

In the late 1950s, there was increasing interest in PV cell design from military scientists as it was realised that this had potential as a power source for use in satellite technology and this remained their major application throughout the 1960s and 1970s (Luque and Hegedus, 2011). Consumer-oriented applications of PV cells gradually

increased, as they began to be incorporated into small-scale electrical devices such as solar-powered watches and calculators. PV cells also began to be used in programmes of rural electrification, in an attempt to help provide access to small amounts of power to inhabitants of remote villages that still remained off-grid (Luque and Hegedus, 2011).

In the 1970s, dramatic rises in oil prices were imposed by the Arab countries of OPEC which led to a global energy crisis. Governments of oil-importing nations began to realize the limitations of conventional energy sources and to grasp the need to begin searching for alternative energy sources for the sake of national security. This led to growing support for research on solar PV technology and its potential applications. As a result, PV technology made rapid progress and investment in solar energy plants began to rise (Hodge, 2010).

In the 1980s, the use of PV systems gradually began to accelerate. Following the signing of the Kyoto Protocol (December 1997), which obligated signatory states to agree on emission limits governing the so-called greenhouse gases, this trend continued with swift growth in this area accompanied by an increased production of solar energy across the globe multiplied nearly twenty-fold during the first decade of the twenty-first century (Hodge, 2010). Current efforts are focused on enhancing competitiveness and performance of solar panels, whilst simultaneously minimising costs. Much of this research has focussed on developing the materials used to manufacture PV cells and on studying methods of enhancing performance of panel cell energy conversion as the yield becomes increasingly important (Hodge, 2010).

1.3.2.2 Grid-connected vs. stand-alone PV solar energy systems

Researchers have studied two main systems for delivering electricity using the PV system: the grid-connected PV system and the stand-alone PV system (Maammeur et al., 2017).

The major benefit of using the grid-connected PV system over the stand-alone PV system is that the former system can be used without the need for batteries to store electricity, which substantially reduces the cost of energy production. PV systems linked to the grid can de sub-divided into three main groups: small systems used for private purposes in domestic settings (generating 1–5 KW), medium systems for commercial, industrial, and big building purposes (10–250 KW), and big system PV power plants for centralised production (100 KW–5 MW) (Castro et al., 2005).

A stand-alone or off-grid PV solar energy system is a self-contained set of interconnected components used for converting solar irradiance directly into electricity and is capable of operating autonomously, since it functions independently of the electricity grid. This system is ultimately completely reliant on solar energy with just a battery backup (Guda and Aliyu, 2015).

As Figure 1-4 illustrates, this type of system usually consists of the PV array, a battery bank, charge controller, an inverter, protection devices and the system load.

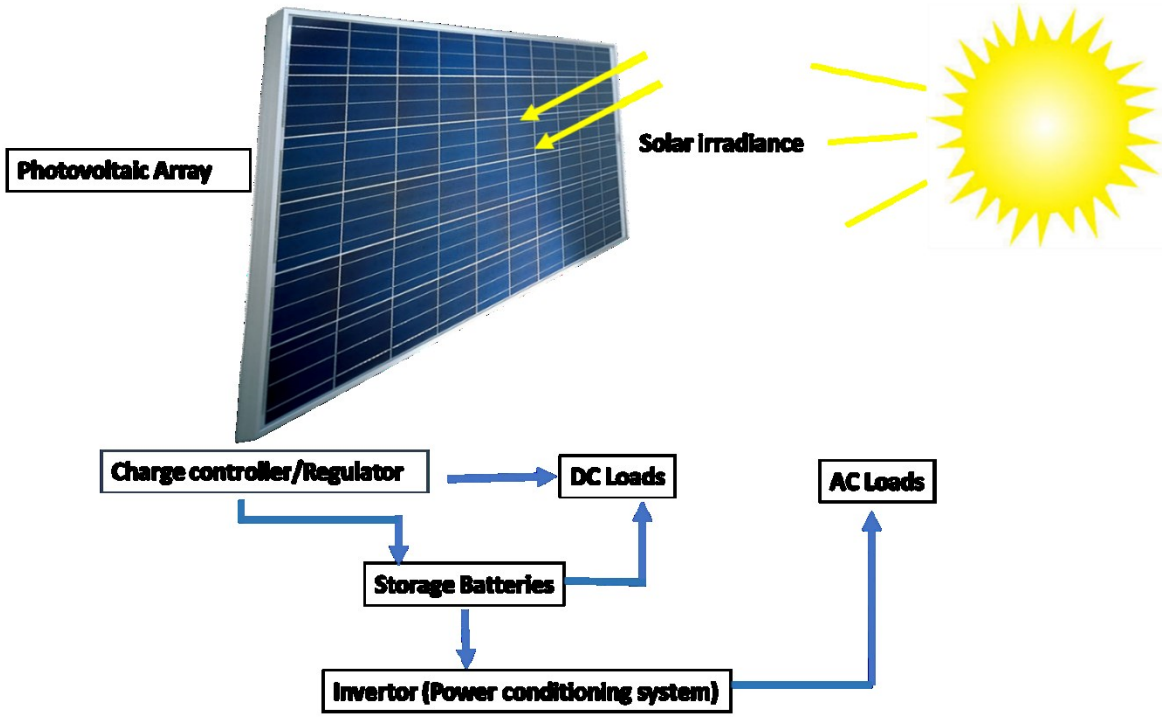

Figure 1-4: Components of a stand-alone PV power system

In grid-connected systems, the owner is able to use the electricity generated or it can be fed into the utility grid. In numerous countries, a tariff is paid for feeding this unused electricity into the grid. In their comparison of the strengths and weaknesses of the two systems, Howler and Fleisher (2015) identify the following points. In a stand-alone system, any excess electricity typically charges the batteries, which once fully charged any surplus electricity will be lost. In a grid-connected system, there is no waste since all the excess in PV-produced electricity can be used. This will allow this energy to be used in distributed energy systems which are likely to become an increasing feature of the future energy landscape.

The reduced number of components in a grid-connected PV system means this is less complex since it requires only PV modules and a grid-tied inverter. Since no storage is

needed, batteries or charge controllers are not necessary. The lead acid batteries required for storage to secure the necessary autonomy for a stand-alone system are expensive and significantly add to the cost of such systems. In addition, these batteries have a limited lifetime which cannot always be easily ascertained (Layadi et al., 2015). Also, depending on the start-up power required, the inverter may need to be oversized to cope with the start-up load also adding to costs. Grid-connected solar energy systems are also more reliable if there are likely to be prolonged periods of low irradiation, for example during bad weather. A stand-alone system is completely reliant on PV power and the storage could run out in a battery-operated stand-alone system.

One important advantage of a stand-alone system is that being independent from the grid ensures that it can still be used during power black outs which may occur frequently in some developing countries and emerging economies, particularly at times of peak demand.

1.4 The role of power electronics in solar PV systems

Figure 1-5 demonstrates a schematic diagram of connection of a PV load to the PV terminal using a DC-DC buck-boost converter. The primary goal of this converter involves matching the load impedance with the source impedance of the PV system in order to deliver maximum power efficiency. The link between the input and output variables of the DC-DC buck-boost converter can be calculated using the following formulae (Astaw, 2007). Equations 1.1 to 1.5 explain the working principles of those converters.

$$V_{out} = -d * V_{PV} \quad (1.1)$$

$$I_{out} = -I_{PV}/d \quad (1.2)$$

$$d = \frac{D}{1-D} \quad (1.3)$$

$$S_L = \frac{I_{PV}}{V_{PV}} = d^2\left(\frac{I_{out}}{V_{out}}\right) = d^2/R_L \ldots \quad (1.4)$$

$$R_L = d^2\left(\frac{V_{PV}}{I_{PV}}\right) = \left(\frac{D}{1-D}\right)^2 \left(\frac{V_{PV}}{v} I_{PV}\right) \quad (1.5)$$

Where

d is a linear control variable between V_{out} and V_{PV},

D is the duty cycle,

R_L is the output load resistance of DC/DC buck-boost converter,

S_L is the slope of load line,

V_{PV}, I_{PV} are voltage and current of PV module, and

V_{out}, I_{out} are output voltage and current of DC/DC buck-boost converter.

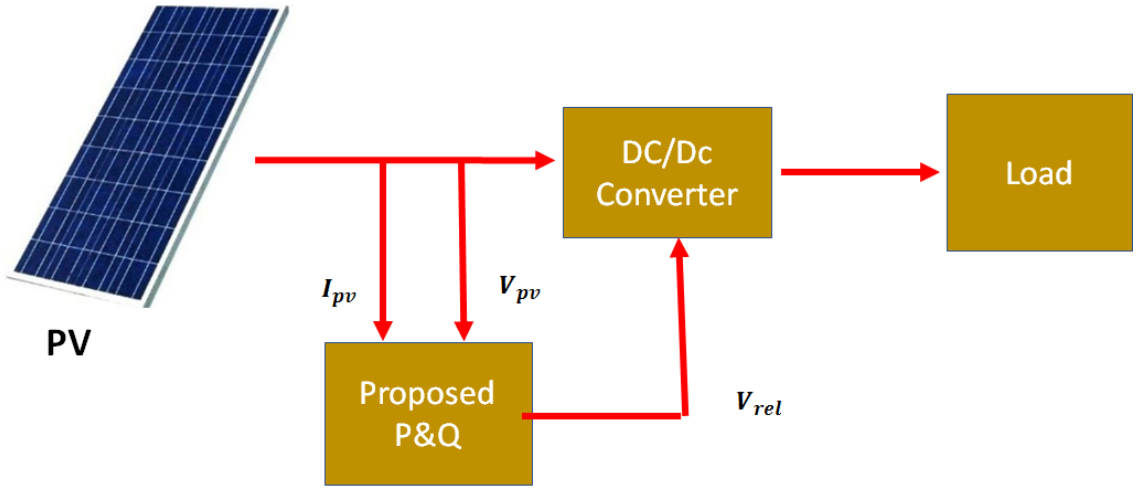

Figure 1-5 Connection of PV load to PV terminal using a DC-DC buck-boost converter

It would be helpful to consider the role of power electronics in today's arena and the changing environment in which grid-connected solar PV energy systems will operate in generating energy, feeding any excess energy into distributed energy resource systems (Molinas, 2016).

As described above, a solar PV system changes energy produced by sunlight into electrical current via PV effects. Solar panels can effectively adapt to demand through being connected in series or parallel, providing one clear strength of power electronics. If two individual solar panels are not identical, a DC-DC converter can be used to improve overall efficiency.

Multiple solar cells are connected inside modules. These modules are then wired together to form arrays and linked to a DC converter and an inverter (AC), thus ensuring that power is produced at the desired voltage and, in the case of AC, at the desired frequency phase, too.

PV systems can be organised into several configurations, each having a basic power electronics interface to convert the DC power produced by the arrays to AC electricity, thus allowing connection both to the grid and for individual consumer use. PV modules can be connected serially and/or in parallel, which are in turn, connected to a centralized DC/AC converter. One option for connecting string-array PV panels to the grid through a single inverter per string is the use of series of PV panels. A third possible configuration involves PV strings with a DC-DC converter plus an inverter as a means of offering the possibility of maximum power point tracking (MPPT) for maximising the power production of the PV system (Blaabjerg et al., 2004a; Kjaer et al., 2005).

Utility interactive DC converters contain electronic components that require a monitoring procedure in order to ensure the prevention of damage to any electronic components and to stop them from breaking down. Research efforts are currently focused on improving the dependability of power electronic systems to enable they are more widely available, are long lasting and sufficiently robust, and have low maintenance costs.

PV panels are utilised to gather and produce the solar energy which is conditioned by embedded PECs. These systems have non-linear current-voltage (I-V) characteristics and the potential degree of maximum power relies on environmental influences such as temperature and irradiance. An example of irradiance level variation over 24-hours in the UK can be seen in Figure 1-6. Weather variations of this type can also cause temperature variation-based stress for the PECs which negatively affects them, shortening their lifetime.

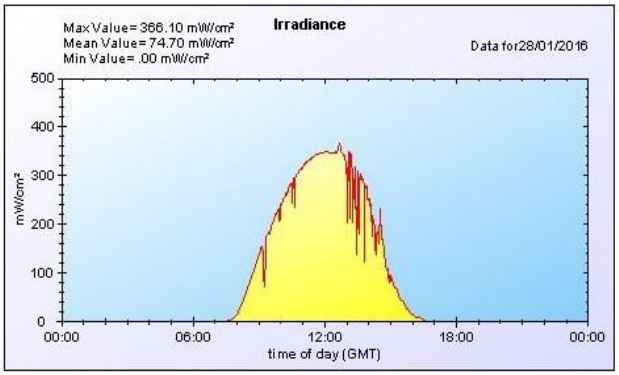

Figure 1-6: Sample irradiance profile for UK (source: WAO, 2016)

The maximum power point changes on the I-V curve of the PV systems as the irradiance varies as shown in Figure 1-7. To harvest the maximum available power

from the solar panels, MPPT techniques are used i.e. incremental conductance and perturb and observe methods. These methods regulate the switching patterns of the PECs to adjust the operating voltage of the PV to the MPPT point.

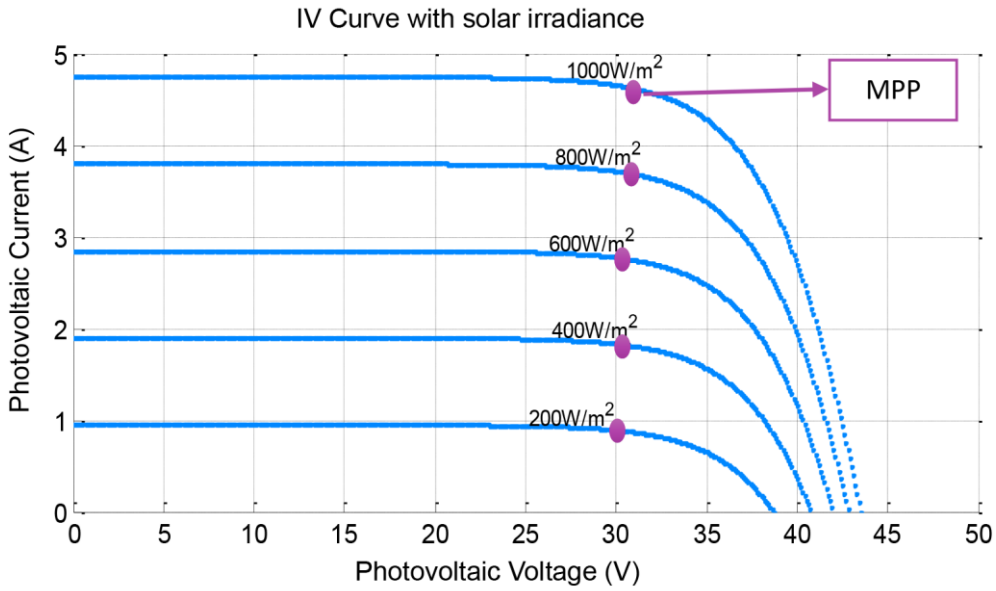

Figure 1-7: Maximum power point variation as irradiance level varies

A fault diagnosis technique using power from a semiconductor device could serve as a target monitoring device that would provide important information based on its operating characteristics. The operator of the system could be notified, in advance, of the need to service the degraded power modules, long before any other device within the power module fails.

It is worth noting also that Blaabjerg et al. (2004a) referred to power electronics as the key enabling technology for grid integration of renewable energy sources, pointing to an idea that has emerged recently as a promising way of meeting growing needs for electric power is known as the distributed energy resource (DER) system. Distributed energy refers to a form of electricity production which makes use of large numbers of

small to medium-sized power plants rather than relying on a reduced number of large capacity plants (Molinas, 2016). As a system, it represents several advantages. In addition to increasing the resilience of the power grid, transmission distances are reduced and consequently so are losses. This also means that the voltage that is needed for efficient transmission can be lower. From the consumer perspective, it provides a wider choice of energy systems, enhances the reliability of supply and would allow users to access alternative less expensive power sources during peak price periods (Kroposki et al., 2006).

If the terms of the Kyoto Protocol are to be met, renewable energy that has been produced from natural sources, including solar PV power, will also need to be incorporated into distributed energy resource (DER) systems (Molinas, 2016). Regardless of the type of renewable energy application that is employed, the control and communication capabilities of power electronics will be the key coupling technology that will enable the efficient use and widespread adoption of DER systems. The advent of extremely reliable power electronics will make it economically feasible to couple even domestic scale co-generation equipment to the electric grid, including solar-generated power systems (Delfino and Procopio, 2008), thus introducing new possibilities for providing ancillary services. In addition, recent advances in power electronics will help to mitigate the previous concerns of electric companies about the safety and quality of domestic surplus energy being sold back to them (Delfino and Procopio, 2008).

1.5 Parameters affecting the efficiency of semiconductor devices

The environmental and economic aims of PV power plants have been critical in the in-depth performance analysis of the output power of solar cells. In addition, the increase

in the global demand for stand-alone PV systems represents a key element in increasing the demand for in-depth performance analysis of the output power of solar cells and providing a greater insight into the main elements determining output efficiency. Three main parameters are acknowledged in affecting the performance of a PV system: PV module degradation, shadows, and the influence of ambient conditions affecting solar irradiance and leading to a reduction in the output power as a result, for instance, dust gathering on the PV module surface (Ketjoy and Konyu, 2014).

1.5.1 Dust deposition

The electricity generated from the sun can be delivered to individual house roofs, to the front windows of big buildings, or to large plants of solar cells that cover hundreds of acres. Usually, standard test conditions (STC) for measuring solar cells are adopted by the manufacturers. The common industry standard used to show the performance of PV modules specifies a cell temperature of 25°C, a solar irradiance intensity of 1000 W/m^2 with an air mass (AM) of 1.5 (Kalogirou, 2013). Measuring the solar cells according to STC is reliable in a factory setting. However, the external conditions in a normal environment, such as dust, temperature, rain, and snow, could all influence the performance of PV devices.

PV power plants are negatively impacted when the electricity produced by a PV system decreases. Pavan et al. (2011) investigated this impact on 1MW PV power plant in Italy. Polycrystalline silicon (poly-Si) was used at this plant, and the study was conducted from June to October. The results showed that there was a degradation in performance of 6.9% as a result of dust settling on the PV power plant (Pavan et al., 2011). When Kaldellis and Fragos (2011) compared the output performance of a fully clean PV panel and one polluted by ash, they found that the latter suffered a

considerable deterioration of up to 27% energy reduction per hour or a 1.5% efficiency decrease in absolute terms.

Bonkaney et al. (2017) compared the impact of cloud cover and the accumulation of dust on the performance of a PV module in Niamey, during the period from June to August 2015. The results of their study confirmed that cloud cover and the accumulation of dust both significantly affected PV module performance. The impact of cloud cover is immediate, with a decrease in output power for a short time, with a long-term effect being observed on output power stemming from dust accumulation (Bonkaney et al., 2017). When dust accumulates on the top surface of the solar panel it decreases transparency, resulting in a decrease in the amount of time that sunlight is able to reach the surface of the PV panel. This leads to a significant decrease in the output efficiency of the solar cell.

An analysis of dust deposition on solar module processing was carried out by Mazumder et al. (2002). They concluded that a number of dust-related factors can substantially affect the performance of PV panels, including dust particle size, the shape and distribution of the dust, deposition mechanisms, and the orientation of the dust (Mazumder et al., 2002).

Tilt angle can also contribute noticeably to the performance of PV panels in dusty conditions (Darwish et al., 2013). An early study conducted by Sayigh et al. (1985) in Kuwait City examined the relationship between the tilt angle and the dust deposition in relation to the glass plates. They found a significant reduction in the transmittance of the plate from 64% to 17% for tilt angles in a range between 0^0 and 60^0 after exposing the panel to a normal environment for 38 days. A study of different glazing

materials was conducted by Nahar and Gupta (1990) in India, examining the influence of dust and tilt on transmittance. They found that the transmittance of glass was reduced with a corresponding increase in the tilt angle, and the transmittances were 19.7%, 13.81%, and 5.67% for tilt angles of 0^0, 45^0, and 90^0 respectively. This study also confirmed that the type of glass material used has a significant impact on the accumulation of dust. More recently, after checking the transmittance of glass plates in various environmental conditions, Hegazy (2001) confimed that solar transmittance degradation and the performance of PV devices is linked to the tilt angle (Hegazy, 2001).

1.5.2 Effects of temperature on PV devices

The effect of temperature on the performance of PV devices is of particular interest to many researchers. The main parameters of PV devices (i.e. maximum current, maximum power, open circuit voltage, and short circuit current) were calculated with the temperature coefficients by Kroposki et al. (2006). Using a cadmium telluride (CdTe) solar cell as a module, they found that although the results for current were not affected by the temperature, those for the voltage were.

The impact of temperature on the performance of monocrystalline Si modules has also been explored by Olchowik et al. (2006) who found that their performance is influenced by the spectral irradiance which reaches the module surface. They concluded that the performance of solar cells can be enhanced significantly by providing an additional cooling system (Olchowik et al., 2006). In another study, Astaw (2007) investigated the impact of the operating temperature on the efficiency of an amorphous silicon solar cell module under normal conditions. He found that the output efficiency compared to initial efficiency decreased substantially by about 65%

from autumn to winter (Astaw, 2007). A thermoelectric cooler was used by Erel et al. (2009) in comparing the performance of PV devices pre- and post-cooling. The authors discovered that a decrease in the temperature of solar cells by 15°C resulted in an increase of 0.01V for each 4cm x 4cm solar cell (Erel et al., 2009). He concluded that cleaner and cooler PV devices lead to enhanced power efficiency of solar cells.

1.5.3 Humidity effects on PV systems

The impact of relative density on the performance of PV devices was examined by Kazem et al. (2012) on three types of PV device (monocrystalline, polycrystalline, and amorphous silicon). During this study, the authors connected the PV system to voltage, current, and humidity measurements. It was found that the relationship between relative density and output parameters were negatively correlated. When the relative density was low, the current, voltage, and efficiency were high. Thus, the performance of the PV system was enhanced when the relative density was low (Kazem et al., 2012).

1.6 Rationale for this research

PV solar energy is regarded as one of the most attractive energy sources due to it is abundance, sustainability, and non-destructive impact on the environment. Moreover, the cost of producing PV system has significantly reduced from $76/ watt in 1977 to $0.3/watt in 2015 as shown in Figure 1-8.

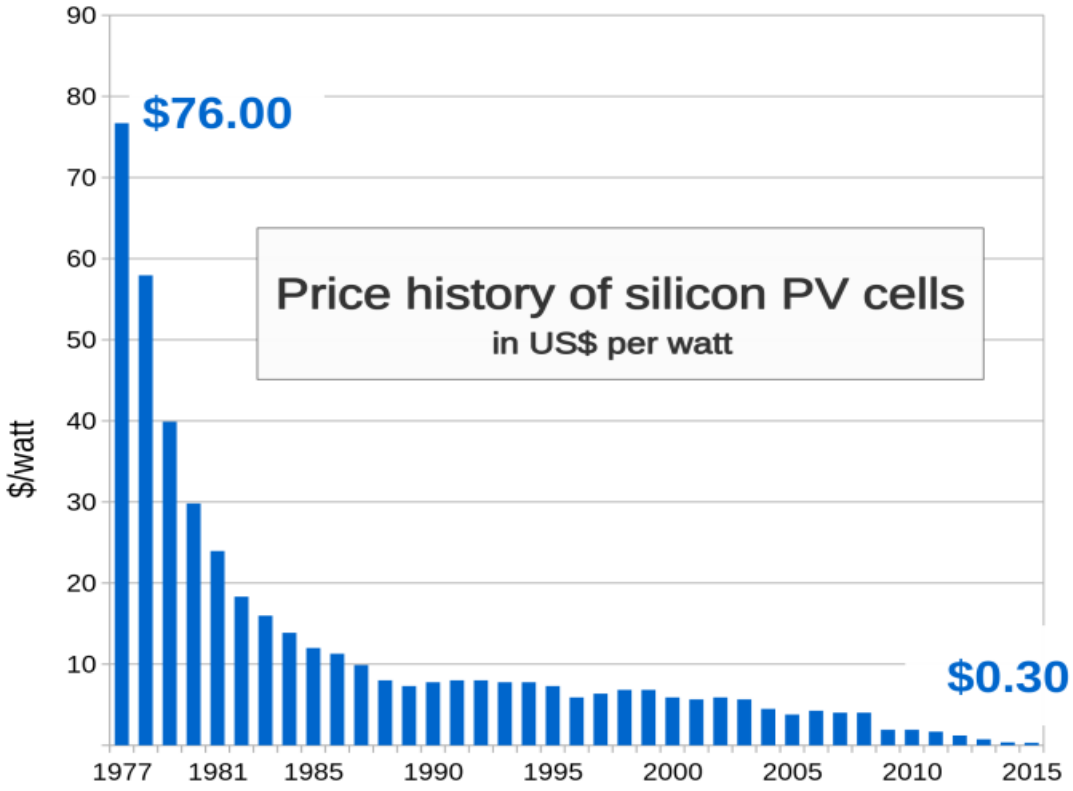

Figure 1-8 Price history of silicon PV cells [Bonkaney et al16]

Figure 1-9 Furthermore, the generation of electricity using PV system has substantially jumped in last two decades from 1.4 GW in 2000 to more than 400 GW in 2018 as illustrated in Figure 1-9. These factors, for example, have led the Saudi government to make increasing production of solar energy one of their key goals in their 2030 Vision national strategy to shape the future of the Kingdom. This has resulted in the installation of PV system solar farms in vast areas of the desert in Saudi Arabia where this geographical feature occupies over half the landmass of this country.[1] However, the power output and efficiency of these PV systems are frequently negatively affected by the range of factors described above, including deposition of dust particles, moisture, and temperature range. Different methods have been used to tackle this

[1] Saudi Arabia announced in March 2018 that it is planning to spend $200 billion on building the world's largest solar farm which would produce 200 gigawatts of energy (England, 2018).

issue. However, they are often complex and difficult to control and do not always detect the faults in a timely manner. Moreover, given the remote location of many of these solar farms monitoring techniques need to be non-intrusive, powerful and reliable, detect potential failures at their early stage from long distance places.

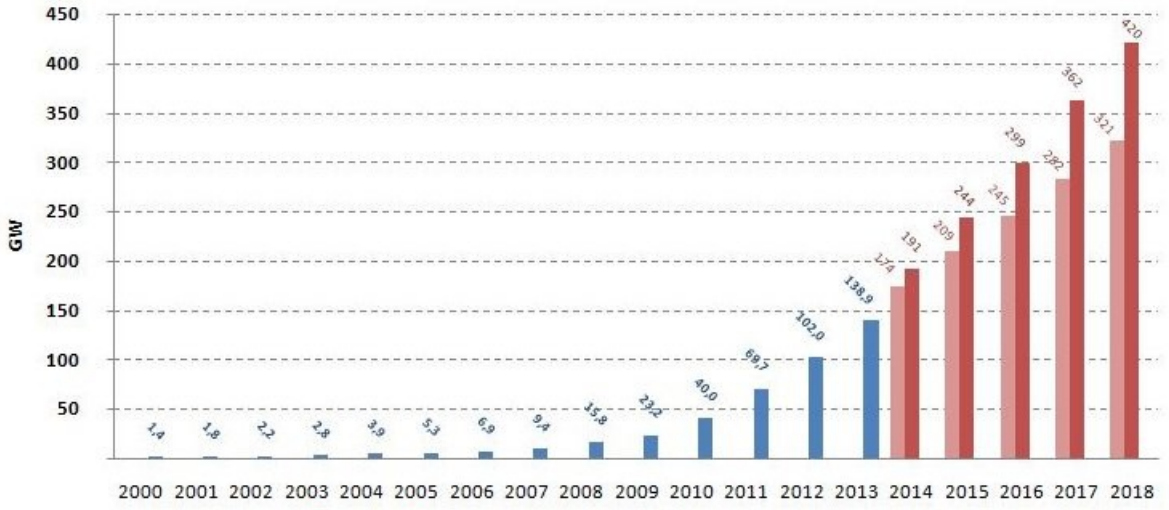

Figure 1-9 Total worldwide installed PV capacity by year: 2000 to 2013 and projected growth scenarios until 2018 (source: Ketjoy and Konyu, 2014)

In addition to thermal measurements, it is also proposed that using acoustic emission (AE) system would provide a novel method of preventing system failure and ensuring continuity of electricity supply. A warning system using this AE technique could be integrated into any existing circuit, allowing data collected to be automatically sent online to alert the system operator to service the degraded power modules, before any other device within the power module fails. It is proposed that a warning system based on acoustic emission (AE) could be developed and implemented within a DC-DC converter of a PV system. This system would then be used to monitor the health of an insulated gate bipolar transistor (IGBT).

Therefore, in-situ health monitoring using thermal and AE techniques is being developed so that this can be integrated into any existing circuit, and any data collected could be automatically sent online. As the literature review will show, previous research has shown that AE can be used in non-destructive testing (NDT) and it has also already been implemented as a condition-monitoring tool for various systems, including engines, pumps and industrial drives.

1.7 Research aim and objectives

1.7.1 Research aim

The aim of this work is to investigate thermal and acoustical characteristics of power electronic devices (PEDs) used for photovoltaic solar systems. The PEDs will be experimentally tested, under different operating conditions, and their thermal and emitted acoustic signals are measured and analysed. By measuring and analysing thermal and acoustical characteristics and any correlation between them, this would pave the way towards the development of a non-intrusive monitoring tool, which can be used as a means of detecting errors on the power electronic circuits before they occur or at early stages of their onsets. This helps in reducing the costs of unexpected down times and would improve maintenance activities, which are currently being conducted in an inefficient and reactive manner.

1.7.2 Research objectives

The aim of this research outlined in Section 1.7.1 will be achieved through the following objectives:

1. To understand the working principles, topologies and roles of power electronic converters in photovoltaic (PV) solar power systems.

2. To conduct an up to date literature review including common failure modes for power electronic devices, in particular those used for PV solar power systems, condition monitoring methods used for detecting those failures.

3. To design and model the DC-DC boost converter circuit using MATLAB and Simulink. This would provide clear understanding of their electrical behaviour and ratings.

4. To derive a realistic finite element model for describing the thermal and acoustical characteristics of semiconductor switching devices used in power electronic converts.

5. To design and build experimental test setup for initial thermal and acoustical data collection and subsequent data analysis.

1.8 Contribution to Knowledge

It is envisaged that this research will provide a valuable contribution to this field by, firstly, providing a viable alternative to existing methods for condition monitoring of power electronics modules and their switching devices (IGBT). Secondly, being able to determine the cause of IGBT failures remotely and quickly with greater accuracy than prevailing methods. Thirdly, diagnosing and resolving faults more quickly since the diagnosis or reasons for failure will already be known, and; finally, being able to determine the most suitable places and/or environments for effective use of AE.

1.9 Thesis organisation

The remaining chapters of this study are structured as follows:

Chapter 2 presents an up to date literature review, offering a critical survey of this field in the last decade. It also identifies the gaps in knowledge within this field of knowledge, noting how these have informed the formulation of the research question. It concludes by providing a rationale for the focus of this research effort.

Chapter 3 focuses on the modelling of solar PV systems. It begins by addressing in detail their structure and design and then modelling these system. The modelling includes component-level analysis, with specific emphasis on power electronic devices. MatLab and Simulink software packages are used for modelling PV solar components.

Chapter 4 develops theoretical modelling for predicting thermal and acoustical characteristics of PEDs. More specifically, it describes simple finite element model using COMSOL and analyses their performance when they are associated with solar PV systems including modelling.

Chapter 5 provides a thorough explanation of the test rig and the experimental setup used during this research to examine and test power electronic devices. It also presents the research findings, together with all the results from both the modelling and the experimental elements of the work, discussing these in further detail.

Chapter 6 outlines conclusions of the carried out research, reviews the objectives for this research, outlining its key achievements, as well as highlighting conclusions derived from the work conducted over the period of this research. It concludes by identifying future research needs in this field and points out some possible directions that may be followed in future work.

2 Literature Review

2.1 Overview

As previously noted, the demand for electricity generation from renewable energy sources (RES) including wind power, PV systems, hydropower and biomass has significantly increased in the last decade and formidable developments have been made in this field. Electricity produced from RES is expected to triple in the next few years. Amongst these RES, PV solar cells and wind turbines have been identified as the most promising technologies for electricity generation (Blaabjerg et al. 2011). However, RES present various drawbacks due to environmental and climatic factors. Subsequently, the provision of reliable energy sources needs to be linked and assimilated into the utility grid or form part of multi-source power generation (Mira et al. 2017). One of key challenges impacting on the adoption of RES is the extensive use of PEDs in the renewable energy sources, especially PV systems technologies, for producing, transmitting and distributing power (Blaabjerg et al. 2011) The main functions of these devices is to transfer renewable energy to the power grid and also support the grid with reactive power injection (Blaabjerg et al. 2011). Thus, these PEDs must be both efficacious and dependable given the vital role they play in the energy transformation of RES. Research has shown that a variety of environmental factors such as dust, moisture, and temperature variation can impact significantly on the performance of the PV systems and cause these to break down. Consequently, detecting or discovering this failure in a PV system at the earliest stage possible is essential in many respects in order to save money and reduce potential losses caused

by system failure. The ability to monitor PV systems remotely is critical as solar farms are often situated in isolated rural locations.

To date, different technologies have been used to control and monitor PV systems such as radiation sensors (in the form of pyranometers or reference cells), data loggers, or other intelligent monitoring. However, these technologies are not only expensive but demand maintenance (Drews et al., 2007*).* Thus, there is a demand for remote detecting technologies which offer effective and credible monitoring. In this thesis, a novel AE technology is used to detect and monitor the failure in a PV system. The intention is that this can be used in individual stand-alone PV systems or in those solar farms occupying vast areas as is the case in Saudi Arabia.

This chapter outlines PEDs and also the use of AE as a NDT and evaluation technique together with a literature review of recent and relevant literature in this field. It begins by briefly outlining the development of AE and then proceeds to consider the context which motivated the need for research in this area and which has continued to underpin its ongoing development and application, namely NDT and evaluation and condition monitoring. After establishing the general advantages that AE offers as a non-invasive method for testing, evaluation and condition monitoring of materials, components, structures and systems, a more detailed review of work on the potential uses of AE in the specific area of power semiconductor devices and their applications in solar energy follows.

2.2 Development of PV systems with PEDs

PV solar cell technology is regarded as a key renewable energy system (RES) for many reasons including the abundance of solar irradiance, its environmentally friendly

credentials and the significant reduction in cost of producing this technology. It has the potential to contribute directly to producing electricity in the future.

The structure of the PV system is based on a P-N junction of semiconductor wafers, which generate electricity upon exposure to sunlight due to the PV effect (see Figure 2-1).

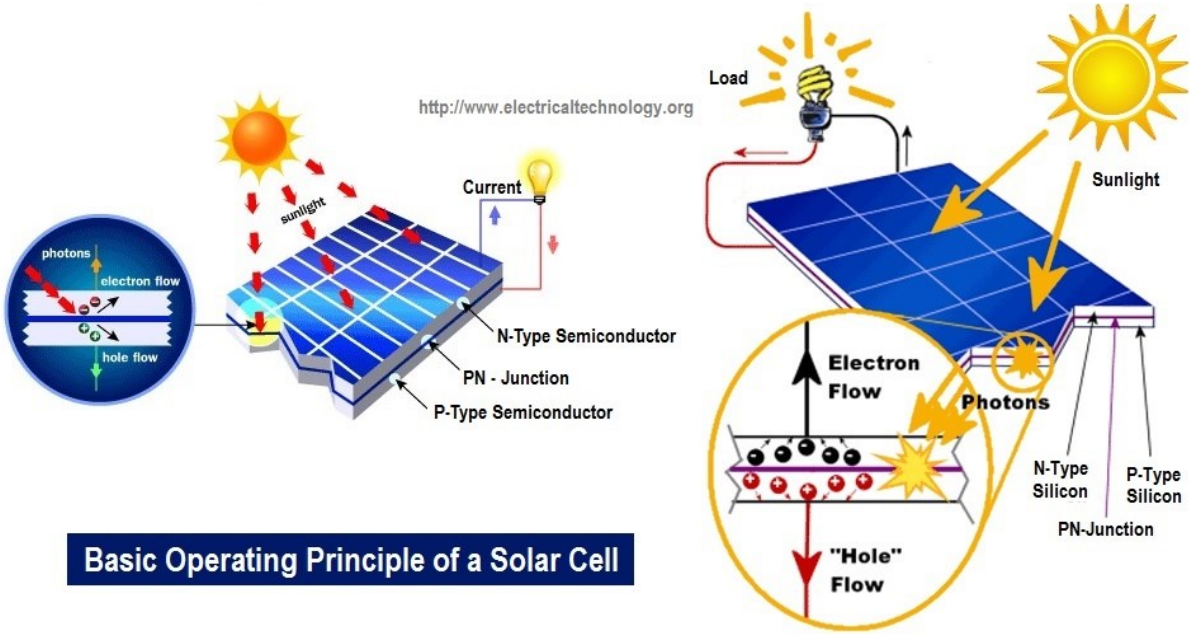

Figure 2-1 PV effect (source: http://renewableenergyplus.com)

In addition to these PV panels, the PV system also contains other components such as inverters, wiring, breakers, ranking and switches. In practical terms, the PV system can be classified into four main groups, namely, stand-alone PV systems, direct coupled PV systems, grid-connected PV systems, and hybrid-connected systems. In the stand-alone system the energy produced is stored in batteries. This system is generally used in rural areas lacking access to the electric grid. In the direct coupled PV system, the PV panels are linked directly to the load and to operate they must be exposed to sunlight. In the grid-connected PV systems, the electricity generated from the PV arrays is either

used straightaway to operate the load or to feed the grid. In the hybrid PV system, another source of energy is used to meet electricity demands in addition to the PV system.

Different semiconductor materials have been used in the PV manufacturing system such as monocrystalline silicon, polycrystalline silicon and amorphous silicon (Kulkarni and Virulkar, 2016). The performance efficiency of these three conductor materials are 22%, 15% and 10% respectively, with amorphous silicon demonstrating the greatest efficiency in terms of voltage output and ongoing maintenance (Kulkarni and Virulkar, 2016). The ideal current-voltage characterisation I-V curve for all PV solar cells measurements is illustrated in Figure 2-2.

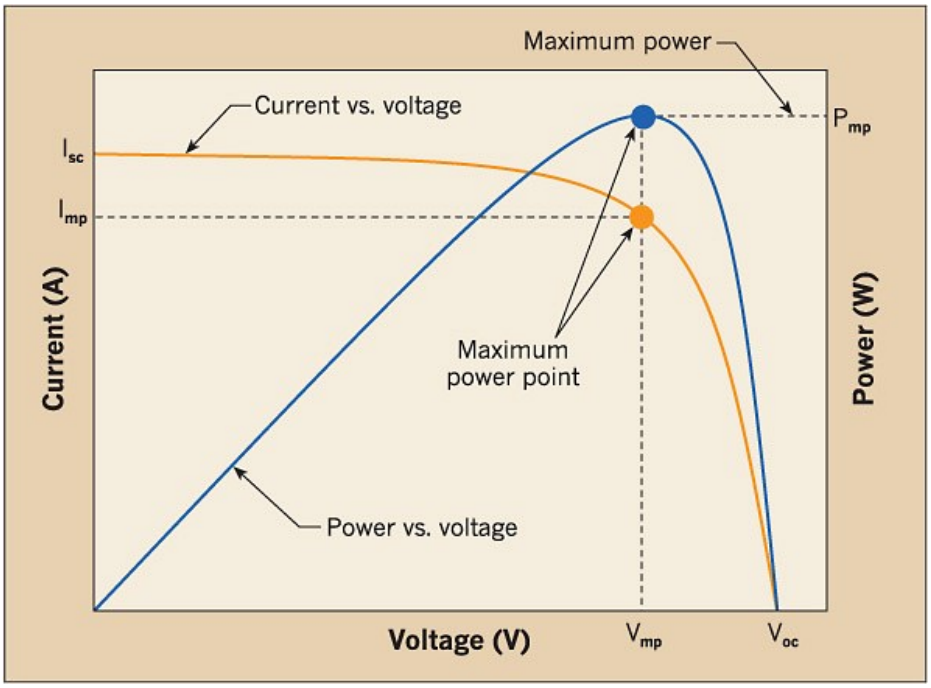

Figure 2-2 I-V characterisation curve (Michalis, 1997)

Due to the rapid development of interest in PV solar cells, new strategies have been developed for operating and managing the electricity grid that allow the energy produced to be stored or promote the power supply reliability and quality. The role

played by power electronic technology in the distribution of the energy produced has significantly increased, allowing RES to be integrated with the electrical grid (Carrasco et al., 2016).

In general terms, PV systems have two broad categories: PV inverters with a DC/DC converter (with or without isolation) and PV inverters without a DC/DC converter (with or without isolation) (Blaabjerg et al. 2004b). Figure 2-3 shows schematic diagram of the power electronic interface for renewable energy sources.

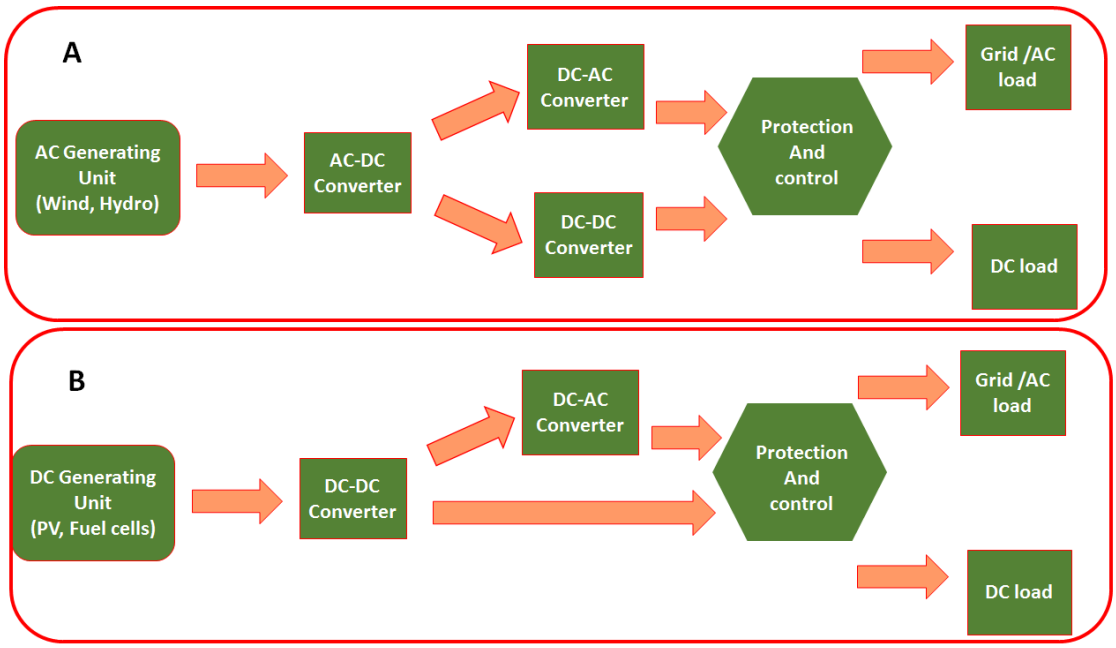

Figure 2-3 Power electronic interface for RES: A=AC generating units, B=DC generating units.

2.2.1 PV system connected to DC-DC converter

Different PECs have been promoted for integrating RES and controlling the power from sources to the load. These converters have five major functions as summarized below:

1. Transforming the variable voltages into regulated output voltages.
2. Confirming high-quality output power by reducing deviations in voltage and frequency.

3. Tracking the maximum power in wind and PV systems
4. Transforming the power to the desired voltage and frequency.
5. Controlling power flow from the source to load.

Power electronics converters which can convert DC to DC or AC to DC and DC to AC are employed for the renewable energy interface. DC-DC converters are considered to be the most frequently used devices for providing and regulating supply from RES which are uncontrolled and unregulated (Chakraborty, 2011). Two major kind of DC-DC converters are employed in renewable energy systems. Isolated type converters are used in medium- to high-power renewable energy applications. Typically, they employ a a high frequency transformer to supply isolation between sources and load (Kim et al., 2017). The second type of DC-DC converters are non-isolated converters which are employed when high frequency transformers are not required for input and output isolation. This kind of converter is used in low-power renewable energy applications and is most common in RES applications owing to their high conversion efficiency, small size and low numbers of components (Du et al., 2017). Non-isolated DC-DC converters may be further subdivided into two types, namely single port and multiport. The former connects a single source to a single load whilst the latter is used to link several RESs to a single load or vice versa.

Two examples of single port converters will be discussed here: the DC-DC boost converter and DC-DC buck-boost converter (Taghvaee et al. 2013). In the DC-DC boost converter, the value of output voltage exceeds the input voltage. This converter is generally utilized when the load voltage demands a higher voltage than the source voltage and is widely used in the PV system in both stand-alone and grid operated systems. In the buck-boost converter, the output voltage value can be greater or lesser

than the value of the input voltage. Cascading the two normal converters (i.e. boost and buck) creates the buck-boost converter (Taghvaee et al., 2013).

Researchers have examined different routes that can be used to achieve high-step-up, low cost and high performance single stage converters, in order to satisfy the requirements for low-cost and high-step-up conversion efficiency in the grid-connected PV system. Various results have been obtained: high-step-up converters with coupled inductor, high-step-up converters with switched capacitor, high-step-up converters with inductor and switched capacitor, high-step-up converters with coupled inductor and switched capacitor (Li and He, 2011)

2.3 Development of acoustic emission (AE) as a field

AE is a naturally occurring phenomenon found within a broad variety of materials, structures and processes. At one extreme, seismic events like earthquakes represent the largest magnitude of AE with the seismologist Kishinouye having been credited with making the first scientific contribution to AE instrumentation in 1933 with his experiments on wood splintering (Grosse and Ohtsu, 2008). At the opposite end of the scale, dislocations in stressed metals have also been observed to produce AE (Miller and McIntire, 1987). Sources of AE can be as diverse as impact, wear, crack propagation and gas flow (Reuben, 1998). The American Society of Testing and Materials defines AE (1990) as: “the class of phenomena whereby transient elastic waves are generated by the rapid release of energy from localized sources within a material”.

AE was first employed as a non-destructive test to examine static structures over 35 years ago, and has been continuously developed, resulting in increased interest in NDT

based on AE leading to its use in many industrial applications (Lysak, 1996). This technique has now been expanded to include health monitoring of rotary machines such as bearings, gearboxes, pumps, etc. (Mba and Rao, 2006).

Initially, experiments with AE began as early as the 1930s (Narzarchuk et al., 2003), while serious investigation in this field can be said to date from the 1950s when Joseph Kaiser published the findings of his doctoral research that was focused on measuring the noise levels generated by various metals when they were subjected to tensile load (Baccar, 2015). Kaiser made two key observations based on the results of his experiments. The first was that all materials tested under load emit AE (Tensi, 2004). The second was that any material under load emitted acoustic waves once the primary load had been exceeded. This phenomenon is now commonly known as the Kaiser Effect, and can be delineated as the, "absence of detectable AE until the previous maximum applied stress level has been exceeded" (Miller and McIntire, 1987: 5). This is very important to understand effects of stress and heat on the emitted acoustic signals. It also explains why the measured acoustic emission signal contain substantial amount of noise and interference, as mentioned in Section 2.5.

This means that during reloading this material will behave in an elastic manner until the previous maximum load has been reached (Grosse, 2007). This information can be utilised to ascertain a link between AE activity and the stress-strain curve (Baccar, 2015).

The value of AE as a technique for carrying out non-intrusive testing and evaluation of materials, components, structures and systems has been recognised since the 1970s (Chretien and Chretien, 1972) but truly came into its own as a condition monitoring

technique in the 1980s (Drouillard, 1996). A non-destructive technique based on AE promises to be one of the most effective methods, particularly for monitoring the condition of components which are subject to tension and distortion (Carpinteri et al., 2007). However, successful application of a non-destructive test based on AE is reliant on the existence of equipment which allows AE signals produced during the early stages of crack or fracture to be received and processed (Lysak, 1996).

The context to these areas and a more detailed review of work on the potential uses of AE in the specific area of power semiconductor devices and their applications is provided below. The principles underlying AE will be discussed in detail in a later chapter.

2.4 Non-Destructive Testing and Evaluation

The mechanical properties of all structures undergo degradation and even a material crack measuring just micrometers is likely to result in some reduction in performance. If left undetected, this damage could eventually produce complete system failure, potentially entailing damage to equipment or to the working environment or beyond, associated economic losses and, in the worst case scenario, personal injury or even death. This explains the growing interest in and demand for developing reliable techniques for identifying early stage damage in structures, materials or systems, and for online monitoring and prognosis of these, that is able to take into account the effects of damage accumulation and estimated future loading (Adams, 2007).

The majority of complex systems must be regularly maintained and inspected to ensure compliance with health and safety and/or environmental legislation, and for reasons of operation reliability and quality control. The frequency with which this

maintenance and inspection must be carried out and the form which they should take are generally determined by the manufacturer although experience also has an important role to play in this decision. This can be affected a number of diverse factors which include the probability of defects developing in structures, the complexity of the system, and the type and age of the material(s) in question (Baccar and Söffker, 2013). The difficulty is that, maintenance and inspection usually prove costly due to downtime and the labour involved and may even be hazardous. For this reason, in recent years, several studies have been carried out in the applied area of non-destructive testing and evaluation (NDTE) which is intended to reduce costs and downtime while at the same time ensuring user safety.

NDTE methods are used, "to determine the integrity of a material, component or structure or quantitatively measure some characteristic of an object" (Diederichs, 2007). These techniques are non-invasive, meaning that this form of assessment does not harm, stress or destroy the object under examination and is performed "without impairing its future usefulness" (Miller et al., 2005). They cover a diverse range of techniques used for detecting and evaluating defects, damage and failures. The oldest and still the most commonly used method is visual inspection while the most frequently applied newer NDTE methods include ultrasonic testing, radiographic testing and electromagnetic testing. Other less widely used methods can involve the use of liquid penetrant, magnetic particles, eddy current, holography, and microwaves, and new techniques are constantly being developed (Diederichs, 2007).

2.5 Condition based maintenance

Condition based maintenance strategy employs continuous monitoring of the operational characteristics of equipment to forecast the requirement for maintenance

prior to a deterioration or breakdown occurring, ensuring that maintenance is only performed when necessary (Tsang, 1995). It is based on “using permanently installed sensors to collect data in order to analyse changes in the performance or condition of a machine component while it is in operation” (The Welding Institute, 2017). If the performance of a component is then found to deviate from its standard parameters, this may point to the onset of wear and deterioration. Thus condition monitoring is a prognostic technique since it “not only describes the present state of a component, but also provides objective data which can be interpreted to predict remaining useful life while in operation” (The Welding Institute, 2017). The need for condition monitoring is particularly important in the case of electrical equipment maintenance as any unexpected fault or shutdown may have extremely serious consequences.

Condition monitoring provides vital information for ensuring the optimal utilization of systems. Rapid changes in computational and data processing capabilities, smart sensors, and transducer technologies combined with those in the fields of signal processing and artificial-intelligence techniques have paved the way toward ever-more effective implementation of condition monitoring techniques that can be applied to electrical equipment. Smart sensors differ from ordinary sensors and usually include microcontroller or processor unit. They are able to capture and analyse signals instantly, as well as being able to achieve the process of ‘capture and analysis’ at higher frequencies. Together, these advances have helped to make the condition monitoring of power generation and distribution systems more reliable and more intelligent (Goel et al., 2014).

AE has been classified as a non-destructive testing and evaluation (NDTE) method since the 1970s and is considered the foremost approach for the detecting, micro-structural

characterization, and monitoring of damage processes (Surgeon et al., 2000) because AE technique has a number of potential advantages when compared to other non-intrusive means of testing or evaluating materials, components or structures. As a technique, AE is usually realized during loading which means it can be used to perform damage inspections and evaluations without the system or device being tested having to be taken out of service. Most other NDTE methods, in contrast, are applied prior to or following the loading of the structure.

Moreover, AE technique detects the elastic waves emitted within the structure during deformation, thus relying on the energy that is released by the object being tested and does not rely on artificial excitation. Thus, it is considered to be a passive NDTE method whilst most other traditional NDTE methods including radiography, ultrasound and eddy currents are defined as active testing techniques. Active approaches employ actuators or piezoelectric wafer active sensors and must be used in conjunction with knowledge about the physical properties of the material being examined in addition to the differing phenomena linked to the characteristics of wave propagation in different materials (Stepinski et al,. 2013). These active methods are still at the embryonic stages of development and are heavily influenced by both environmental and operational conditions including levels of pressure, temperature, and humidity, together with structural boundaries (Stepinski et al,. 2013). Passive approaches, like AE, however, rely on the dynamic response of the structure to mechanical and environmental stress which is applied in service. In this case, any waves detected can be interpreted as having been caused by the actual damage (Romanowicz, 2014).

AE can be considered an effective tool for studying material damage due to its ability to provide information that is both detailed and immediate. Some NDTE techniques

can be considered indirect, meaning they measure changes which have occurred during machine operation, seeking to deduce its condition from these. Indirect approaches are generally unable to provide data on the exact location of any changes occurring in the signal. Since sources of AE are diverse and can include, for example, impact, wear, crack propagation or gas flow, the signal they produce is potentially more direct. This is due to the fact that it based on a degradation process, as opposed to it being merely a symptom that degradation has occurred, which may be the case with a rise in temperature or vibration at a particular frequency, for example. Thus, AE can identify any changes happening in the material, component or structure at an early stage and has the potential to pinpoint the source of the emission and hence, determine the location of the degradation events (Wang et al., 2012).

AE has two further strengths for NDTE. Firstly, by using suitable hardware, it allows the dynamic processes or changes in a material to be continuously monitored in real-time (Vallen, 2002). Secondly, it can be employed as a 'global' monitoring tool (Holford et al., 1999) and in comparison with other NDTE techniques it can provide inspection over a wider area. All of the benefits listed above serve to make AE one of the most appropriate NDTE methods for health monitoring applications carried out in-situ, particularly when these are related to examination of dynamic failures (Fouvry et al., 2003).

According to the American Society of Non-destructive Testing, the two key disadvantages of this using AE are, firstly, the fact that signals display a tendency towards attenuation and when placing sensors, care must be taken to ensure that the whole structure is monitored. Secondly, because the voltages induced in the transducer are very small, it is necessary to eliminate background noises to prevent

this from corrupting the signal before it is amplified which can prove difficult. In practical terms, this means that the signal will often be dominated at lower frequencies by mechanical and external noise while at higher frequencies, attenuation constrains the applicability and effectiveness of AE as an NDT method outside the laboratory environment (Miller, 1987). In addition, although the unique properties of the Kaiser effect (see section 2.3) are generally helpful in this technique, this may also sometimes represent a hindrance to the AE testing process (ASNT, 2006).

It has been argued that AE analysis is most effective when used in combination with other techniques, such as stress-strain or crack growth measurements (for example, the Krak gauge) or with visual methods such as microscopy or digital image correlation (Pollock, 1989). When combined with these techniques, AE can offer additional information concerning the dynamics of any underlying deformation or damage processes and can also identify transitioning from one type of deformation or damage to another when this occurs (Pollock, 1986).

Since the latter part of the twentieth century, AE and its applications have been researched intensively in diverse fields including condition monitoring of rotational machines (Navarro et al., 2010; Wang, W. et al., 2013), concrete structures (Nair, 2006; Lamonaca et al., 2012;), steel pipes and tools (Lim and Kaewkongka, 2007; Martins et al., 2014; Shukri, 2012), and fibre reinforced plastic (Costa Oliveira, 2004).

2.6 Power electronic converters (PECs)

2.6.1 The importance of PEDs

PEDs such as PECs and power semiconductor devices are used in an increasingly wide variety of industrial applications, being “a key and enabling technology for many

industrial segments such as automotive, home and office, communication, automation, energy supply and distribution" (Elbuluk and Idris, 2008: 14). In particular, they play a key part in the growing area of renewable power generation, in the technology of both wind power turbines and solar power PV fuel cells (Elbuluk and Idris, 2008), the latter being the focus of this research. The main functions of PECs as outlined by Hingorani (1995) are:

- Power conversion,
- Power conditioning to remove distortion, harmonics, voltage dips and over voltages
- High speed and/or frequent control of electrical parameters such as currents, voltage impedance, and phase angle, and
- High speed and/or frequent circuit interruption transfer, and current limiting functions.

Authors stress the importance of power semiconductor devices, the focus of this research. For Kärkkäinen et al. (2014a: 1) they represent "the workhorse of power electronic converters" whilst according to Bose (1992: 403), they can be called "the heart of modern power electronics". However, the same author observed that the power semiconductor device can also be considered to be "the most complex, delicate and 'fragile' element in a converter" (Bose, 1992: 403). There is evidence to support this opinion. For example, focusing specifically on the renewable power generation industry and more specifically on wind production, electrical faults and especially faults in power semiconductor devices have been found to cause a significant proportion of all downtime (Ribrant and Bertling, 2007). Citing statistics from an evaluation of

reliability of offshore wind power generating systems by Zhu et al. (2011), Kärkkäinen et al. (2014a: 1) note that the failure of power semiconductor modules was reported to have been responsible for some 19% of power converter failures. Field experience suggests that PEC failure was responsible for 37% of the unscheduled maintenance in PV generation systems (Moore and Post, 2008).

There are a range or variety of other devices currently available in the field that can serve the same or similar functionality to PECs, their main task being to process and control the flow of electrical energy efficiently, so that it is able to optimally suit the load requirements. These include DC-DC converters, DC-AC rectifiers, AC-DC inverters such as buck-boost and Cúk converters and electronic circuits that rely on the use of a transistor. All of these devices generally operate in the same way and are relevant to this current field of research but the major focus here will be on the Insulated Gate Bipolar Transistor (IGBT), one of these semiconductor devices used as switching elements in PECs in high switching frequency and current-voltage rating applications (Iov and Blaabjerg, 2007).

As noted above, PECs are extensively used in solar PV energy systems, representing part of the renewable energy sector that has rapidly expanded over the last decade. Since the efficacy of these systems is strongly affected by levels of irradiance and load variations, PECs in the form of DC-DC converters are embedded within solar energy applications to ensure that the minimum power can be extracted despite variable operating condition. This control strategy has been referred to as Maximum Power Point Tracking (MPPT) (Ferranda and Leva, 2008). PV systems can be structured using several configurations but each makes use of a basic power electronics interface to convert the DC power generated by the arrays to AC electricity, allowing this to be

interconnected to the grid for conditioning the energy flow (i.e. voltage and frequency regulation) and thus permitting safe consumer use. Configurations for maximising the power production of the PV system can vary:

- PV modules can be connected in series and/or in parallel and then connected to a centralized DC-AC converter.
- In string-array PV systems series of PV panels are connected as a single string with one inverter per string being used for connection to the grid.
- PV strings can consist of a DC-DC converter plus an inverter (Blaabjerg et al., 2004a; Kjaer et al., 2005)

Damage to any single component either reduces the efficacy of the complete system or causes it to malfunction. Thermal behaviour and electrical stresses of switching devices used in PECs are major contributors to failures in those systems. Looking towards the near future, it is expected that the control and communication capabilities of PEDs will be principally responsible for facilitating the widespread growth of newer Distributed Energy Resource (DER) applications, including solar PV applications. This add extra emphasis to their importance as the role of DER applications is expected to rise significantly, motivated by significant changes to the energy utilities market. Currently, however, power electronics is considered to be the least reliable part in the whole system design (Molinas, online), with the failure of PEDs being one of the most common causes of generation loss in renewable applications (Musallam and Johnson, 2012).

In countries like Saudi Arabia, PV cell systems are placed under extra strain due to the extreme environmental conditions which exist there. In addition to very high

temperatures and sometimes extreme daytime-to-night-time variations (Alawaji, 2001) high winds in desert regions can produce dust storms leading to dust accumulation (Al Helal and Alhamdan, 2009) and levels of humidity can also be high in the eastern and western coastal areas. This, together with the fact that solar power farms in the Kingdom are often situated in remote locations (Hepbasli and Alsuhaibani, 2011), makes it all the more crucial that effective and efficient condition monitoring of these devices can be carried out.

The lifetime of the DC-DC converter which operates the MPPT has a crucial effect on the dependability of the solar PV application in which it is embedded (Daliento et al., 2017) but currently estimates put the lifetime of the solar energy conversion system at only 20-25 years as a result of a number of issues that remain outstanding. These include the growing role and complexity of the PEDs they contain (Iov and Blaabjerg, 2007) and current lack of knowledge about their failure mechanisms of converters despite the fact that the ability to analyse their reliability could play a key role in increasing the lifetime of solar energy systems and preventing permanent damage (Poller et al., 2012). Therefore, there is a need for non-intrusive, powerful and reliable monitoring techniques that can detect any potential failure at their early stage.

Unexpected failures in power semiconductor devices can bring a range of negative consequences depending on the situation. In an industrial context, this may lead to shutting-down the operation of an entire plant, thus bringing production to a halt. For the company concerned in a situation of this kind, in addition to paying for repairs to the system itself which can be enormous (Wu et al., 2014), an even more serious implication could be the massive loss of revenue resulting from this stoppage. In his analysis of the potential financial implications of a prolonged unscheduled interruption

to production, Eade (1998) calculated that these losses could be substantial, running into hundreds of thousands of pounds. Most worryingly, in other cases, the failure of a power semiconductor module may create a hazardous situation or lead to injury or even death. Ji et al. (2013) for example, reported that solder layer fatigue in IGBTs could potentially be one of the weakest parts in the traction drive of Electric Vehicle as their failure can result in a sudden breakdown of the power converter causing human lives to be put at risk.

In the last decades, a significant development has been made to the technology of power electronics and inverter types. Figure 2-4 illustrates the design of a modern RES-based power generation system, in which the power electronics device represents the core of the system. The central inverters were commonly used for most PV applications in the last few years (Gazis et al., 2010). In order to avoid amplification, the PV modules were linked into a series connection (strings), which generates an appropriate high voltage. To achieve the highest power level, these strings need to be connected in parallel via the string diode (Gazis et al., 2010). Many obstacles were encountered when using the central inverter including MPPT power losses and other losses which result from the difference between the high voltage DC cables and the modules from the PV arrays to the inverter. Initially, these inverters were applied using thyristors which resulted in low harmonic performance (Gazis et al., 2010). Currently, the string inverter is considered to be one of the most common inverter types, and by connecting one or two strings to each inverter, losses are substantially reduced (Kjaer et al., 2005).

Nowadays, the string inverters are obtainable in the range between 2-30 kilowatts peak (kWp), although until 2008 their maximum production did not exceed 5 kWp. In

PV panels, single phase string inverters were used to produce power up to 2MWp. Then, a leap in quality occurred after the development of the three phase string inverter which came onto the market in 2010. This product provides a simple design, electrical connections and produces a symmetrical power output (Gazis et al., 2010).

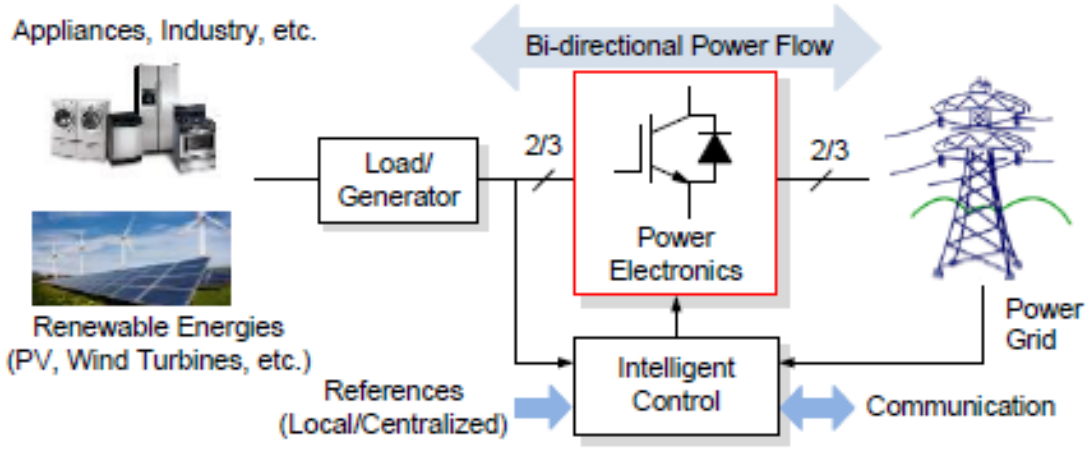

Figure 2-4 Advanced modern power electronics technologies and intelligent control techniques for RES and loads (Blaabjerg et al., 2011).

2.6.2 Transistor voltage regulators: IGBTs

Since the mid-1980s, IGBTs have become the leading devices in the power electronic areas in the power range higher than 1KW. IGBT manufacturers took advantage of the development of semiconductor technologies to reduce the cell size while trench gate technology further decreased chip size (Omura, 2010).

IGBTs have the potential to approach 500 A/cm^2 in the next decade if they are not replaced by new technologies. IGBTs also have the potential to significantly improve their performance, allowing them to compete with SiC devices in the high current range. The main benefits of IGBTs are not only their dramatic reduction in both cost

and chip size, but also the fact that parallel IGBT chips provide tens of kilowatt output in power inverters (Omura, 2010).

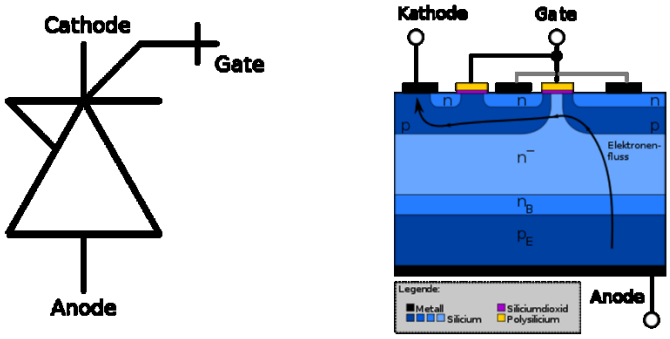

Figure 2-5 The IGBT system

In order to accomplish pulse width modulation (PWM) control efficiently for the inverter, two main devices have widely used as switching systems, namely, the IGBT (Figure 2-5) and the metal oxide semiconductor field effect transistor (MOSFET). In the inverter products surveyed here, 70% use IGBT and 30% MOSFET.

The switching frequency of IGBTs is about 20k Hz and it is possible to use them for large power capacity inverters higher than 100 kW. In contrast, although the MOSFET can achieve a higher switching frequency of around 800 kHz, its output power range capacity is between 1 kW -10 kW. Therefore, both IGBTs and MOSFETs can be used for power capacity between the range of 1-10 kW in the PV system while IGBTs are employed in large scale power plants with higher power capacity of about 100 kW. The harmonics in output current, size and weight of the inverter can be decreased using high frequency switching (Mohanty, 2014).

2.6.3 Reliability of power semiconductor devices

Given that non-functioning power semiconductor devices may cause potential implications in terms of downtime, financial losses and legal liability it is perhaps not surprising that more recently, interest has greatly increased in the issue of improving

the reliability of power semiconductor devices in terms of their material, fabrication, structure and design (Song and Wang, 2013; Wang, H. et al., 2013; Wu et al., 2013; Batunlu and Albarbar, 2015a; 2015b). In addition, research has addressed condition monitoring of power semiconductor modules in order to identify any significant changes that may indicate a developing fault or to provide early indications of imminent wear-out, which would enable replacements to be carried out (Musallam et al., 2008; Kärkkäinen and Silventoinen, 2013; Oh et al., 2015; Degrenne et al., 2015).

Kärkkäinen et al. (2014a: 6081) argue that the current problems caused by unexpected or catastrophic failures in power semiconductor devices could be significantly decreased by an appropriate and effective condition monitoring method but note that "a generally accepted and widely implemented method does not yet exist".

To date, an extensive variety of methods and techniques have been put forward for condition monitoring of PECs that would signal early warning of failure and the great majority of these previous attempts have chosen to focus on gathering data from electrical measurements of transistors (Anderson and Cox, 2011;. Wagenitz et al., 2012; Xiang et al., 2012; Ji et al., 2013; Zhou et al., 2013). In the case of IGBT power modules, studies have investigated saturation voltage for this purpose. The approach adopted by Anderson and Cox (2011) was to use an on-line condition-monitoring scheme for determin potential faults. They devised an algorithm based on principal components analysis that could be used to extract data about relevant features of these devices (including, for example, $V_{CE,ON}$ and $R_{DS,ON}$). They demonstrated that this could be compared to data values previously recorded from similar devices correctly functioning in a variety of operating conditions. Their on-line feature

extraction scheme, applicable to both IGBTs and MOSFETs, simplified the measurement process by exploiting the nature of carrier-based PWM.

Turn-off time has also been proposed as another possible failure indicator specifically for IGBTs. After reviewing the types of primary failure modes related to IGBT latch-up fault, Brown et al. (2012) studied the effects that occurred prior to these faults in IGBTs. Noting that elevated junction temperature led to a rise in IGBT turn-off time, they modelled the correlation between junction temperature and turn-off time. They were then able to derive a metric from this model and use it to standardize the estimated junction temperature based on measurements relating to turn-off time. Fault testing conducted in situ on a three-phase power inverter with aged transistors involved inducing a fault situated in the die-attach solder layer and demonstrated the feasibility of using this metric to predict IGBT latch-up.

Zhou et al. (2013) proposed identification of dynamic changes in gate current as a means of health monitoring and diagnosing failure inside an IGBT module. Their method works on the principle that elements inside IGBTs are affected by localised damage as they age. When an IGBT is about to wear out, these effects can be easily distinguished by measuring dynamic changes in the gate current. Their approach uses a relevance vector machine framework to provide accurate predictions, thus allowing operators to identify any failing IGBT modules and avoid breakdown by taking appropriate measures in a timely fashion. They were able to verify the applicability of their proposed method experimentally.

Mingxing et al. (2012) investigated the potential of using externally measurable characteristics related to changes in exterior electrical signals in IGBTs in order to

detect bond wire failure in these power modules. They demonstrated that during the turn off process prior to bond wire failure in an IGBT there are measurable changes in gate-emitter voltage, saturated collector-emitter voltage, collector-emitter voltage and collector current. They were able to validate their theory experimentally, using simulations and a test circuit.

However, all of these methods share a common drawback, namely, that a fast measurement must be carried out for every power transistor in the power semiconductor device (Kärkkäinen et al., 2014a). Kärkkäinen et al. (2014a) demonstrated that the switching transient in a power semiconductor module leads to an AE. They suggested that the wave propagates through the heat sink surface of the electronic module and can be determined by an acoustic sensor. Analysis revealed that the propagation delay of the observed acoustic signal increases as the distance from the source to the sensor increases. In subsequent investigations, Kärkkäinen et al. (2014b) confirmed that during switching periods, AE occurs within the electronic power devices and they also observed that the output voltage signal of an AE sensor is different from that of the transistor during the switching period. This prompted them to propose the idea that AE might be a suitable method for condition monitoring of PECs.

2.6.4 Failure mechanisms of IGBTs

In comparison to other converter components in renewable energy applications, research suggests that IGBTs are more vulnerable to earlier break-down (Busca et al., 2011) and that long-term exposure to high temperatures plays a role in this failure (Ribrant and Bertling, 2007). It has been calculated that over half of these failures are

induced by temperature (Lu et al., 2009). Moreover, this level of failure almost doubles for each 10 °C increase in temperature that occurs in the operating environment.

IGBTs are typically composed of a single or several semiconductor chips and their package, and both of these components are of equal importance in ensuring reliability and high performance. The IGBT is constructed of layers of bonded materials, which typically include silicon, ceramics, plastics and metals such as copper, tin and aluminium. These components are largely connected togehter by means of bond wires and soldering (see Figure 2-6). The IGBT assembly is covered with an insulating gel and enclosed in a polymer housing so that only the metal connectors of the terminals of the device protrude. The baseplate of the IGBT is mounted onto a heat sink or other cooling device. Thermal interface material is greased between them to enhance thermal contact.

The materials from which the IGBT is assembled may display very different electrical, thermal and mechanical properties. In addition, package designs can also vary in terms of their layout, geometry and size. It is worth noting that like other power modules, IGBTs are manufactured with less silicon area in an attempt by the industry to reduce costs and this results in higher power density. Manufacturers also attempt to integrate the power semiconductor in a common substrate (a direct copper bonding substrate) using bond-wire connectors as a method of increasing power density within the circuit (Ji et al., 2015).

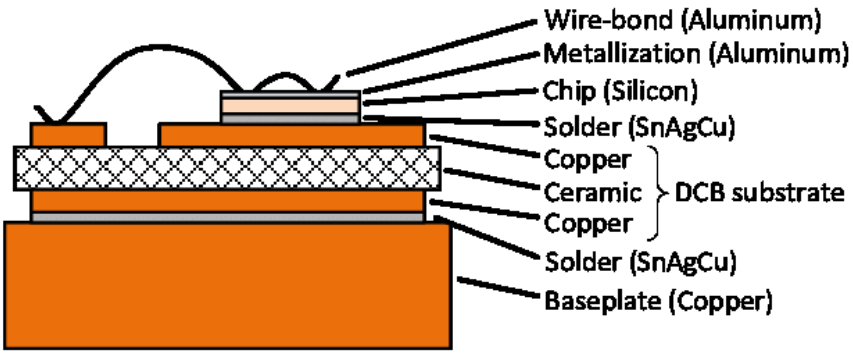

Figure 2-6: Cross-section of layers of IGBT module (Bahman, 2015)

When the IGBT is in operation, heat flux is transferred from the die chip to the cooling system via different heat paths and fluctuations in temperature are generated within these layers as a result of cyclic temperature swings and exposure to extreme temperatures. In practice, IGBTs face harsh operational conditions given that they must function at high temperature, undergo frequent temperature cycles and also intensive vibrations. Since these bonded materials possess different coefficients of thermal expansion (Lutz et al., 2011), this mismatch can lead to the creation of fatigue in particular locations within the IGBT. The introduction of these stressors to the system may seriously impact on the reliability of the entire device. Lab-based aging tests conducted by different researchers concluded that typically the dominant wear-out mechanisms responsible for the eventual occurrence of failure in these power modules are bond wire lift-off, together with die-attach and baseplate solder fatigue (Bi et al., 2015). As it relates to bond wire, lift-off is usually the result of temperature swings and the large coefficient of thermal expansion (CTE) mismatch between aluminium bond wires (24 ppm/^{o}C) and the silicon die (30-300 ppm/^{o}C) (Ji et al., 2013). Solder fatigue/cracking usually occurs because plastic deformation of the layers of solder occurs when these are subjected to temperature cycling loads. The CTE mismatch between the different bonded materials (ceramic and copper) causes

temperature swings which induce thermo-mechanical stresses in the module. This becomes crucial at the interfaces of the assembled layers (Ji et al., 2015). Moreover, if one component fails within a power electronics module, this may lead to over-voltage stress on other switching devices, increasing the likelihood of further faults arising as the current density in the remaining contacts continues to rise towards a critical value (Gorecki, 2013).

2.7 Acoustics of semiconductor devices

Until the initial observations published by Kärkkäinen et al (2014a) that formed part of his doctoral work (Kärkkäinen, 2015), work in the field had been limited to analysing fault progression in power semiconductor devices using acoustic microscopy (Moore and Frank, 1995; Haque et al., 2000) together with Smulko et al.'s (2011) more recent research on capacitors and Stumberger et al.'s (2013) work on acoustic noise emissions from a transformer in a DC-DC converter. Kärkkäinen's work with wind turbines points to the potential for the development of AE as a condition monitoring tool for use with solar PV systems.

As well as enhancing the durability and reliability of power converter components, there is also considerable interest in developing a system that would be capable of actively monitoring these components with the aim of alerting the user when failure is likely to occur. To date, various failure prediction systems based on thermal and/or electrical measurement have been trialled (Anderson and Cox, 2011; Brown et al., 2012; Ji et al., 2013; Wagenitz et al., 2012; Xiang et al., 2012 ; Zhou et al., 2012). More recently, experiments have been carried out using sensors readily available on the market with the aim of establishing if AE from components might be a better way of predicting component failure (Kärkkäinen et al. 2014a; 2014b; 2015a; 2015b).

However, there are a number of drawbacks to running tests with this type of sensor, even if it is intended to be used as an AE sensor. Some of these sensors can be sensitive to the displacement of the surface they are supposed to measure; others may be sensitive to the displacement velocity. In addition, sensors which are typically employed to capture AEs from gases (including air) are pressure sensitive. Moreover, taking these measurements requires extremely fast electromagnetic and electrical transients as a result not only of the switching operation and the high temperatures involved, but also due to the as yet unknown nature of the phenomena under investigation.

Kärkkäinen et al. (2014a; 2014b) were interested in addressing some of the limitations that currently prevent greater exploitation of AE. Findings from their experiments on power modules suggest that AE occurs due to semiconductor switching somewhere within the power module, but the precise mechanism that causes this AE remains unknown. It is thought that electromagnetic interaction between the various components in the power module may be caused by the fast switching transients producing a magnetic force within this module. However, since a force of this nature would only exist for tens of nanoseconds during the switching transient, it has not yet proved possible to test this hypothesis. It is this gap in current knowledge that represents the basis for this study and the methodology employed within measuring the on/off power frequency will determine this interaction.

In their experiments, Kärkkäinen et al. (2015a) recorded the acoustic propagation delays that occurred to different locations in the test module and discovered that the duration of these delays lengthened as the distance to the test module increased. Having determined that the most likely source of AE in the experimental set up was

the test module itself, they then carried out tests using the same device in an identical measurement setup, but this time incorporated two different AE sensors. Whilst the propagation delay remained consistent in both of the tests they performed, the waveforms were found to differ significantly. This implied that the signal they had observed had been affected by the sensors. These sensor effects also help to highlight the difference recorded between the two sensors. Although both sensors show that an acoustic event takes place, and that the results of the propagation delay analysis indicate that the power module is the likely source of this, neither of the sensors actually provides a 'true' illustration of the acoustic phenomenon that occurs. It is unclear whether other analyses, such as frequency content, would yield more reliable results due to the difficulty of knowing whether the data obtained actually represents the system itself or the acoustic source.

Another experiment aimed to determine what type of AE occurs when semiconductor components fail. Thus, initially the semiconductor components in an IGBT were heated until they failure occurred (Kärkkäinen et al., 2015b) and at the same time, the transistors and acoustic events were monitored. A similar experiment was repeated using a device under test (DUT) connected to the AE sensor by means of a piece of sheet metal. This was intended to allow the acoustic waves to propagate from the DUT to the sensor. Unfortunately, using this metal sheet means that any heat produced within the DUT is able to reach the sensor. Since the sensor in the experimental setup was not designed for temperatures over 60°C, the heat generated by the metal sheet proved problematic.

Results showed that when the DUT temperature is rapidly increased, the amount of thermal energy produced from the system is smaller than if the temperature is

increased gradually. When the thermal energy total decreased, the increase in temperature at the sensor also decreased. Thus, a current was passed through the DUT to heat it up while the DUT remained in the active region.

Although this experiment may be criticised on the grounds that the DUT was not intended to be used in this way by the manufacturer, it proved to be the easiest method of achieving a result. The key point observed in this study was that two types of AE can be observed under these circumstances. The first acoustic event (immediate emission) occurs when the semiconductor fails; the second (the post-failure emission) takes place just tens of milliseconds after but these two types of AEs can be clearly distinguished.

When these three AE types are compared (Figure 2-7), it is evident that the failure-related AE closely resembles the switching-related AE. The post-failure AE, however, is totally unlike the other two types of AE because it does not appear to contain any components that suggest resonance. The oscillation that is visible in the immediate emission attenuates more quickly than the oscillation produced by the switching related emission. These results suggest that even where resonance might be present within the sensor, it does dominate the measurement.

Efforts were made to separate the sensor from the heat source in these tests using thermal shielding gel but results showed that this was not successful since the water contained within this gel quickly vaporises. It was thought that this heat problem might be solved by using a laser doppler vibrometer to provide a contactless measurement. However, when a test was carried out, the vibrometer was unable to pick up any signal from the test setup.

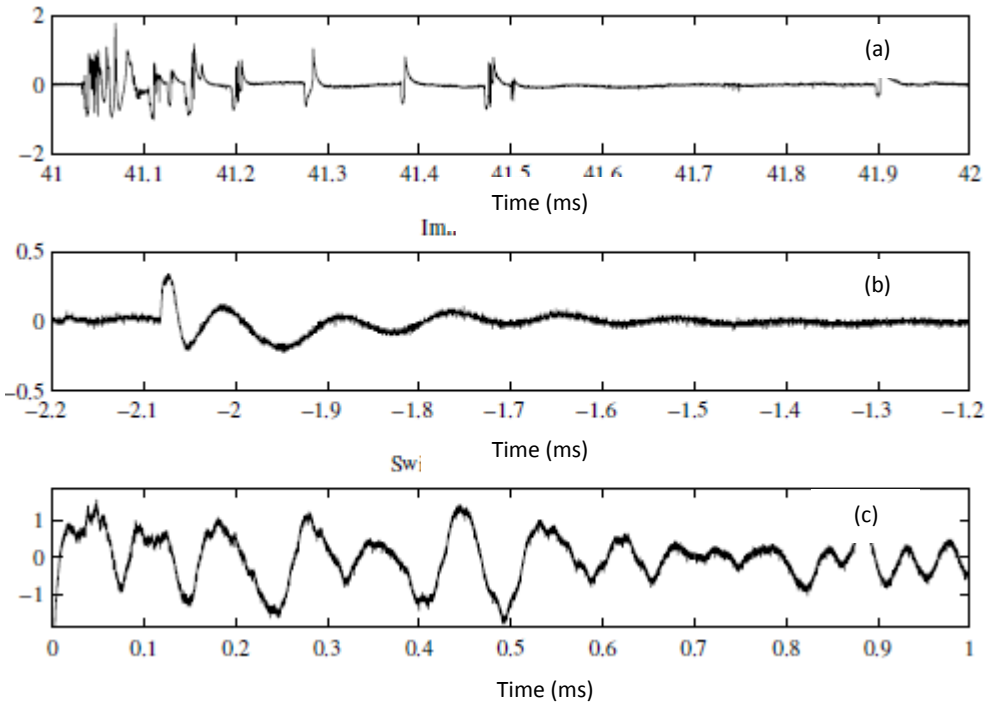

Figure 2-7: Comparison of three AE types: (a) Post-failure emission, (b) Immediate emission, (c) Switching-related emission (Kärkkäinen et al., 2015b)

2.8 Summary

Failure or breakdown of PEDs/PECs is one of the most frequent causes of problems with the PV solar energy systems. The research presented in this literature review has highlighted that the reliability of PEDs and PECs has the greatest potential to affect the overall lifetime of renewable energy systems. Moreover, condition monitoring can be used as a technique to provide an effective means of predicting the adverse effects they are likely to create. To date, a number of solutions have been proposed for facilitating effective condition monitoring of PECs that would address this problem and a range of disparate techniques have been proposed in the literature to extend the reliability of these devices. However, no single generally accepted method exists since all have shortcomings. Recent research focusing on PECs in wind turbines has suggested that techniques using acoustic emissions (AE) might provide a useful solution to condition monitoring of these semiconductors devices.

As previously mentioned in section 1.8 (see page 25), it is envisaged that this research will provide a valuable contribution to this field by, firstly, providing a viable alternative to existing methods for troubleshooting PEDs (IGBT) failure. Secondly, being able to determine the cause of IGBT quickly with greater accuracy than prevailing methods; thirdly, diagnosing and resolving faults more quickly since the diagnosis or reasons for failure will already be known, and; finally, being able to determine the most suitable places and/or environments for effective use of AE.

3 Modelling of Photovoltaic Solar Systems

3.1 Overview

This chapter focuses on the modelling of PV solar systems. It begins by providing a brief overview of modelling techniques and then provides a detailed structural description of PV solar systems. Having established the structure of these systems, a component-level analysis of the design and modelling of these systems follows. This will include a discussion of the PEDs that are crucial in maximising the efficient operation of these systems.

3.2 Modelling techniques for PV solar power systems

The decrease in the cost of PV cells and the subsequent increase in interest in solar PV energy systems had led to the development of numerous sizing and simulation software tools for commercial use (see, for example, photovoltaic-software.com) intended to offer quick analysis of system behaviour and suggest potential improvements to design. Software tools designed for academic purposes include TRNSYS (Transient System Simulation Tool), WATSUN, Polysun and PVSYST which allow for more sophisticated calculations simulating long-term performance of systems and a broad range of variables (Kalogirou, 2013).

Modelling a PV solar power system is a useful means of observing the behaviour of a range of variables including temperature, power, etc. for different input parameters with the primary goal/objective of optimizing system performance. However, modelling the components of a PV solar system to a high degree of accuracy is a complex issue since it involves unpredictable parameters such as weather data including levels of solar irradiation, temperature and shading. All of these factors can

impact on the functioning of a solar array. Moreover, software tools do not usually consider non-ideality and non-linearities of PV modules as they are based on manufacturer's specifications obtained in standard testing conditions (STC). Mathematical models are very complex and need expertise, skill and careful handling.

3.3 PV solar power system components

As shown in Chapter One, various configurations can be employed for solar PV power systems. Stand-alone systems generally supply power to remote, off-grid areas while utility-Interactive/grid-connected systems are connected to the power grid and operate in parallel with this, allowing any surplus electricity which has not been utilised by the household to be fed into the utility grid so that it is not wasted. Hybrid systems, as their name suggests, incorporate an energy source other than the solar PV cell array, for example, a wind-operated or micro-hydroelectric turbine. In this chapter, the focus is on the components that make up a fully operational stand-alone PV power system.

3.3.1 PV array

The PV array which may consist of hundreds of individual PV cells is the crucial component of any stand-alone PV system, as it converts sun photons into electricity. Each solar PV power cells consists of a p-n junction fabricated in a thin layer of semiconductor material, usually silicon. Figure 3-1 shows schematic diagram of the stages of forming solar cells to the PV system.

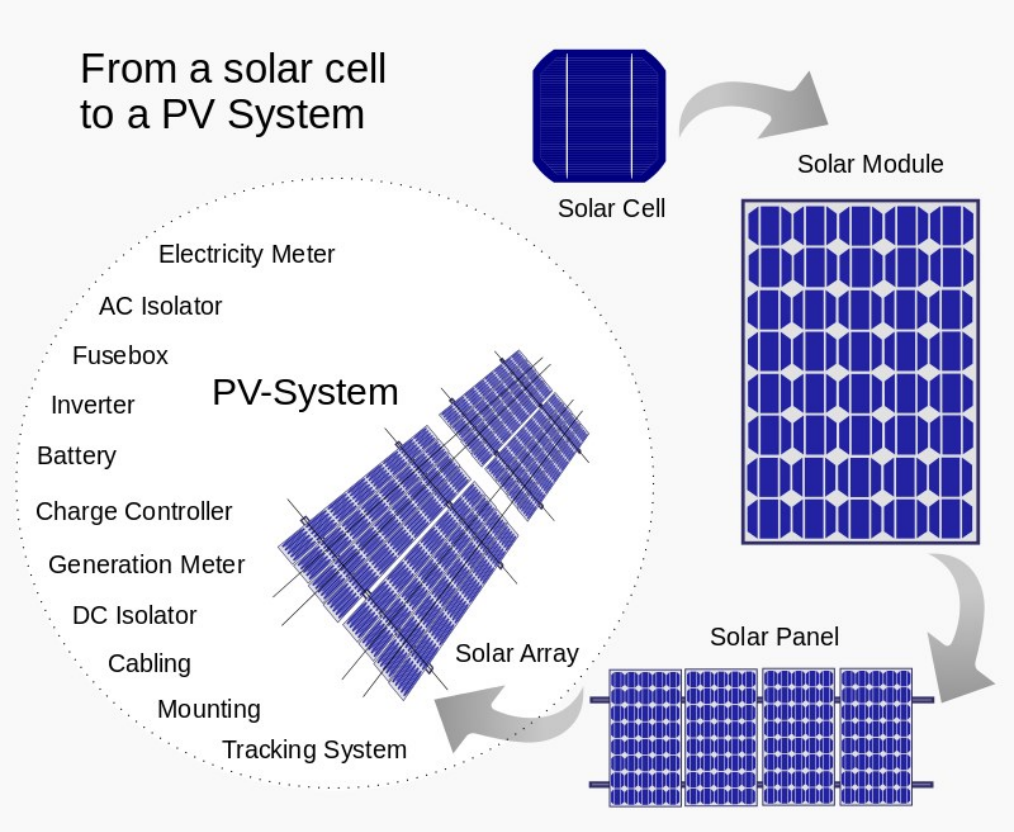

Figure 3-1: A solar PV array (Source: Miguel, 2008)

The PV array system can be classified into silicon and non-silicon based semi-conductor solar cells as shown in Figure 3-2. The main reason of this wide classification is that silicon-based solar cells which typically include monocrystalline silicon, polycrystalline silicon and amorphous silicon control approximately 90% of the PV market worldwide for both solar farm systems and individual PV systems on the roof of buildings. Solar cells based on silicon material are more stable and efficient and can deliver high performance for a long lifetime.

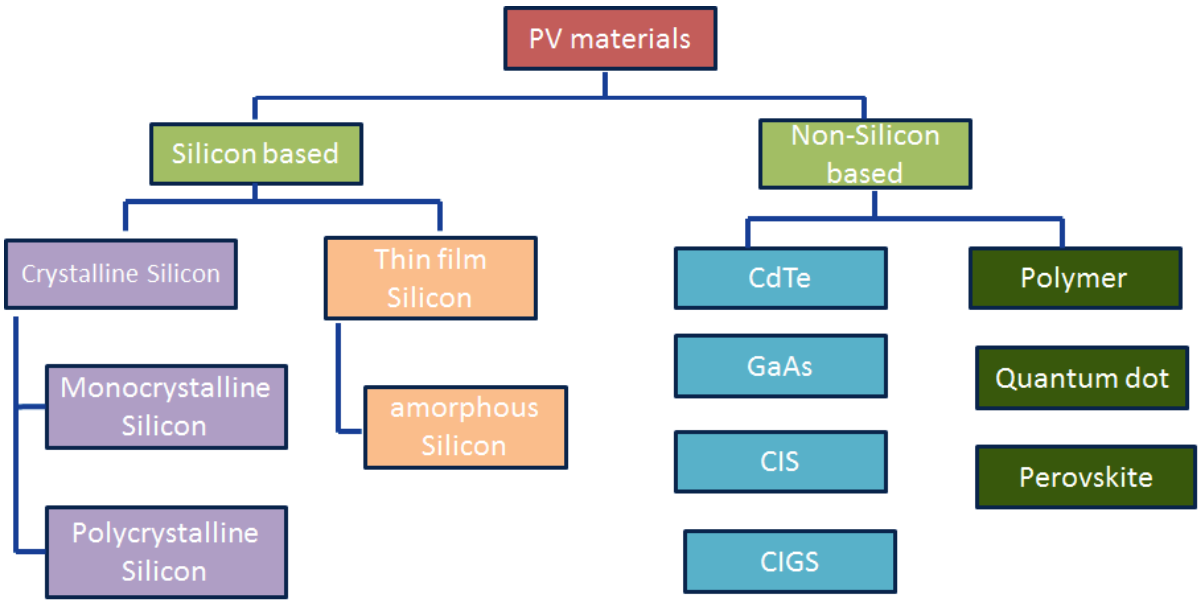

Figure 3-2 Different materials used to fabricate PV solar cells.

Non-silicon-based materials represent the second and third generation of solar cells. The second generation include cadmium telluride (CdTe), copper-indium-selenide ($CuInSe_2$ or CIS) and copper-indium-gallium-selenide ($CuInGaSe_2$ or CIGS). The solar cells based on these materials are expensive and cannot currently compete with silicon-based solar cells. Recently, third-generation materials based on thin film semi-conductor materials have emerged and these might have the potential to compete with silicon-based materials in the future. These materials are inexpensive, simple, widely available, and easy to fabricate using solution-processed methods such as the roll-to-roll method similar to the technology employed for printing newspaper.

These materials include polymer, quantum dot and, most recently, perovskite. Of these materials, perovskite-based solar cells have the most promising properties to date. However, these third-generation materials are still at the development stage and may take a long time before they are commercially viable.

Table 3-1 Efficiency levels of different types of PV panels

TYPE	CELL CONVERSION EFFICIENCY	MODULE CONVERSION EFFICIENCY
Monocrystalline silicon	25%	16-18%
Polycrystalline silicon	21%	14-16%
Amorphous silicon	13.6%	10%
Cadmium telluride (CdTe)	22%	9-12%
Perovskite	22%	N/A
Group III-V Technologies (e.g. GaAs)	25%	N/A
CIGS	22%	8-14%

When solar radiation, in the form of sunlight, strikes a solar cell, photons with an energy exceeding that of the band-gap energy of the semiconductor material produce some electron hole pairs creating an electric field across the layers (Lorenz, 1994). Consequently, the influence of the p-n junction's internal electrical fields, these carriers are driven apart, creating a photocurrent which is directly proportional to the solar radiation. The stronger the sunshine, the more electricity is produced. During daylight hours, a solar PV power cell produces non-linear output characteristics (I-V and P-V), which vary in accordance with the amount of solar radiation and the temperature of the cell. At night-time, solar PV power cells are not active, functioning like diodes (Walker, 2001).

PV cells are produced in a range of shapes, sizes, structures and semiconductor materials, but silicon-based material is the most widely used. The power output of a typical PV cell is usually approximately 2W at 0.5V (Miguel, 2008). Therefore, to increase their power output, groups of PV cells are usually mounted together and connected using a series-parallel configuration to form a module or panel. In PV solar

power systems, groups of these modules are typically connected in series to begin with, and then individual strings are connected in parallel circuits to form an array which can produce the necessary voltage and amperage required by a particular system to meet a residential power requirements (Miro, 2014). In terms of size, an array could be similar to a single pair of modules, or sufficiently large to encompass acres of ground. The power of a PV cell is measured in kilowatts peak (kWp) which refers to the rate of energy is generated during peak performance in full direct sunlight during the summer. As Table 3-2 shows, the cell's ideal factor (*F*) is dependent on the semiconductor material used in fabrication while

Table 3-1 shows the efficiency levels for different types of solar panels.

Table 3-2 Ideal factor (*F*) for different solar PV power cell technologies

SOLAR PV POWER CELL MATERIAL	IDEAL FACTOR (*F*)
Si-poly	1.3
Si-mono	1.2
a-Si-triple	5
a-Si:tandem	3.3
a-Si:H	1.8
CdTe	1.5
CIS	1.5

A 12-volt module is the industry benchmark for battery charging and this is acceptable for systems processing up to about 2000 watt-hours. Systems processing 2000-7000 watt-hours ted to operate more effectively at 24 volts, whereas those running over 7000 watt-hours should ideally operate at 48 volts.

3.3.2 Storage unit (battery system)

PV systems cannot store electricity; thus, batteries are used in conjunction with stand-alone systems. Figure 3-3 illustrates an electrical equivalent circuit of a battery. The PV system supplies the load during the high solar radiation hours in daylight with surplus electric energy being stored in the battery. When there is reduced solar radiation or at night time, the storage batteries are used to supply the load whenever needed. A PV system with a battery is configured by connecting the PV array to a module inverter. The inverter is connected to the battery bank and to any AC loads.

A battery is an electrochemical cell, which is able to hold electrical energy as chemical energy. The battery size required in a PV solar power system is determined by the kind of the battery and the maximum amount of energy required for storage. Batteries forming part of a stand-alone system need appropriate storage to avoid humidity, have to be routinely maintained and typically need changing at approximately every eight year interval (Layadi et al., 2015).

Two key concepts are relevant to a battery, namely, depth of discharge (DOD) and state of charge (SOC). DOD refers to the maximum amount of output energy that can be extracted from a battery for a particular application while SOC refers to the amount of charge energy remaining in the battery. Every battery has a different DOD rating which depends on its chemical composition and type.

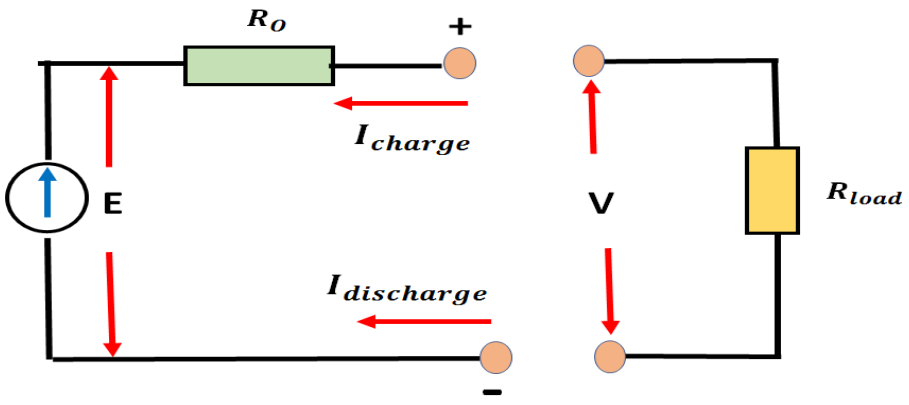

Figure 3-3 Schematic diagram of the battery [adopted from Layadi et al., 2015].

It is preferable not to discharge energy below the DOD level specified for a battery as this will have a detrimental effect on battery life, decreasing the number of charge-discharge cycles. Once fully charged, a battery has 100% energy. Deep discharge lead-acid batteries which have a DOD of up to 80%.are recommended for use in stand-alone PV power systems because of their high performance (Assad, 2010).

In addition, another important concept relevant to the battery is nominal capacity, which is defined as the number of amperes per hour which is produced maximally from the batteries. Battery efficiency is represented by the ratio between the charge extracted during discharge and the amount of charge required to restore the optimal state of charge (Hansen et al., 2000).

The lifetime of the rechargeable battery is specified as the number of charge-discharge cycles the battery can maintain prior to losing 20% from its initial capacity (Hansen et al., 2000). However, this specification is only valid if the charging and discharging currents are well below the rated value, highlighting the importance of the charge controller to cost-effective running of this component in the PV solar power system.

3.3.3 Charge controller modules

The charge controller, also referred to as the voltage regulator, is another vital component of the PV solar power system. It can be thought of as the brain of the system as it organises the power flow between the main components of the stand-alone system (i.e. the PV generator and storage batteries) and the load. It ensures the battery bank is fully charged and by regulating the system voltage to the specified range it prolongs battery life by protecting it from being overcharged or completely discharged while preventing any reverse current flow as a result of over discharge. As previously noted, recharging generally takes place during the hours of darkness (Energypedia, 2014).

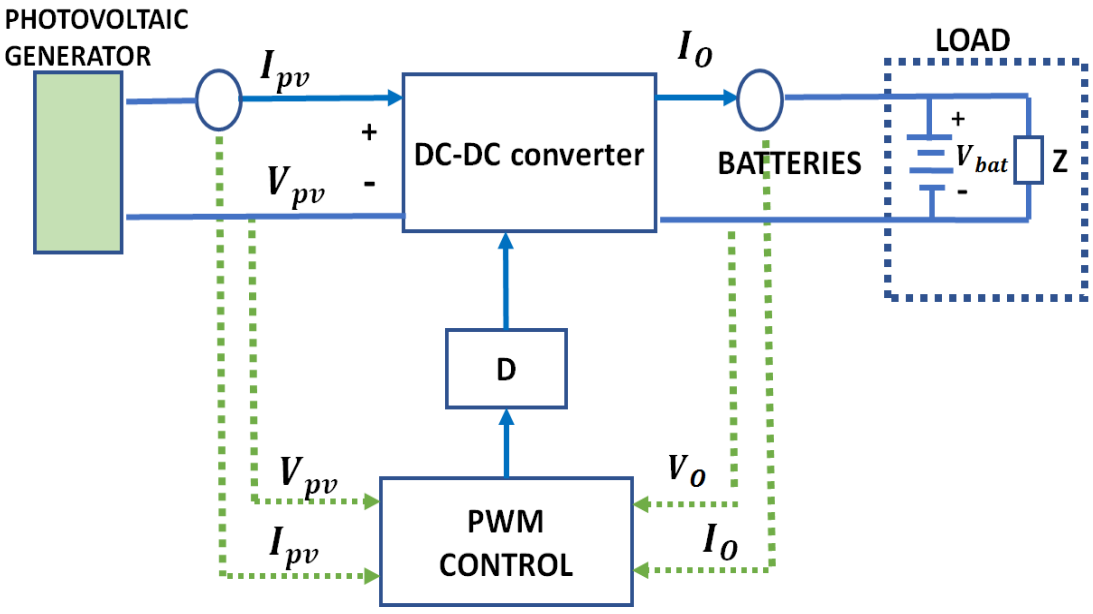

Figure 3-4 General block diagram of a stand-alone PV system with MPPT

Inserting the DC-DC converter between the PV arrays and the batteries is an important method of overcoming any undesired impact on the output power and achieving maximum performance. The importance of these DC-DC converters lies in seeking the maximum power point in addition to other typical functions of the converters which are determined by the controllers. These converters are usually known as maximum

power point trackers (MPPTs) (Salas et al. 2006). Figure 3-4 shows a block diagram of a stand-alone PV system with MPPT.

Typically, the two principal kinds of charge controllers widely utilised in current PV solar power systems include PWM and MPPT. Each of these techniques has its own appropriate specific function for monitoring the charge status of the battery when the difference results from the charging mode. Both types regulate charging rates based on the battery's charge level to enable charging at an optimal level which is nearer to maximum capacity and also to monitor the temperature of the battery in order to prevent overheating. Furthermore, the major function of the MPPT in the PV system is to operate the PV generator at its maximum power and to extract the maximum obtainable power.

3.3.4 Power conditioning system (PCS)

The PCS processes and controls the flow of electrical energy efficiently, so that it can optimally suit the load requirements. PECs form a key part of the PV system architecture and power semiconductor devices are fundamental components in determining the efficacy of PECs for power conditioning. They play a significant role in converting the disparate kinds of electricity, in order to benefit end users. Since the solar cell produces a DC-type of electricity, various types of power electronic converters are needed. Inverters transform the direct current (DC) power coming from the solar PV array into an alternating current (AC) which is then ready to be connected to the load. The inverter, sometimes referred to as a module-level power converter, also ensures the optimum usage of the PV generator, i.e. the MPPT (Femia et al., 2013), modifies the power to maintain the required power factor, and protects the grid-interface against unexpected events (Ruiz et al., 2011; Kjaer et al., 2005).

An inverter is vital in helping to meet load requirements. If the inverter is connected directly to the PV panels, it has to mirror their PV voltage and input current. Solar inverters are sized to work with the highest possible average efficiency to ensure that the total energy output is as high as possible. When PV solar power systems are installed in regions with lower irradiance levels, inverters are undersized to move the peak efficiency of the curve to an output power facilitating maximum energy gain. In sunny regions, conversely, inverters are oversized to accomplish the same purpose.

The total energy output of a PV solar power system is determined by the number of PV panels connected per inverter. In the cheapest systems, only one central inverter is connected to all PV panels. Figure 3-5A shows a central inverter that connects PV modules to the grid in series known as strings. These series connections are linked in parallel via string diodes to a single central inverter to obtain a high power output between 10-250 kw (Hassaine et al. 2014). If each panel has its own inverter (referred to as a microinverter or module inverter) then every panel can work at the maximum power point. One of the major benefits of using central inverters is the high efficiency and the reduction in cost owing to usage of a single inverter. However various limitations have been found when using this central inverter including losses in string diodes, power losses due to the centralized MPPT and high voltage DC cables are required between the PV modules and the inverter (Hassaine et al., 2014). Failure in the central inverter can cause the entire PV system to cease operating (Nazeer et al., 2017).

Using string inverters is another possibility that can be used for coping with the shading of panels which can reduce output (see Figure 3-5B). Shading analysis is carried out to configure how the string inverter should be used to connect to several

PV panels experiencing similar levels of shading, thus improving the efficiency of the whole system. Lee and Raichle (2011) found that under partial shading conditions, a system with microinverters produces 26% more power on average in comparison to a PV system employing a central inverter. Multiple MPPT systems can maximise power yield for a PV solar power system, even if part of the array is shaded.

In this type of the inverter, each individual string of PV modules is linked to a separate inverter resulting in no loss of power related to the string diodes (Kjaer et al., 2005). Using the string inverter, the MPPT can be utilized for every string which leads to increased output efficiency of the PV modules compared to the PV modules with the central inverter and also reduces the cost as a result of mass production (Nazeer et al., 2017).

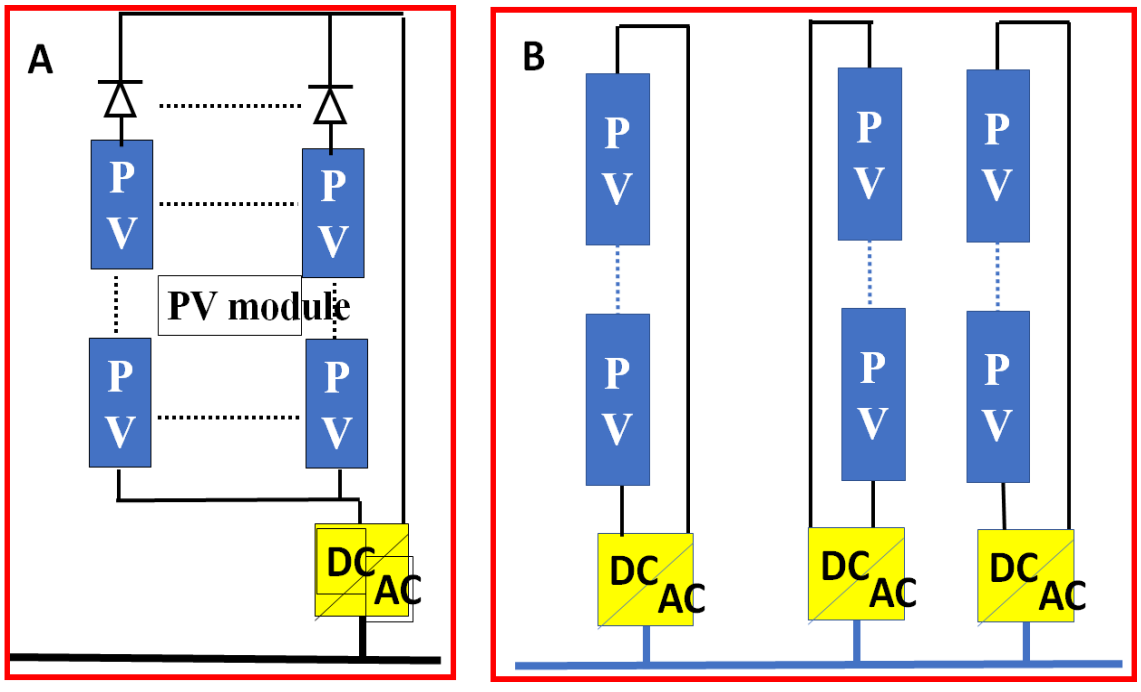

Figure 3-5 A=central inverter, B=string inverter

As with the charge controller, the inverter is too equipped with MPPT electronic technology which is capable of detecting the maximum power point for each module.

The point of maximum power output of a solar PV cell can be determined by a mixture of current or voltage. Where this is situated is likely to fluctuate constantly based on environmental factors such as irradiance, light levels, shading, temperature and the characteristics of the solar PV panel. A MPPT system constantly looks for this point to obtain the maximum power available from the cell. Two MPPT tracking algorithms, incremental conductance (IC) and perturb and observe (P&O), are used for this purpose.

3.3.4.1 DC-DC boost converter

Usually, DC-DC power converter devices are utilised to alter the output voltage from any level in the PV system to any other level. Figure 3-6 illustrates typical renewable energy system with a DC–DC converter. In order to produce the available power from the PV arrays using the tracking method, the DC-DC converters are connected between the PV arrays and the load. The popular DC-DC converters which typically used for power conversion are: boost converters, buck converters and buck boost converters. In these systems, the DC-DC converters are converted with the maximum power operating and the power generated from the PV system (Rajesh and Mabel, 2015).

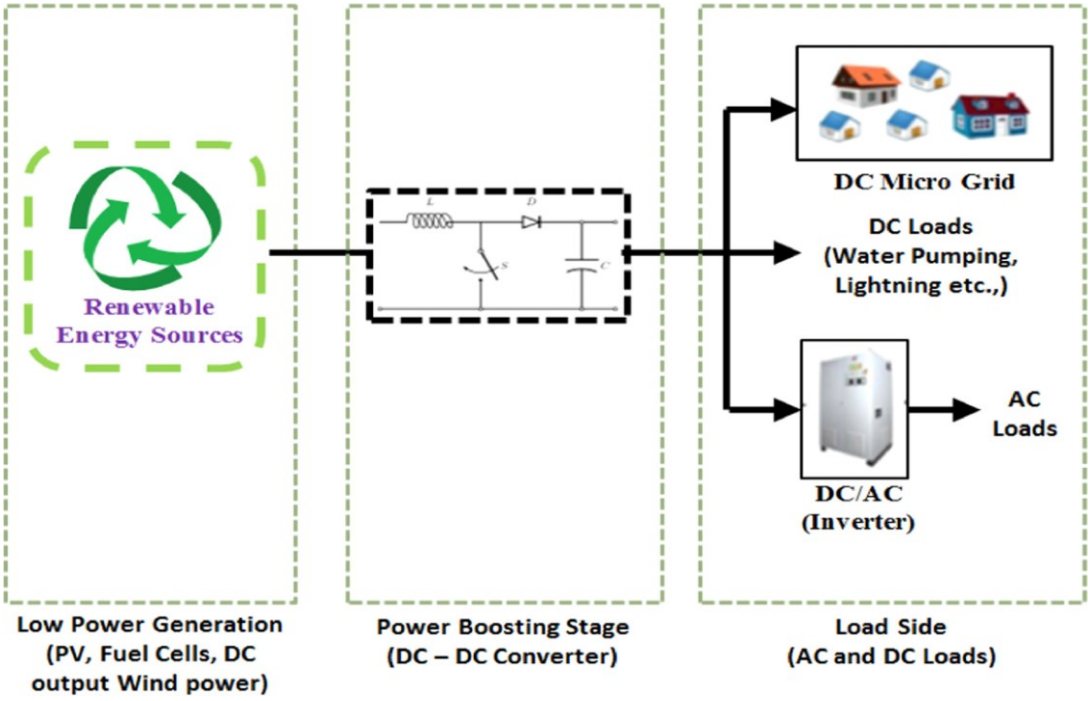

Figure 3-6 Circuit diagram of DC–DC boost converter [Rajesh and Mabel, 2015]

3.3.4.2 DC-DC boost converters modelling

There are numerous kinds of DC-DC converters. Generally speaking, they can be categorised into: step-down and step-up (boost converter) or a mixture of both these types. They are extensively employed in energy conditioning in fuel cell systems and MPPT to maximize the electric energy obtained from solar energy applications. The converter accepts a DC input voltage, producing a DC output voltage in those cases where the output voltage produced differs to the input. Some of the key parameters utilised in the converters incorporate silicon-controlled rectifiers (SCR), gate turn-off thyristors (GTOs), MOSFETs and IGBTs. The latter is used as a switching element in PECs in high switching frequency and current-voltage rating applications.

A boost converter is an electronic circuit that converts a DC source from a low to a higher voltage level. The principal boost converter components are the switching device (IGBT or MOSFET), power diode, inductor and input/output ripple capacitors.

Figure 3-7 shows a common schematic circuit of a boost converter in which the switching device takes the form of an IGBT as this is preferred for high power levels.

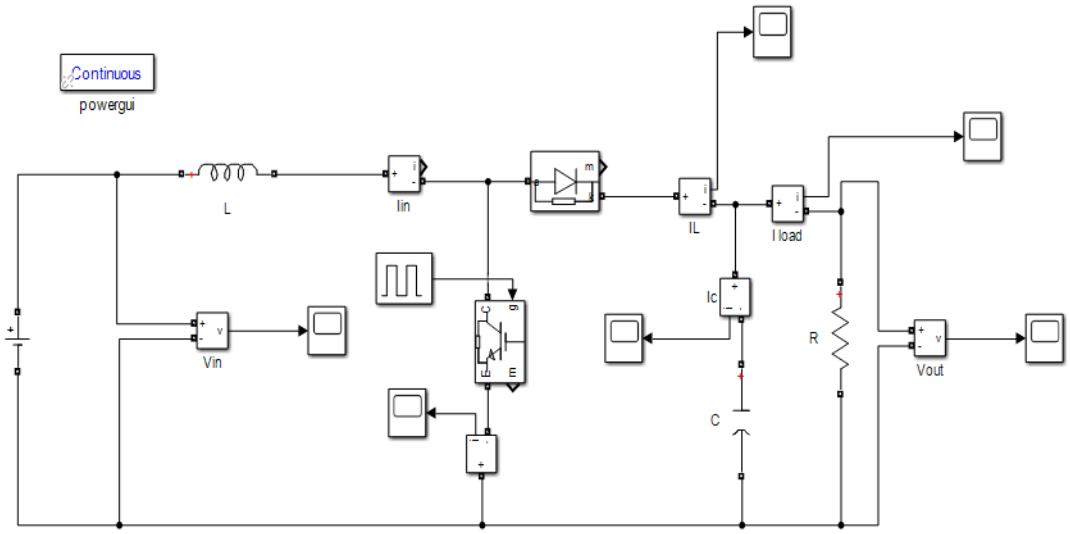

Figure 3-7: IGBT in DC-DC boost converter

MATLAB and SIMULINK:

The simulation circuit diagram illustrated in Figure 3-7 was created by utilising MATLAB software (Bonkoungou et al., 2013). The circuit used comprised: an IGBT, inductor, diode, capacitor and load. In terms of parameters, the input voltage was denoted by V_i and was constant at a value of 5V. As for the Output voltage(V_o) in the circuit, this was connected to the VPV connector and illustrated the output voltage of the boost converter. Initially the voltage increased rapidly up to 9V finally dropping and stabilising around 7.7V as shown in Figure 3.8.

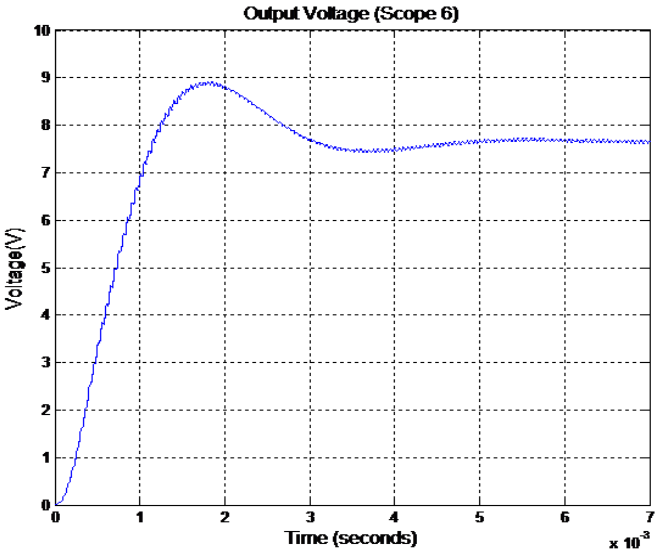

3-8: The output voltage of the boost converter

As for the other parameters, the Pulse Width Modulation (PWM) operates at a 50% level of the duty cycle and is calculated based on the size of the pulse divided by the period multiplied by 100. The IGBT emitter current increased spontaneously to reach a maximum value of 1.47A, then decreased rapidly to 0.39A, finally stabilising at 0.56A.

Figure 3.9 shows the emitter current of the IGBT which has the same variation shape as the collector current.

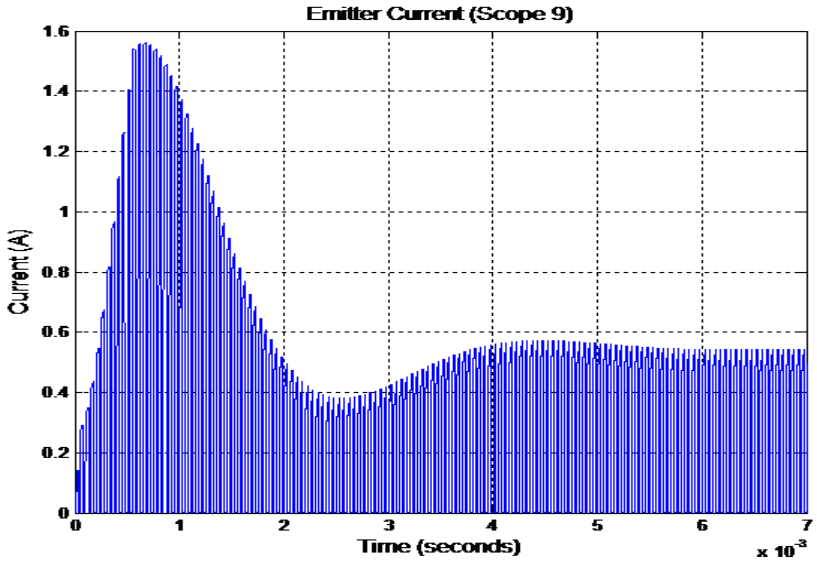

Figure 3-9 The variation in the IGBT current emitter

Based on the above mentioned data, it was concluded that the results of the simulation revealed that the simulated boost converter worked correctly and that the data obtained concurred with that which had been found experimentally.

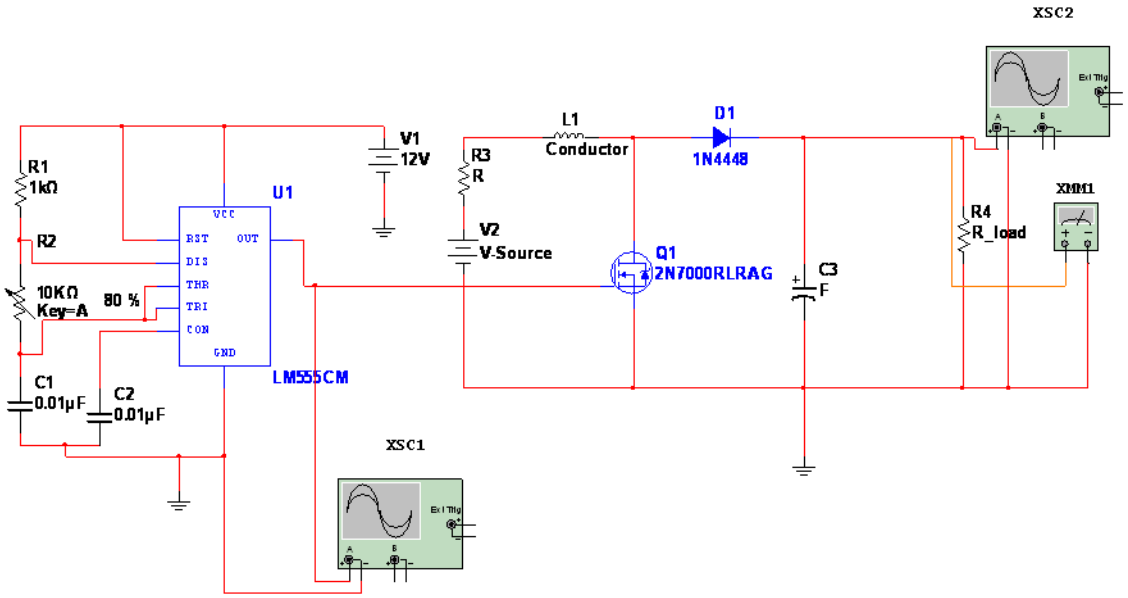

Figure 3-10 IGBT Block diagram for DC-DC Boost converter

Figure 3-10 demonstrates the direct control technique used for boost converters, highlighting the block model of the controller.

Figure 3-10 was used in order to provide a detailed explanation for the components contained in figure 3.7. Figure 3.10 represents two circuits : the one on the left being the control device, with the one on the right hand side representing the boost device. The gate, inductor, diode, capacitor and the load are the components of the first part. The second part is the controller device, which includes the boost output voltage signal, a desired output voltage, hysteresis controller, a constant switching source, and a second gate controller. The parameters that were investigated using this block diagram consisted of output voltage, current and output frequency at different loads.

Since the IGBT is most commonly used for the purposes of switching, it is important to fully understand the conduction mode (on-state) or the cut-off mode (off-state) (see Figure 3-11a). During the on-state the semi-conductive switch is conducting and current builds up in the inductor producing an electromagnetic field that is able to store energy. In this state, the switch (S) is closed, producing an increase in the inductor current (see Figure 3-11 below). The IGBT's on- and off-states are regulated by appropriately designed gating circuits which activate and deactivate the gate terminal. Where a positive input voltage signal across the gate and the emitter is applied the device will remain in an on state, while contrastingly, a zero or slightly negative input gate will result in an off state.

During the off-state, the semi-conductive switch is not conducting which leads to a collapse of the electromagnetic field. In this scenario, the switch is open (Figure 3-11c) with the sole path to the inductor current being offered via the flyback diode (D), capacitor (*C*) and the load (*R*). This leads to a transfer of energy into the capacitor, which will have accumulated during the on-state.

Where the field collapses, any energy stored does not escape through the semi-conductive switch; rather, it passes through the diode and into the load/capacitor at a far higher voltage. This happens several thousand times per second via the pulses delivered by a timing circuit, enabling the charge of a high-voltage capacitor from a low-voltage source.

For a boost converter running on continuous mode, the current passed via the inductor will never drop to zero. During the on-state, the switch (*S*) is closed, making the input voltage (V) appear across the inductor, causing the current (*I*) that flows

through the inductor to alter during a time period (t), which can be expressed formulaically as illustrated in equation 3.1:

$$\frac{\Delta \boldsymbol{I_L}}{\Delta_{\boldsymbol{t}}} = \frac{\boldsymbol{V_i}}{\boldsymbol{L}} \quad (3\text{-}1)$$

At the end of the on-state, the increase in current (I) is represented by equation 3.2:

$$\Delta I_{L_{On}} = \frac{1}{L}\int_0^{DT} V_i dt = \frac{DT}{L} V_i \quad (3\text{-}2)$$

This formula shows that the variation of the inductor current (I) is determined by the inductance (L), the duty cycle (*D*), the period (*T*) and the input voltage (*V*).

During the off-state (Figure 3-11c), the switch (*S*) is open, which results in the inductor current (I) flowing through the load, as given by equation 3.3.

$$V_i - V_o = L\frac{dI_L}{dt} \quad (3\text{-}3)$$

Therefore, the variation of the current (I) during the off-state can be represented as follows:

$$\Delta I_{Loff} = \int_{DT}^{T} \frac{(V_i - V_o)dt}{L} = \frac{(V_i - V_o)(1 - D)T}{L} \quad (3\text{-}4)$$

Thus, the inductor current has to be identical at the start and end of the commutation cycle. In other words, the overall change in the current (the sum of the changes) is zero:

$$\Delta I_{L\,on} + \Delta I_{L\,off} = 0 \qquad (3\text{-}5)$$

By rearranging the above equations, the input/output characteristic of a boost converter is only dependent of the duty cycle (*D*) as given in the following equation:

$$\frac{V_o}{V_i} = \frac{Ts}{t_{off}} = \frac{1}{1-D} \qquad (3\text{-}6)$$

V_o= average output voltage

V_i= the input voltage, PV voltage

Ts= switching period

D= duty cycle

t_{off}=switching off of the IGBT

Equation 3-6 shows that the link between input and output voltage is regulated by the switch duty cycle (*D*). According to this equation, output voltage always exceeds the input voltage (as the duty cycle goes from 0 to 1), which increases with *D*, theoretically to infinity as *D* approaches

Boost converter models, in general, can be determined by three elements: the inductor current *IL* when the IGBT is on, the output voltage of the converter *Vout* and the duty cycle value *D.*

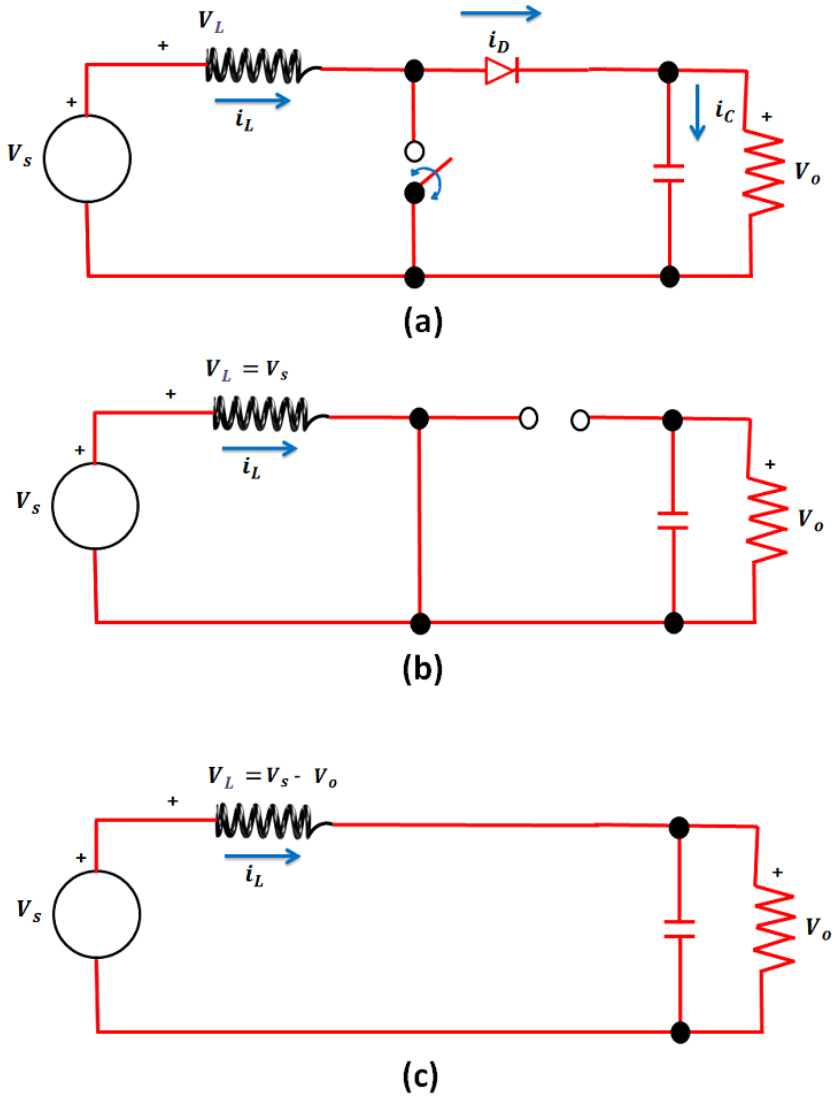

Figure 3-11: (a) A schematic diagram circuit of a boost converter (b) The equivalent circuit for closed switch mode (c) The equivalent circuit during open switch mode.

3.3.4.3 Principle Operations of control for DC-DC Boost Converter Modelling

Figure 3-12 illustrates two square wave control signals. One of these signals represents the hysteresis controller, while the second represents a constant frequency source, which is composed of a fixed duty cycle (which is also followed by a second block switch). The final device contains the main controller, with the controller law highlighted in Table 3-3 below.

Table 3-3 Main Controller Law

$V_{2(t)} \leq V_{ref(t)}$	$V_{3(t)} \rightarrow V_{out}$
$V_{2(t)} > V_{ref(t)}$	$V_{1(t)} \rightarrow V_{out}$

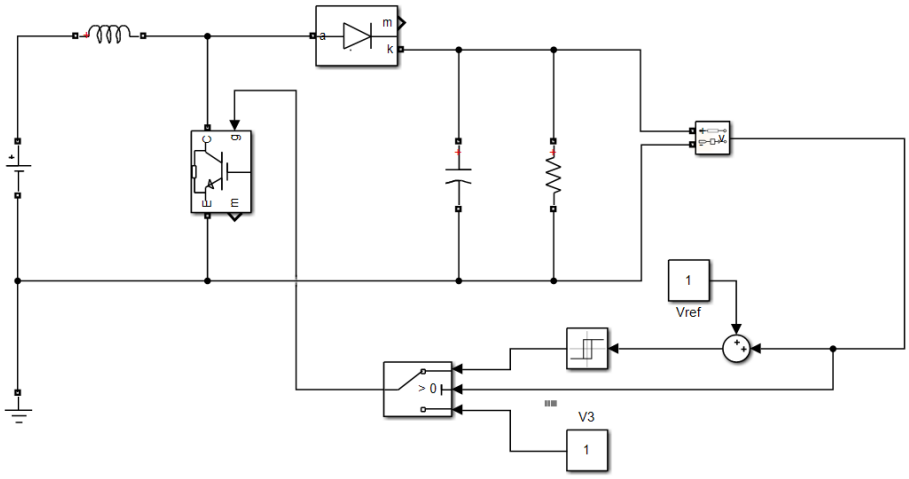

Figure 3-12 voltage controls for Boost converter

In transient response, provided the output voltage exceeds that of the reference, it is generally observed that the main controller tends to function with the first condition or state. This leads to an increase in voltage. In this process, the role of the diode is to prevent any possibility of a reverse current, and by doing so this ensures the flow of the current from source to load (in one direction). During the process, the power of the inductance current is raised, prompting a corresponding increase in voltage; this rise is regarded as being linear in equating power analysis (power average).

Turning the switch off causes an alteration to the inductance current. The result of which means the positive voltage becomes negative and vice versa, based on Ampere's Law. The last effect leads to the voltage increasing (the source voltage besides the accumulated energy in coil). At the last moment, the current flows from the coil to the low-pass filter, thereby producing an increase in the output voltage. In the last state, this process can achieve a discontinuous mode (where the inductor current drops to zero); alternatively, it can remain within a continuous conduction mode. The role of the constant switching source is critical here as it not only determines, but also controls the rise time, transient time and maximum voltage. The reason being that the main controller would not have selected the hysteresis controller at this juncture. This point is only achieved once the system reaches the reference value. Once attained, the system commutates to the hysteresis controller, thus administering the direct voltage

control. In other words, the system begins to start ringing into the hysteresis band. While this process does have its strengths, one of its primary drawbacks is that the output will reach the hysteresis band, and once the system achieves its limit, modulation is produced due to the interaction between the hysteresis band and switching source. The hysteresis band also functions to determine the maximum tolerance ripple.

Once the system begins to commutate, transient time will eventually occur and switching frequency will rely on filter values, inductance and the hysteresis firing. A Variable Pulse Width Modulation Frequency System (VPWM) has been created in order to assist the system in self-stabilization. Within the VPWM, the firing frequency of the transistor turning on/off action dictates the switching period. This process continues until a stable state within the system has been achieved, as well as when load changes occur, due to the variations in output voltage which are being generated.

B. Steady State Response

As soon as the controller law produces V2 (t) as the output signal from the main controller (transient operation has disappeared), this leads to a system state change (switching on and off) which in turn leads to a ringing between the hysteresis band. This is due to the change in output voltage, as it seeks to achieve a state of stability. Table 3-4.(below) which expresses the control law.

Table 3-4 Hysteresis controller law

Intput	Outout
$e_{(t)} > +\delta$	1
$V_{(t)} > -\delta$	0

As the boost output voltage is judged against a “desired” value that is known, this leads to the creation of an error signal, which triggers the hysteresis being switched to the on position, and being at a fixed point where it will remain up until the error value reaches a point below -δ.

This error value symbolises the reference signal of the hysteresis controller. Since the main controller is moving between the constant signal and the hysteresis, this causes a

direct output voltage control, which prompts the variations in frequency reflected in the switch and duty cycle respectively.

It is worth mentioning that the implementation of a hysteresis controller does not provide any assurances of achieving the hysteresis band. It is possible to replicate the inductance action as a current source, and this will produce a charge in discharge in the capacitor, where the frequency being generated will be contingent on the fixed frequency source or hysteresis.

Consequently, the output filter's parameters may be ascertained by offering a minimum switching frequency that is analogous to the fixed one. This will tend to remain as the switching action of the main controller and switching will commutate between the hysteresis and fixed source.

The switching frequency produced as a result of the hysteresis controller can be determined by the following equation:

$$f_s = \frac{f_c}{2\Delta V_0} \tag{3-7}$$

In Figure 3-13 the current control has a multitude of applications in power converters. It is utilised as a control boost converter and from amongst its benefits are its ability to eliminate the external compensation ramp as well as being able to achieve an increase gain for DC and low frequencies. It is also able to counter noise that is produced in the sensed current signal.

Proteus represents just one of a range of simulation packages that can be used, and includes integrated circuits modules for this purpose.

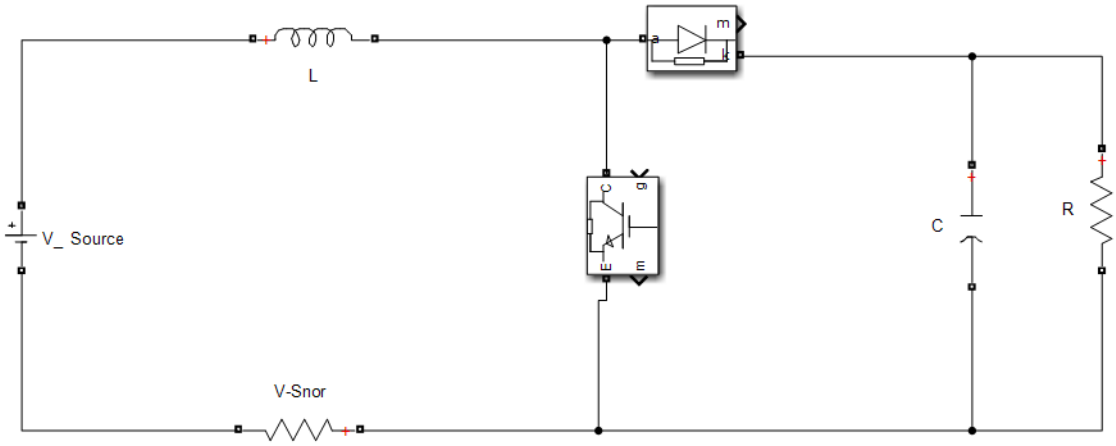

Figure 3-13Boost converters with current sensing

It is noted that where the sensing resistor's value is small, its overall effect on Boost Converter activity is negligible. Furthermore, a few assumptions are made in this model – the first being that the switches were ideal and the second that output had a low overall ripple.

In this process, Equation 3.8 expresses the duty cycle, where t_{on} represents the time duration the MOSFET is switched on and T_s refers to the switching period. This is expressed below:

$$Duty = \frac{t_{on}}{T_s} \qquad 3\text{-}8$$

The value of the controlled current source is derived from Equation 3.13, with Equation 3.10 expressing the voltage value across the controlled voltage source. In this second equation, I_L refers to the current through the inductor when the MOSFET is on, and V_{out} denotes the Boost Converter output voltage.

$$i_Q = \frac{t_{on}}{T_s} I_L = dI_L \qquad 3\text{-}9$$

$$V_D = \frac{t_{on}}{T_s} V_{out} = dV_{out} \qquad 3\text{-}10$$

In general terms, Boost converter models can be said to be governed based on three variables: the inductor current I_L when the MOSFET is on, the output voltage of the converter V_{out} and the duty cycle value which is represented by d.

For the current control, the reference current i_{ref} refers to the control variable which is likened to the sensed current signal, highlighted in Equation 3.11.

$$V_{senser} = R_{senser} * I_L \qquad 3\text{-}11$$

In order to determine the duty cycle value of the current control, the sensed current and reference current values need to be included. Once the duty cycle value has been obtained, it can be fed into the DC-to-DC converter model to determine the required waveforms.

The current control scheme with pulse width modulator PWM is illustrated in Figure 3-14.

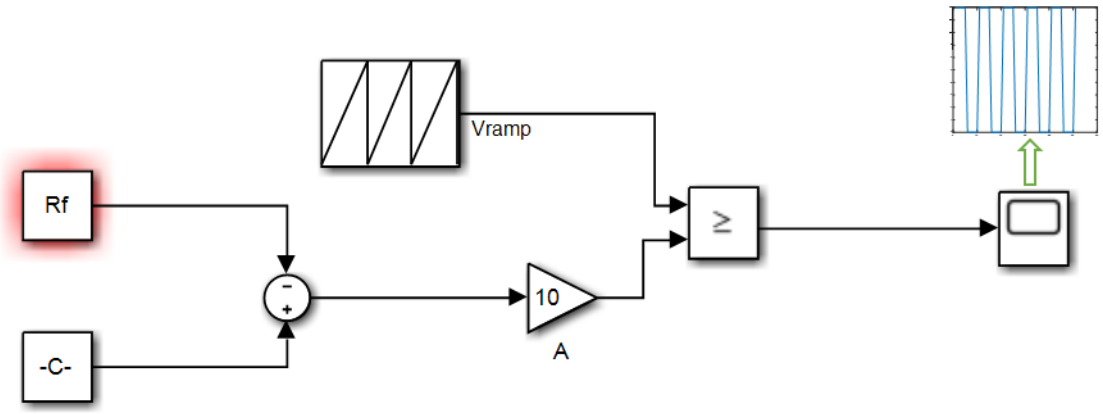

Figure 3-14 current control with PWM

Once the inverting terminal is linked to the capacitor and resistor in parallel, the amplifier functions as a low pass filter, which means it is possible to disregard the ripple switching in the inductor current I_L and V_{sense}.

The inverting terminal of the Op Amp connected to R_2, is sustained by the sensed current signal, while the non-inverting terminal of the Op Amp is connected to i_{ref}.

In this process, the signal icon functions as the comparator output, and works by comparing between V_{sense} and i_{ref}, amplifying any discrepancies between the two. The signal icon works by feeding into the inverting input of the comparator, thereby generating the duty cycle d. The non-inverting terminal element of the comparator is sustained by a saw tooth signal, which is expressed by the value $V_{sawtooth}$ and frequency $f_{sawtooth}$. It is the resulting signal from the comparator d, which is deemed the pulse width modulated signal (PWM) and is responsible for controlling the converter duty cycle.

It is possible to model the PWM circuit as a constant multiplier $^{1}/_{V_{sawtooth}}$ and voltage limiter. The latter of which aims to restrict the duty cycle between d $_{min}$ and d $_{max}$.

Figure 3-15 provides a pictorial representation of the PWM circuit model with current control scheme.

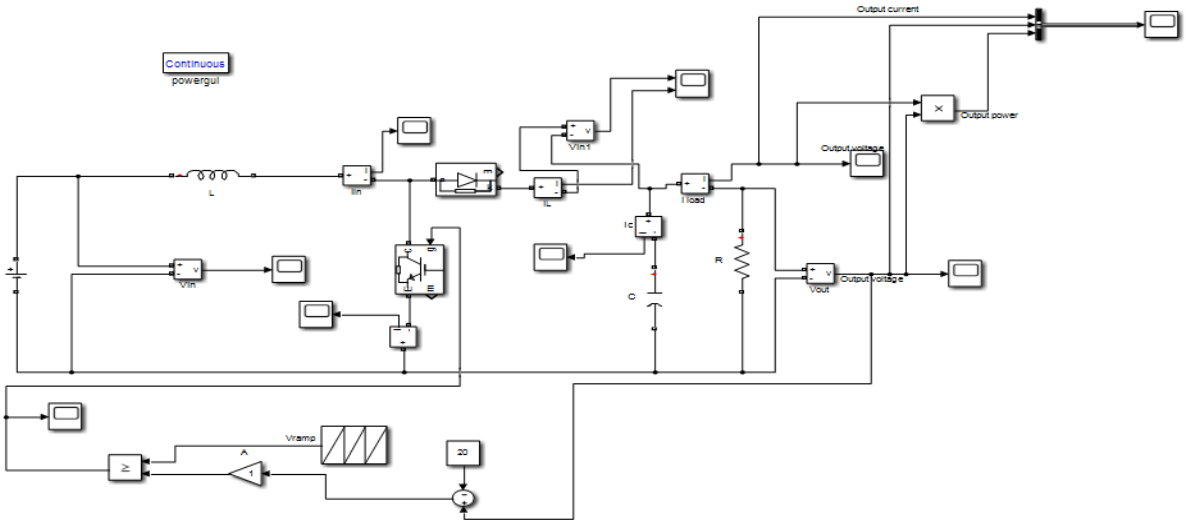

Figure 3-15Design of current control

From the data provided in Figure 3-15, it is possible to derive the transfer function of the duty cycle for the current control scheme, which is denoted by the following formula:

$$d(s) = {}^{1}/_{V_{senser}} (i_{ref}(s) + H(s)(i_{ref}(s) - R_{senser} IL(s)) \quad 3\text{-}12$$

Where H(s) is the transfer function from the inverting terminal to V_d.

$$H(s) = \frac{K_c(1+\frac{s}{w_L})}{s(1+\frac{s}{w_L})} \quad 3\text{-}13$$

And Kc, ω1 and ω2 can be defined as:

$$K_c = \frac{1}{R_2(C_1+C_2)} \ , \ w_1 = \frac{C_1+C_2}{R_1 C_1 C_2} \ , \ w_2 = \frac{1}{R_1 C_2} \quad 3\text{-}14$$

3.3.4.4 DC-DC buck converter

The circuit diagram of the buck-converter is shown in Figure 3-16. Owing to its simplicity and high efficiency, the DC-DC buck converter plays an important role in PV systems (Karatepe et al., 2009). Buck converters regulate the voltage, current and power from the PV system and charge the battery effectively at times of uncertain power output (Ko and Chao, 2012). This type of the converter can be utilized to connect high module voltages to the low module voltages (battery, load) owing to the lower voltage value of the output voltage compared to the higher input voltage magnitude (Mohan et al., 2004).

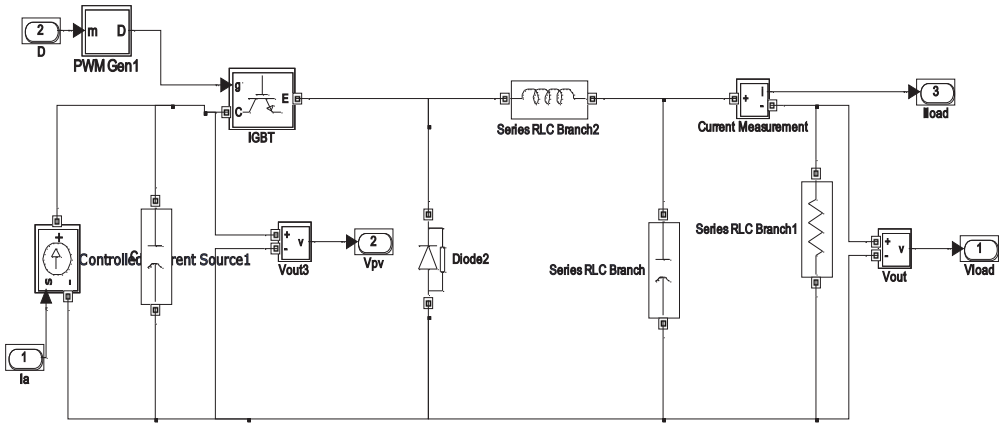

Figure 3-16 Circuit diagram of DC–DC buck converter

3.4 PV solar cell characteristics

An ideal solar cell may be modelled by a current source in parallel with a diode. As no solar cell is considered ideal in practical terms, this necessitates the addition of a shunt resistance and a series of resistance components to the model. In order to understand the process of electronic behaviour as it pertains to a solar cell, models can be created which are electrically equivalent, and use discrete ideal electrical components with well-defined behaviour. An example of this type of equivalent circuit is highlighted in Figure 3-17 (Lorenzo, 1994).

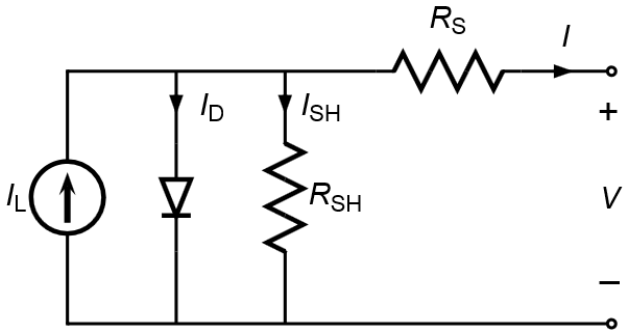

Figure 3-17: The equivalent circuit for a solar cell [Oi, Akihiro 2005]

The internal photocurrent of the PV solar cell (*IPH*), within PV cell equivalent circuit is shown in Figure 3-18 along with the boost converter for the MPPT application.

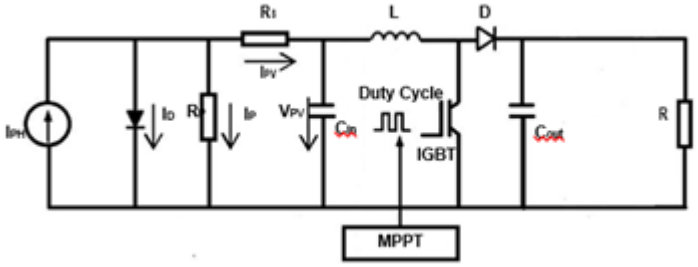

Figure 3-18: PV solar cell equivalent circuit integrated within a MPPT system

A parallel diode (*D*), internal series and parallel resistances (R_S and R_P) are clearly visible in this circuit, as well as the total current and voltage I_{PV} and V_{PV}, respectively. Total current (I_{PV}) can be demonstrated in relation to diode (I_D) and parallel resistance currents (I_P) using the following formula:

$$\mathrm{I_{PV} = I_{PH} - I_D - I_P} \tag{3-15}$$

$$\mathrm{I_{PV} = I_{PH} - I_O\left(\exp\left[\frac{q(V_{PV} + I_{PV}R_S)}{AkT_C}\right] - 1\right) - \frac{V_{PV} + I_{PV}R_S}{R_P}} \tag{3-16}$$

where I_0 represents the total diffusion current, V_{PV} represents the output voltage, q is the charge of one electron, Tc is the solar cell temperature, k is the Boltzmann constant and A is the junction perfection factor, responsible for determining the diode deviation from the ideal p-n junction.

In order to derive the numerical model of a PV module, this can be extended as:

$$I_{PV}(1+\frac{R_{ST}}{R_{ShT}} = n_P I_g - n_P I_O \left(\exp\left[\frac{q\left(\frac{V_{PV}}{n_S}\right) + I_{PV} R_{ST}}{AkT_C} \right] - 1 \right) - \frac{V_{PV}/n_S}{R_{ShT}} \quad (3\text{-}17)$$

where I_g is the photo-generated current, cells in parallel n_p and cells in series n_s the $R_{shT} = \frac{n_P}{n_S} \times R_P$ and $R_{ST} = \frac{n_S}{n_P} \times R_S$

P_V voltage, V_{PV} as a function of the current, I_{PV} is represented as:

$$V_{PV} = 2n\left(KT_C/q\right) n_s \ln(\frac{n_P I_P - I_{PV}}{n_P I_o} + 1) - \frac{2n_S R_S}{n_P} I_{PV} \quad (3\text{-}18)$$

Figure 3-19and Figure 3-20 illustrate the impact of cell temperature and internal resistance (Rs) on the I-V curve respectively.

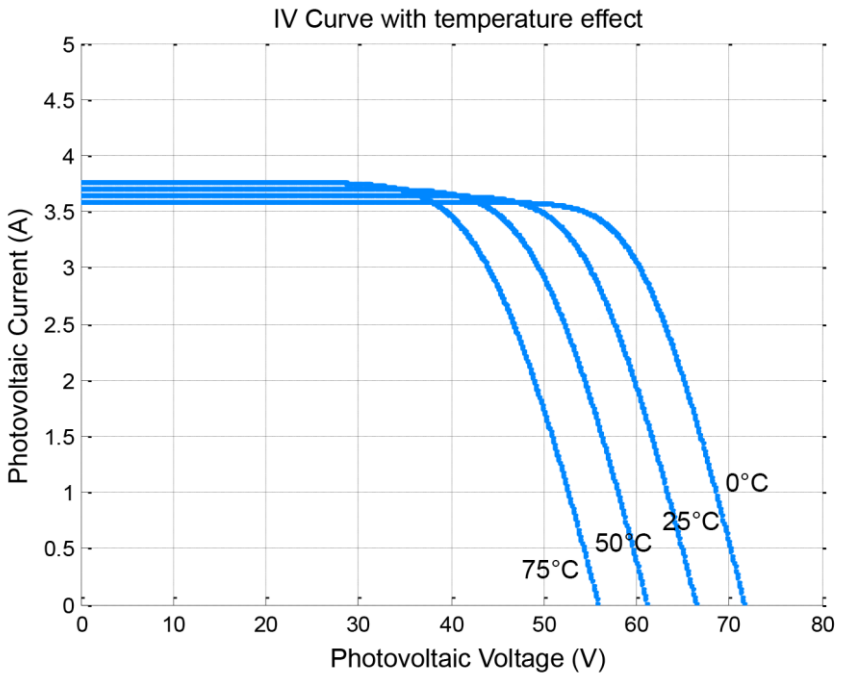

Figure 3-19I-V characteristics (temperature and the light radiation) in (1kW/m²).

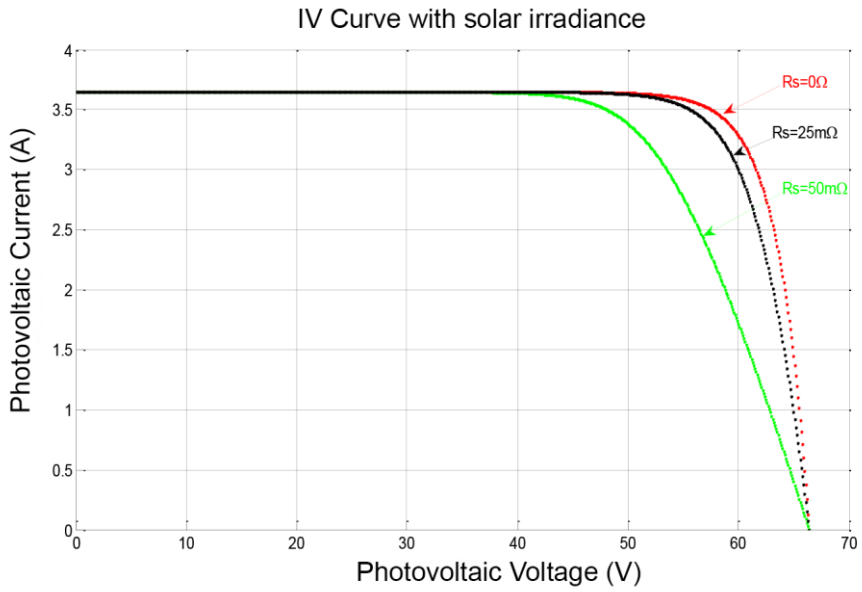

Figure 3-20 Illustrate impacted of chains resistances during (1KW/m², 25°C) on the PV unit by using MATLAB simulation.

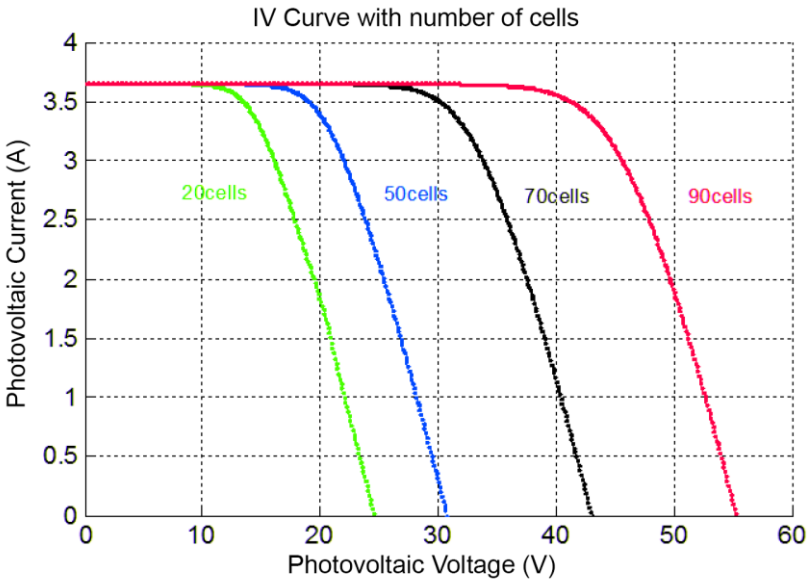

Figure 3-21 PV effect systems by number of cells.

3.4.1 The main parameters for measuring the PV system

The primary electrical parameters that can be used to characterize PV modules are shown in Figure 3-22 and listed below. These are usually measured under STC (see 1.5.1):

Open circuit voltage (V_{OC}): The highest value of voltage of the PV solar cells under the open circuit conditions (I =0).

Short circuit current (I_{SC}): The highest value of current produced by the PV solar cells under the short circuit current conditions (V=0).

Maximum power ($p\ max$): The operational point $p\ max$ ($I\ max,\ V\ max$) which is the highest efficiency that can be obtained from PV solar cells.

$$p\ max = I\ max * V\ max$$

Fill factor (FF): The ratio of the maximum power that can be produced from the solar cells to the load and the produced I_{SC} and V_{OC}.

Voltage at maximum power (V $p\ max$): The voltage value generated by the module which is linked to the maximum value of power for that module.

Current at maximum power (*I max*): The current value produced by the module which corresponds to the maximum value of power for that module.

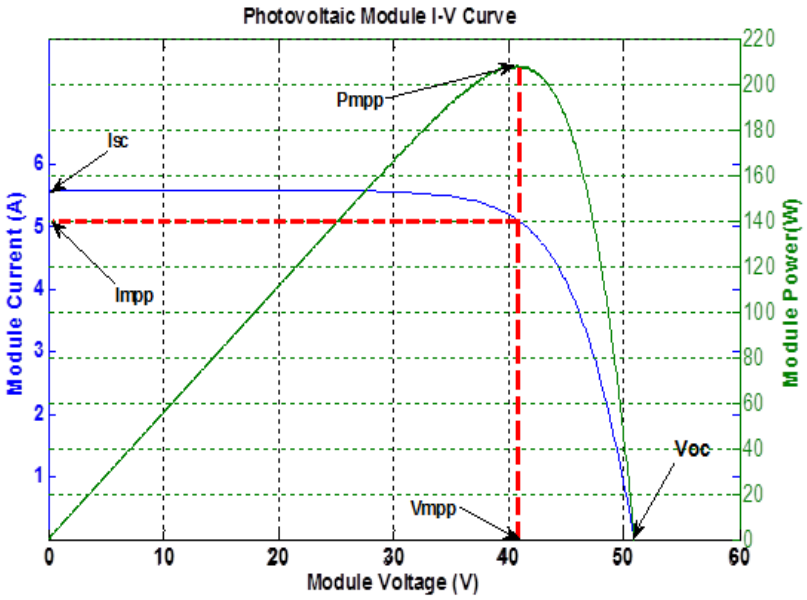

Figure 3-22 I-V curve (blue) and P-V curve (green)

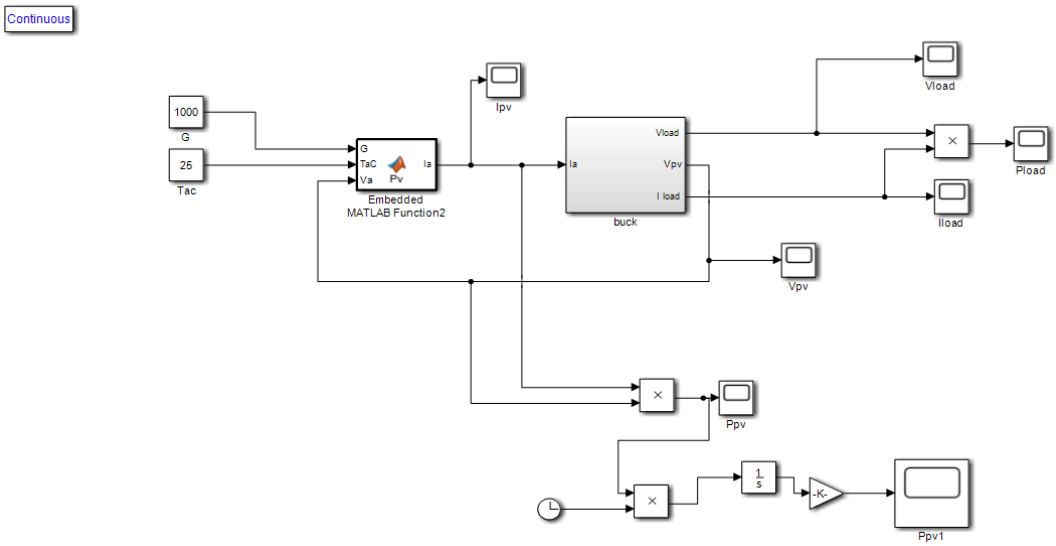

Figure 3-23 Modelling of PV system

3.4.2 Failure in PV systems

Although there are major advantages in using PV systems to supply electricity, these systems may be exposed to various operational issues, which may result in fluctuation in their output power or even occasionally in breakdown. As previously noted in Chapter 1, these may be caused by a range of environmental factors that affect the PV arrays such as a reduction in solar irradiance due to clouds, dust, high temperatures or moisture. In addition, this can also be the result of the degradation of the PV system over time, module defects or string defects (Stettler et al., 2005). Although the power conditioning system can be used to detect failure in a large scale PV power plant, it is harder to monitor this in a PV string/panel. Thus, identifying a novel early stage failure detection method is essential for developing an effective PV system.

3.5 Summary

The primary objective of this chapter has involved utilising MATLAB and SIMULINK to design and model a DC Boost converter. The DC Boost convertor has been used to generate low DC voltage, thereby converting low levels of DC voltage into a higher DC voltage. In order to achieve this, certain parameters were used by the convertor, and these were: Input voltage, Output voltage, duty cycle, collector and emitter current. These parameters are considered to be important because they provide a control for and regulate the output voltage from the DC Boost convertor unit itself.

As is known, the DC Boost convertor regulates/controls how the PV system operates and so one can infer that it represents the core or heart of the PV system, analogically speaking. Therefore, in order to truly determine how the PV functions and is able to

operate effectively whilst being subjected to a myriad of environmental factors, it is only logical that the DC Boost convertor must be designed and modelled optimally in order to produce the desired outcome from the said PV system. The link of the environment to the efficiency of the PV system cannot be underestimated, and so this must be harnessed to produce a PV system that is fit for purpose and able to work harmoniously with the environment, rather than trying to control it.

With regards to determining the relationship between the operation of the PV system and the different environmental factors it may encounter, the modelling of the DC Boost convertor system in this chapter has determined that changes in temperature do affect the PV system's voltage output. Higher temperatures have significantly affected the voltage of the PV system. This issue can be resolved, to an extent, by increasing the number of solar panels used in the PV system as an increased number of panels will yield a greater output voltage and thereby offset the effects of an increase in temperature.

The other issue to consider is the effect of the environment on the operation and efficiency of the PV system itself. Factors such as humidity, dust, and high temperatures all need to be considered, as they can all have an impact of the output voltage produced by the PV system. This is where the design of the DC Boost convertor is critical, as a 'built in' early fault diagnosis system triggered by the abovementioned environmental factors would clearly need to be an integral aspect of the design. This would help to detect changes in environmental factors which may adversely affect the PV system.

In conclusion, this study has established a clear, causal link between temperature and the efficiency of the PV system. The effects of temperature can be mitigated to an extent by using more solar panels in the PV system. However, given the temperatures that may be produced in hotter climates such as Saudi Arabia, it is clear that this relationship needs to be monitored so that optimal results are being produced for this kind of technology. All of this must consider the costs and expenditure involved in producing, maintaining and monitoring this type of technology, if in the long run, it is to be considered a viable, worthwhile alternative to the older, more established fossil fuels.

4 Thermal and Acoustic Modelling of Power Electronics

4.1 Introduction

Previous research has classified AE as an appropriate NDT method for detecting micro-structural characterisation and monitoring damage processes due to its sensitive transient response. During heat and under any harsh conditions, the power semiconductor modules of PV systems experience high mechanical and thermal stresses, which can lead to bond wire lift-off and solder joint fatigue faults. These stresses can in turn lead to malfunctions of the electronic power modules. The current research and development status of AE measurement techniques have allowed the field of NDT of condition monitoring to be expanded to power electronics. It is envisioned that by merging different signal conditioning and analysis, useful information can be extracted from AE signals, which can provide information regarding the health of PEDs, AE technique could serve as a method of early detection of such defects and be used to monitor any unexpected anomalies in the power semiconductor devices of a PV power system.

The chapter begins by explaining the theoretical background to thermo-acoustic behaviour for power electronics applications and then discusses more technical information concerning the acquisition and analysis of AE signals to describe the thermo-acoustic behaviour of PEDs.

4.2 Thermal modelling

Researchers have shown that due to its operating characteristics, the IGBT module deteriorates after undergoing a significant amount of thermal stress cycle. Chibante et al. (2003; 2005) investigated a physical model of IGBT hole/electron distribution to

describe the electro-thermal effect of IGBT. A later study by Tang et al. (2012) explained how the different temperature characteristics during turn-on and turn-off transient affect lifetime of IGBTs.

The electro-thermal temperature dispersion from an IGBT can be mathematically explained using a Foster network thermal model (Allbabar and Batunlu, 2018) as shown in Figure 4-1. Its formula can be expressed as:

$$T(s) = \sum_{k=1}^{N} \frac{1/C_{thn}}{s + 1/(C_{thn} \cdot R_{thn})} P_L(s) \qquad (4\text{-}1)$$

where T represents the emitted temperature, and;

P is the power loss.

N is the order polynomial regression

C is the capacitor

R is resistance

The summation annotation indicates an equivalent thermal Foster network as shown in (4-1). This represents the summation of the response of the first order system of RC circuits, in which $C_{thn} \cdot R_{thn}$ is equivalent to the time constant of the system. P_L is the power loss in the energy conversion of the IGBT. Technically, by determining the transient characteristic of P_L, it is possible to verify the electro-thermal temperature, thus predicting the condition of an IGBT.

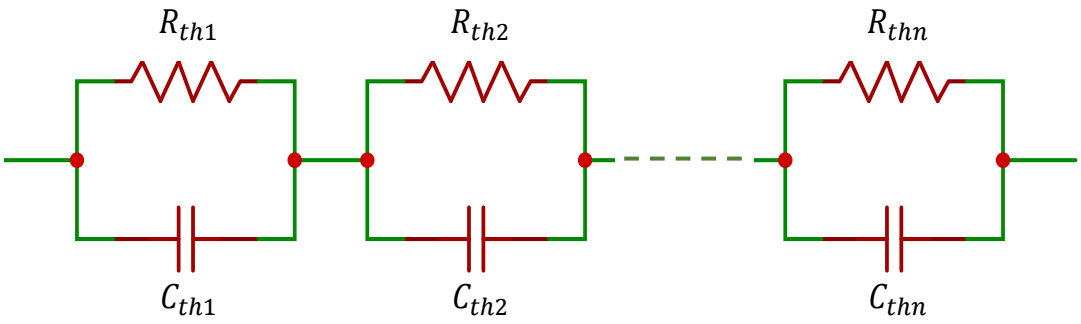

Figure 4-1: Thermal Foster network

4.3 Acoustic Emissions

4.3.1 Characteristics of AE

According to the American Society of Testing and Materials Terminology for Non-Destructive Examination (1982), AE is defined technically as "the class of phenomena whereby transient elastic waves are generated by the rapid release of energy from localised sources within a material." AE is identified to be a naturally occurring phenomenon that has been observed in a broad scope of materials, structures and procedures. At one extreme, seismic events are a form of AE whilst in extreme comparison, AE has been observed in the dislocations produced in stressed metals (Miller and McIntire, 2005).

When a material cracks under stress, the cracking process emits acoustic waves that emanate in an omni-directional manner from the source. An AE sensor (usually piezo-electric based as detailed above) in contact with the material being monitored, is used to detect the mechanical shock wave and convert the low displacement into an electronic signal that is amplified by a preamplifier and processed by the AE instrument. As previously noted, AE is usually transient in nature, occurring in discrete bursts, interpreted as AE "hits". Through the analysis of aspects of the waveforms associated with each of these hits, AE systems are able to analyse each hit individually.

Stress plays an important role in the AE generation process. In many AE applications, stress is automatically applied by the process itself (for example, pipelines) while in other cases, the stress is the result of an externally induced force. The most important thing, however, is that the stresses being applied are non-destructive, and also that they are well below the expected defect tolerance of the material.

AE testing can be performed in the field with portable instruments or in a laboratory setting. A typical design system contains a sensor (ultrasound transducer), preamplifier, filter, and amplifier, along with measurement tool, display, and storage equipment (e.g. transducer, pulse generator, oscilloscopes, voltmeters, and personal computer). Figure 4-2 shows the typical set-up for running an AE test.

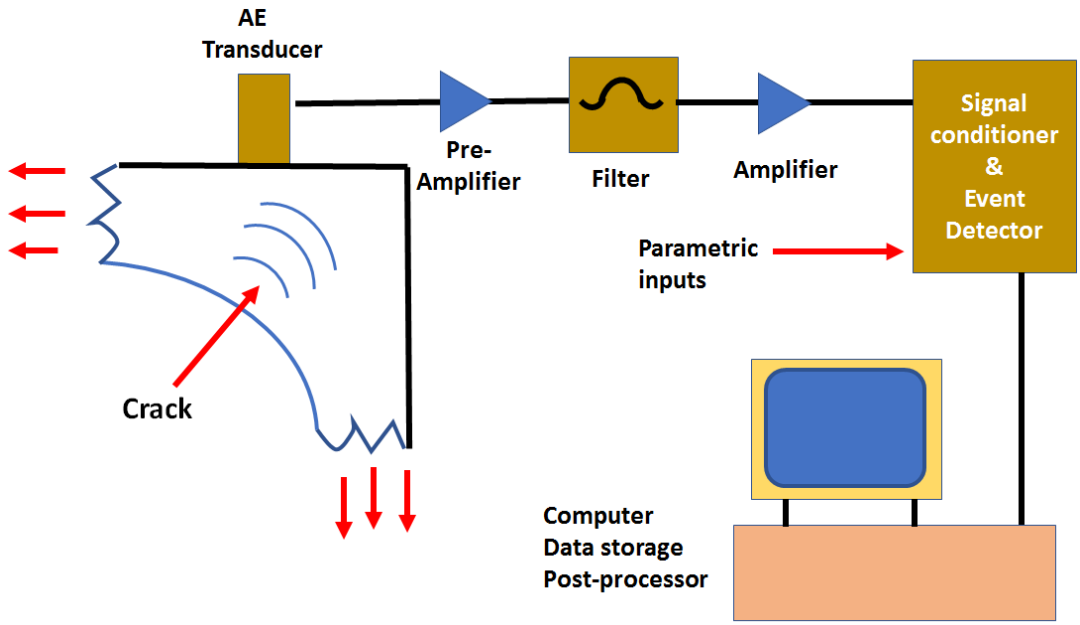

Figure 4-2: A typical AE test set-up [adapted from Huang, 1998]

One significant barrier to the use of AE techniques is that it requires a suitable hardware set-up for accurate and effective data acquisition. More knowledge about signal processing and analysis is crucial to identify the useful information which lies within the AE signal.

AE is usually in the form of an elastic stress field and there are no emissions without this stress. For this reason, Pollock (1989) recommends that AE testing generally requires controlled loading of the structure under examination. Any displacement within the structural surface being tested is identified by the AE sensors which convert these movements into an electrical signal by making use of a piezoelectric crystal. Following this process of sensing and subsequent pre-amplification, the signal will then be transmitted to the main instrument for filtering and amplification. A digital output pulse is generated every time the AE signals exceed the voltage which has been set at a fixed threshold level with a comparator circuit being used to detect this signal. The operator generally sets this level and this key variable effectively determines the sensitivity of the test (Miller and McIntire, 2005).

The operating frequency of the equipment used for AE testing typically has a range of 20 to 1200 kHz and is extremely sensitive to any surface displacement. This sensitivity means that the equipment is able to detect material deformation, crack growth and processes such as phase transformation, flow and solidification (Miller and McIntire, 2005). Technological advances mean that AE systems can handle increasingly high rates of data acquisition and faster signal processing. This ability to store ever greater quantities of waveform data has helped to improve our understanding of AE wave propagation.

4.3.2 Signal measurement parameters

Five key signal measurement parameters are used in AE signal analysis, namely, amplitude, counts, the measured area under the rectified signal envelope, also known as relative energy, duration and rise time. Figure 4-3 shows a typical AE "hit waveform" with all its related features. These parameters have become standardised within the

field although a number of other parameters are sometimes used in test and analysis including average frequency, count-to-peak, absolute energy, and spectral moment (Miller and McIntire, 2005).

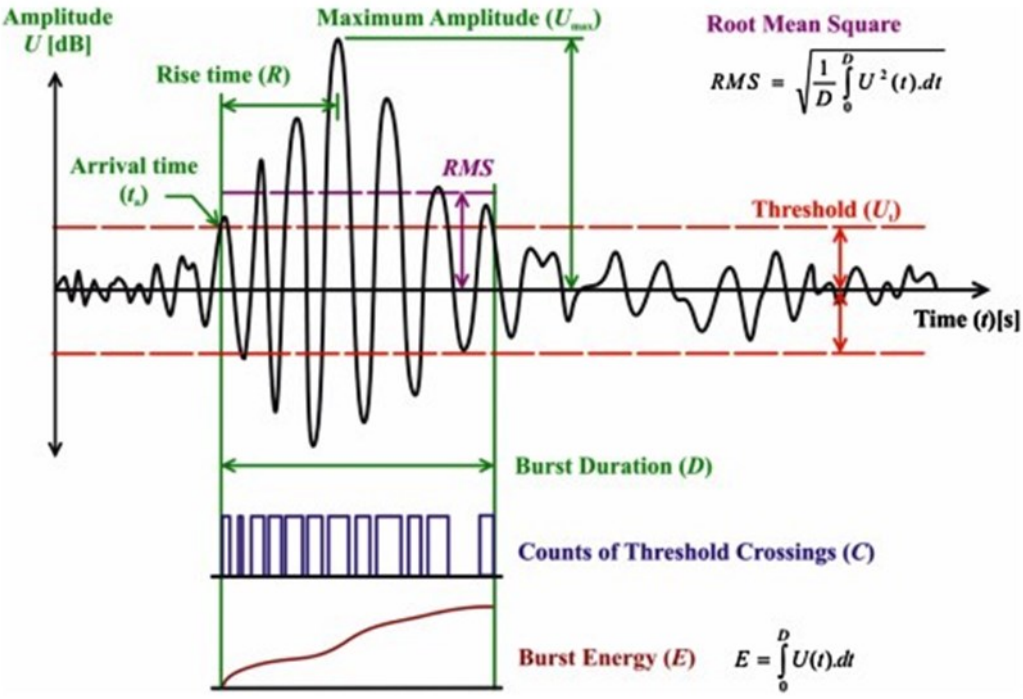

Figure 4-3: Definitions used for recording AE events (Shukri, 2012)

Amplitude (A) is a crucial parameter. It refers to the maximum peak voltage reached by an AE waveform and has an explicit connection to the magnitude of the AE source event, determining its detectability. AE amplitude can vary widely from micro-volts to volts and is usually conveyed utilising a decibel scale, which defines 1 μV at the transducer as 0 dB, 10 μV as 20dB, 100 µV as 40dB, continuing on.

One of the easiest and longest established ways of quantifying the AE signal is through threshold-crossing pulses or **counts**, also referred to as ring-down counts (N). This measure relies heavily on both the acoustic properties and reverberant nature of the material specimen and the sensor itself.

Energy (E) is the measured area under the rectified signal envelope (MARSE). Since this is less dependent on threshold settings and operating frequencies and is sensitive to amplitude and duration, it is usually preferred over counts. **True Energy** measures the true energy of an AE event through using transient signals or particular data rate intervals from uninterrupted AE signals. It is calculated in atto-joules ($1x10^{-10}$ J = 1 aJ). **Absolute energy** is calculated through the integral of the squared voltage signal divided by the reference resistance (10 kΩ) over the duration of the AE waveform packet (PAC, 2005).

Duration (D), measured in microseconds, refers to the length of the time from the first threshold crossing to the last. It is useful for noise filtering and for other types of signal qualification. Finally, **rise time** (R) can be defined as the time elapsed between the first threshold crossing and the peak of the signal.

Using signal processing software, current AE systems can identify these parameters, denoted as feature data. This process is conducted through isolating the value of said parameters from waveform data. This process is reliant upon the wave propagation process between the source and sensor and can be utilised for a number of signal qualification and noise rejection processes. Pollock (1989) provided a useful summary of AE data display, categorising this in the following way:

1. History/Time plots
2. Distribution functions showing the statistical properties of the AE
3. Channel plots showing the distribution of AE detected by each channel
4. Location displays showing the position of the AE source
5. Point plots showing correlations between various AE parameters and
6. Diagnostic plots showing the magnitude of AE from various parts of a structure or locations within it.

4.3.3 AE source mechanism

As noted previously, AE consist of stress waves created through the rapid release of elastic energy in stressed materials, with emissions being classified as continuous or transient waves. The former are typically produced by processes involving rapid repetition including fluid flow, machine vibration and continuous friction between surfaces. In the case of continuous waves, amplitude and frequency may fluctuate but there is no end to the AE signal Figure 4-4.

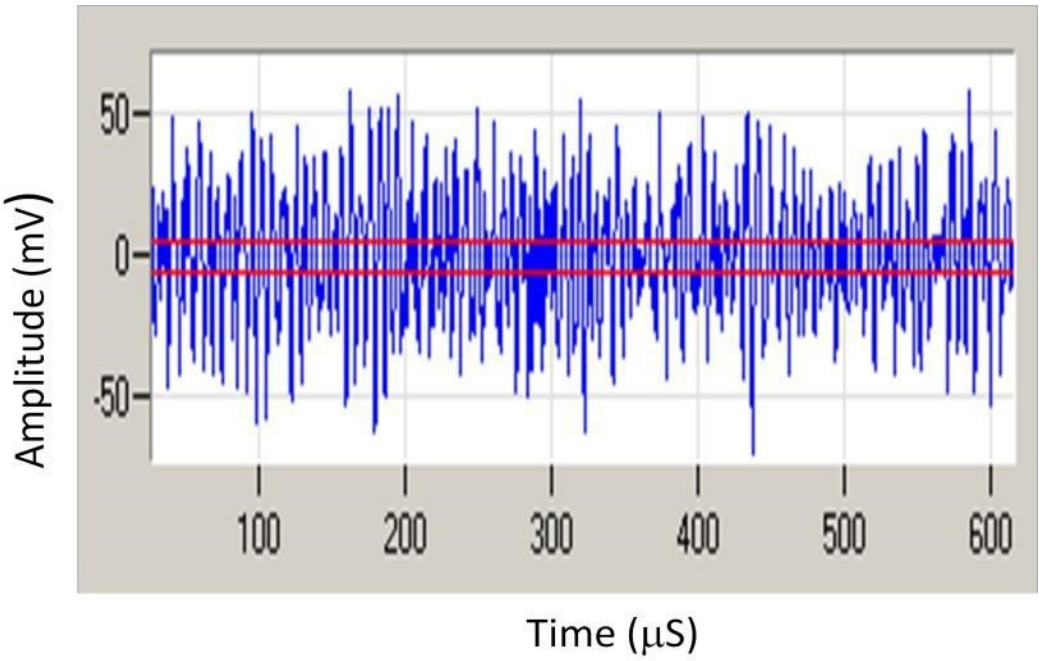

Figure 4-4: Typical continuous AE signal

Transient waves, on the other hand, produce burst-type signals since they are generated through a sudden and permanent change in the material. These may take the form of corrosion and deformation processes caused by defects. In this case, the discernible start and end of the signal can be detected and it clearly differs from the noise signal (Figure 4-5).

Scruby (1987) identifies the classic sources of AE as being defect-related deformation processes, for example, plastic deformation. In metals specifically, other mechanisms causing AE include formation and growth of micro cracks, sudden crack growth, frictional processes caused in crack closure and opening, and also movement and multiplication of dislocations (Heiple, 1987).

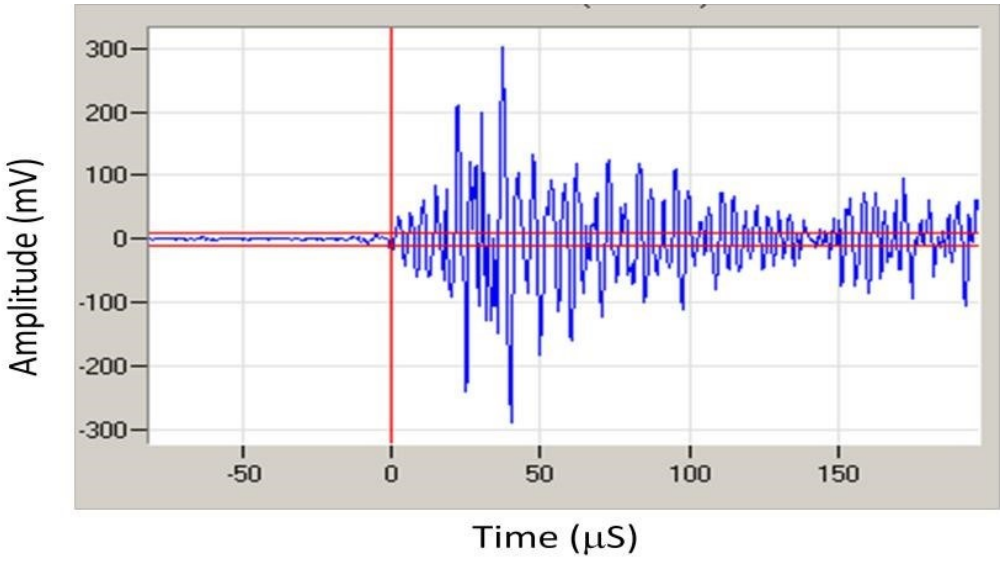

Figure 4-5: Typical transient AE signal

The amount of AE energy that is released is principally dependent on the speed of these deformation processes and their size. Thus, although the formation and then subsequent movement of a single dislocation will create an AE stress wave, an isolated process of this type will not be sufficiently large to produce a detectable result. However, millions of combined dislocations all moving simultaneously will cause individual stress waves to overlap and this superimposition will mean detection is likely to occur (Heiple, 1987).

AE can provide data that are detailed and immediate making it a very valuable tool for studying material damage. AE analysis proves most useful when it is used with other techniques. Some of the best known ones include stress-strain measurement,

measurement of crack growth using a Krak gauge, or employing visual techniques, for example microscopy or digital image correlation. AE can be said to complement these techniques by providing additional data on the dynamics of the damage that has occurred or on underlying processes of deformation. It can also shed light on the progress of transition from one form of deformation or impairment within a material to another (Pollock, 1989).

4.3.4 Ultrasound wave properties

Acoustic or ultrasound waves are a type of longitudinal wave that propagates by means of adiabatic compression and decompression. Their direction of vibration follows their direction of travel. Acoustic waves travel at the speed of sound which is dependent upon the medium they are passing through and are characterised by the following parameters:

- **Velocity** refers to the speed at which a sound wave propagates through a specific medium. This is inversely proportional to the density of that medium and is directly related to its stiffness.
- The maximum distance that particles move from their normal position is known as **amplitude**. The louder a sound is, the more energy that it carries and the greater its amplitude.
- The **frequency** of the sound wave is the number of oscillations it generates per unit of time (usually per second).
- W**avelength** is the term used to designate the distance from one pressure peak to the next one. Wavelength depends on the frequency with which the sound wave propagates and the medium involved.
- **Attenuation** causes a travelling wave to decrease in power as the distance from the reflective material increases. The power of the reflected wave decreases in comparison to the power of the incident wave.

Sound pressure, particle velocity, particle displacement and sound intensity are all important quantities for describing acoustic waves.

4.3.5 Propagation of AE waves

AE signals constitute the response produced by a transducer to the sound waves generated in a solid medium (Miller and McIntire, 2005). Figure 4-6 shows that AE waves released at source can fundamentally be considered to be a stress pulse caused by permanent displacement in a material.

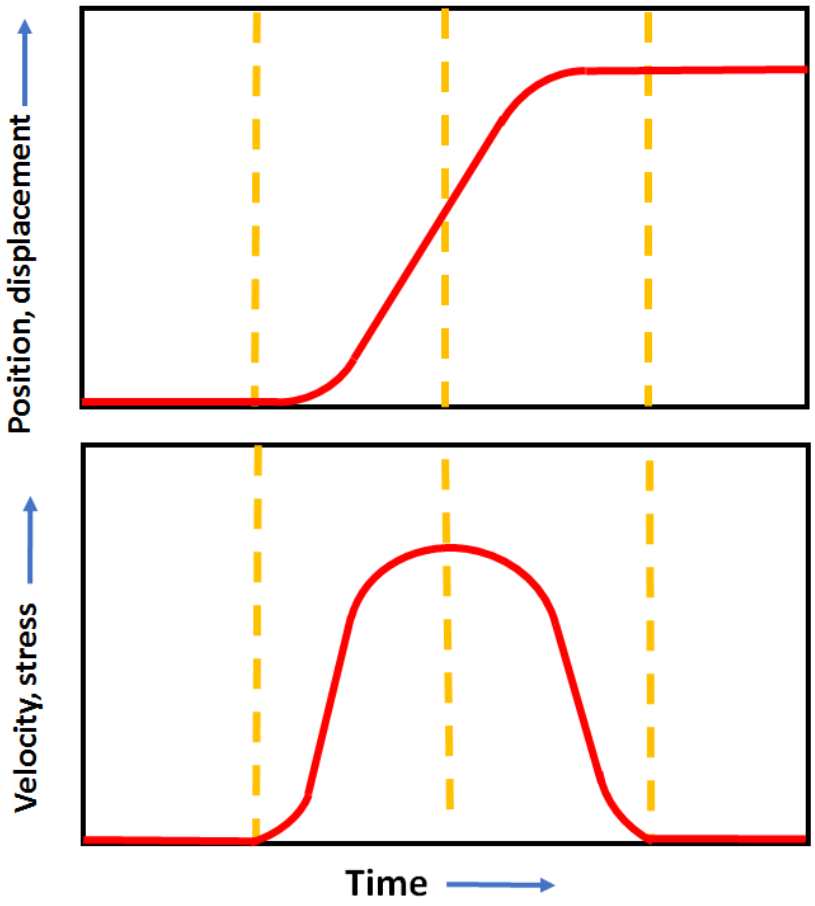

Figure 4-6: Stress waves released at AE source [adopted from Pollock 1989]

This displacement waveform corresponds to the permanent change that is related to the source processes. The height and width of the pulse that is generated is dependent upon the dynamic of these processes. Thus, if crack growth occurs at the microscopic level this may last only a few microseconds and consequently the pulse that is produced has a similarly brief duration. It should be noted that the amplitude and energy of stress pulses can vary greatly, ranging from sub-microscopic dislocations at

one extreme to major crack extensions at the other. As Figure 4-7 illustrates, a stress wave is dependent on the nature of the source (in this case, a growing micro-crack) and often possesses strong directionality, radiating outwards from the original source in all directions.

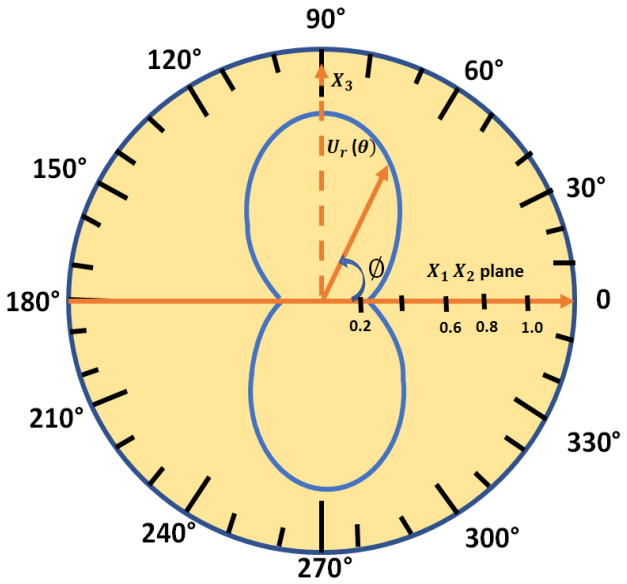

Figure 4-7: Angular dependence of AE radiating from a growing micro-crack [Pollock, 1989]

Figure 4.7 is used to measure the length, width and angle of the wave frequency generated from the AE sensor. This helps to measure and determine the changes in any wave frequency. In this study more specifically, it will help to record the changes in the transistor when it goes from on to off.

AE is initially propagated from a point source as bulk waves, taking two basic forms, as transverse and longitudinal waves, as seen in Figure 4-8 (Rindorf, 1981).

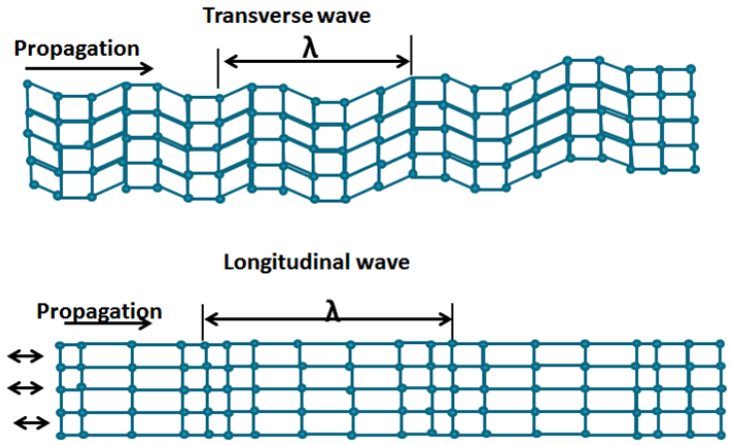

Figure 4-8: Basic modes of wave propagation in solid media [Rindorf 1981]

When longitudinal waves strike the surface of solid materials, this may create a further wave mode referred to as a surface wave or a Raleigh wave (Figure 4-9).

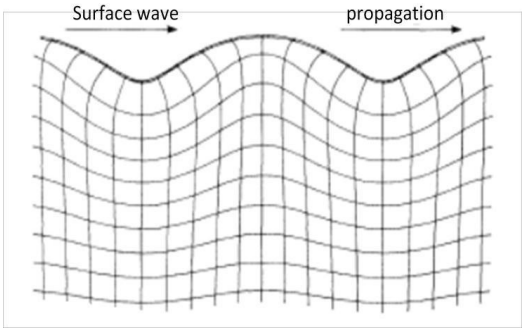

Figure 4-9: Surface wave particle motion (Rindorf, 1981)

The test specimens used in many AE studies consist of plate-like structures (Aggelis et al. 2011; Holland et al. 2000; Grondel et al. 2002) which propagate Lamb waves using two modes of propagation, known as symmetric (S_0) and asymmetric (A_0) (Figure 4-10). The former refers to plane of the late which forms the larger component of displacement with the latter referring to the larger displacement component flexural mode, which is perpendicular to the plane of the plate. These types of propagation are also sometimes referred to by the terms extensional and flexural.

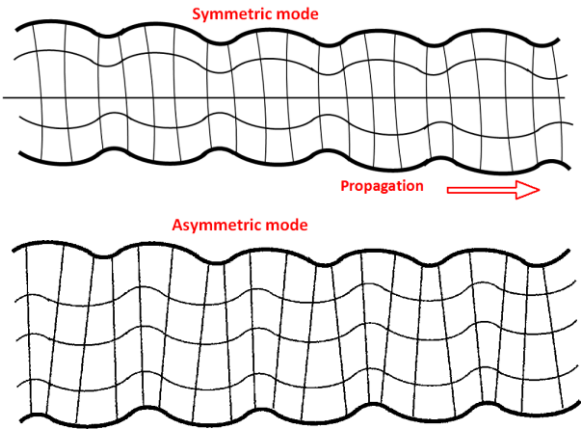

Figure 4-10: Lamb waves [Rindorf 1981]

In the symmetric mode, the plane of the plate forms the larger component of displacement while in asymmetric mode, the larger displacement component in the flexural mode is perpendicular to the plate's plane. Lamb waves can only occur if the plate's thickness is much smaller than its other two dimensions while the wavelength is much larger than the plate thickness (Gorman, 1991).

4.3.6 Wave attenuation

When waves travel through propagate within a medium, the subsequent AE response can be explicitly impacted by the reduction of energy. This decrease of amplitude as waves of media is denoted as attenuation (Miller and McIntire, 2005), evident in the near and far field. Near-field attenuation refers to the loss of amplitude which occurs in close proximity to the source. When this occurs further from the original source, it is known as far-field attenuation.

Pollock (1986) identifies four main causes of attenuation, namely, geometric spreading, internal friction, velocity dispersion and dissipation of acoustic energy into adjacent media. The first of these, geometric spreading, is considered to be a major contributor to near-field attenuation mechanism, causing significant decreases in amplitude. Wave propagation away from the source leads to energy redistribution

within the medium creating a corresponding decrease in amplitude. In the case of a bulk wave, the amplitude decreases by a proportion of 1/r (r = distance of propagation). In wave propagation involving two dimensional waves, such as Lamb waves, the amplitude of the signal decreases by a proportion of $1/r^{1/2}$ (Miller and McIntire, 2005).

Energy absorption caused by internal friction may be responsible for far-field attenuation since this can convert acoustic energy into thermal energy within a material. Since the absorption mechanism is usually frequency dependent, larger losses typically occur as a result of the fact that AE waves propagate at a higher frequency.

When Lamb waves spread within a plate-like structure, attenuation that is caused by dispersion usually takes place. When the frequency components of different modes of Lamb wave are superimposed at source their propagation distance varies in relation to their velocity. In the case of examples such as guided waves employed for ultrasonic testing, levels of attenuation can be extremely large.

In the case of the final type of attenuation mechanism, acoustic energy may dissipate into adjacent materials; thus grains in metals, surface coating or fluids contained in piping systems or vessels may all result in internal scattering of AE signals and subsequently act as sources of attenuation.

In order to ensure that attenuation does not impact on the detection of an AE signal, several transducers need to be arranged in close proximity so that it is possible to detect any AE events originating from any part of the structure under examination. It is possible to identify the minimum spacing that is required between two sensors

empirically by making use of simulated AE testing or by basing this on prior experience with structures of a similar type and composition. Through positioning multiple sensors in varying distances from the AE source it is possible to measure attenuation levels. It is possible to calculate attenuation using the following equation:

$$\gamma = 20/x \log A1/A2 \qquad (4\text{-}2)$$

where γ is the attenuation coefficient (decibels over distance); x is the distance between detection points; A1 refers to the amplitude of the signal at point 1; and A2 is the amplitude of the signal at point 2. The attenuation coefficient is calculated as a function of the AE wave's frequency content and the medium of wave propagation.

4.4 Analysing AE signals

A number of different signal-processing techniques and algorithms can be employed for mechanical diagnosis, and it is important to select the correct approach to gather the data required for an investigation. Three types of data acquisition techniques exist, which can be referred to as value type, waveform type and multidimensional type. The first of these, value-type data, consists of a single value collected at a specific time; data of the waveform type must be gathered as a series over time; while multidimensional-type data comes from multiple dimensions and is collected in a time epoch. For the purpose of condition monitoring, the most commonly used waveform data come from vibration signals and AEs. Others include ultrasonic signals, the current produced by a motor and partial discharge. For the purposes of waveform data analysis, three principal categories of analysis are employed, which are referred to as time-domain, frequency-domain and time-frequency, each of which are outlined in the following sections (Jardine et al., 2006).

Before data from the acoustic event itself can be analysed, it must be cleaned for the purposes of eliminating or reducing any noise disturbance and errors. This process must be carried out employing manually operated graphical tools. A range of signal processing techniques have been created to facilitate analysis and interpretation of condition monitoring and fault diagnosis data as, in reality, images taken from raw signals are generally used for feature extraction. However, data that can be used immediately for fault detection is unavailable. Therefore, better results and interpretation may sometimes be produced by combining image and waveform processing (Jardine et al., 2006).

4.4.1 Time-domain analysis

Time-domain analysis is widely used for the purposes of calculating impedance values along a transmission line, in addition to determining engine faults, with this being based directly on the time waveform itself. Typically, time-domain analysis involves calculating characteristic features from time waveform signals using descriptive statistics. These can include mean, peak, peak-to-peak interval, standard deviation, crest factor, together with other high-order statistics, for example, root mean square (RMS), skewness, kurtosis, etc. (Jardine et al., 2006).

Many time-domain analysis techniques can be used to analyse waveform data for machinery fault diagnostics, with time synchronous average (TSA) being one of the most popular time-domain approaches. The TSA makes use of the ensemble average of the raw signal over a number of evolutions in an attempt to remove or reduce noise and effects from other sources, so as to enhance the signal components of interest. TSA is given by equation 4-3.

$$\bar{S}(t) = \frac{1}{N}\sum_{n=0}^{N-1} s(t + nT), 0 \leq t \leq T \qquad (4\text{-}3)$$

where s(t) is the signal, *T* is the averaging period and *N* is the number of samples for averaging.

In more developed time-domain analysis approaches, time-series models are applied to waveform data. The primary basis behind time-series modelling is fitting waveform data to a parametric time series model in which to then obtain features built on this parametric model. Two models are most frequently cited in the literature: the autoregressive (AR) model and the autoregressive moving average (ARMA) model. An ARMA model of order *p,q*, denoted by ARMA(*p,q*), is expressed by equation 4-4:

$$x_t = a_1 x_{t-1} + \cdots + a_p x_{t-p} + \varepsilon_t - b_1 \varepsilon_{t-1} - \cdots - b_q \varepsilon_{t-q} \qquad (4\text{-}4)$$

where *x* is the waveform signal, ’s are independent normally distributed with mean 0 and constant variance ^{2}, and a_i, b_i are model coefficients. An AR model of order *p* is a special case of ARMA (*p,q*) in which *q* = 0. Poyhonen et al. applied the AR model to vibration signals collected from an induction motor and used the AR model coefficients as extracted features.

4.4.2 Frequency-domain analysis

Frequency-domain analysis is based on the transformed signal in the frequency domain, which makes it easier to identify and isolate certain frequency components of interest than is the case for time-domain analysis. Spectrum analysis using FFT is the dominant form of conventional analysis. This analysis technique either examines the whole spectrum or focuses on particular frequency components of interest, extracting these from the signal. The most commonly used tool in spectrum analysis is the power

spectrum which is defined as $E[X(f)X*(f)]$, where X(f) is the Fourier transform of signal x(t), E denotes expectation and $*$ denotes complex conjugate. Other useful auxiliary tools for spectrum analysis include graphical presentation of the spectrum, frequency filters, side-band structure analysis and envelope analysis (also called amplitude demodulation). The Hilbert transform is a useful tool in the latter form of analysis which has also been used for machine fault detection and diagnostics (Jardine et al., 2006).

Although the power spectrum has gained widespread acceptance, other spectra have been shown to possess specific benefits for signal processing analysis in certain cases. Among these, power spectrum, described as the inverse Fourier transform of the logarithmic power spectrum, is widely favoured for detecting harmonics and sideband patterns in power spectra. High-order spectra, such as bi- or tri-spectrum, can provide more diagnostic information for non-Gaussian signals than the power spectrum. These are actually the Fourier transforms of the third- and fourth-order statistics of the time waveform respectively. Bi-spectrum analysis has been shown to have wide application in machinery diagnostics for mechanical systems including gears, bearings, rotation and induction machines (Jardine et al., 2006).

Two approaches are generally adopted to power spectrum estimation. Initially, the non-parametric approach, estimates the autocorrelation sequence of the signal and then applies a Fourier transform to this estimated sequence. The second class, the parametric approach, involves creating a parametric model for the signal and then estimating the power spectrum on the basis of the model fit. The AR and ARMA models, respectively, are the two most commonly used parametric spectra in machinery fault diagnostics (Jardine et al., 2006).

4.4.3 Time-Frequency

One of the limitations of frequency-domain analysis is its inability to handle non-stationary waveform signals, which frequently occur in the case of machinery faults. Thus, time-frequency analysis, which investigates waveform signals in both time and frequency domains, has been developed for analysing non-stationary waveform signals. Typically, time-frequency analysis uses time-frequency distributions, which represent the energy or power of waveform signals in two-dimensional functions including both time and frequency. This provides more accurate diagnostics by more clearly revealing any fault patterns.

Short Time Fourier Transforms (STFT) or spectrogram (the power of STFT) and Wigner–Ville distribution are the most popular time-frequency distributions. The technique of STFT splits the entire waveform signal into segments within a short-time window and then applies a Fourier transform to each of these segments. As a result of this segmentation, spectrogram has constraints for time-frequency resolution, meaning that it can only be applied to non-stationary signals with slow-changing dynamics. However, bi-linear transforms such as the Wigner–Ville distribution, do not involve signal segmentation enabling them to overcome this time–frequency resolution limitation. Unfortunately, bi-linear transforms also have a major disadvantage due to the interference terms formed by the transformation itself. This makes it difficult to interpret the estimated distribution. Improved transforms have been developed to overcome this disadvantage such as the Choi–Williams distribution.

The analysis of engine data through time-frequency techniques relies upon both domains in order to generate a comprehensive illustration of engine state, explaining the evolution of the spectral of a signal content over time. Developments for analysing

non-stationary signals of time-frequency technology include the widely used STFT and the wavelet transform. The STFT captures the frequency characteristics as a function, using a sliding window. The resulting spectra correspond with the duration of this window. However, the limitation between the time and frequency resolution is an inherent drawback of STFT.

Another transform for time–frequency analysis is the wavelet transform. Unlike a time–frequency distribution, which is a time–frequency representation of a signal, wavelet transform is a time-scale representation of a signal. The wavelet transform is similar to the STFT but has been improved by achieving higher frequency and sharper time resolutions. Wavelet analysis can be used for constructing a normality model in both frequency and time. The wavelet transform represents a signal in terms of a family of wavelet basis functions, shifted in time and scaled in frequency. These basis functions are typically irregular in shape, making them suitable for the analysis of non-stationary signals with sharp changes, and compactly supported in time, enabling localization of a signal's features in time (Jardine et al., 2006; Clifton and Tarassenko, 2006).

One of the main advantages of wavelet transform is its ability to produce a high frequency resolution at low frequencies and a high time resolution at high frequencies for signals with long duration, low frequencies and short duration, high frequencies. Another advantage of wavelet transform is its ability to reduce noise in raw signals. Wavelet theory has developed rapidly in the past decade and has wide application. It has been successfully applied to waveform data analysis in fault diagnostics of gears, bearings and other mechanical systems. Time-frequency analysis of engine data combines both domains for a more complete representation of engine state,

describing the evolution of the spectral content of a signal through time (Clifton and Tarassenko, 2006). Recently, more extensive applications of wavelet transform for signal processing in machine condition monitoring and fault diagnostics have been successfully attempted (Jardine et al., 2006).

4.5 3D Finite Elements Result

The tested power electronic device was modelled using COMSOL finite element software package, see Figure 4.11.

A 3-D finite element IGBT model was derived using COMSOL Multiphysics modelling software to provide a simulation that can be tested and then used in a real situation. The heat distribution through each material was determined, as were the collector and emitter, all of which formed the parameters.

The mesh size for the transistor is based on the surface area covered, with the transistor itself comprised of three distinct separate parts; a thin top structure, a slightly thicker bottom portion and the three pins which are connected to the thicker base. The whole structure is made of ceramics. As for its measurements, the thinner, top part of the transistor is 1.39mm in its thickness, with its height expressed as 6.47mm. The hole which appears in this structure (in the centre) has a diameter of 3.61mm. The thicker base is 4.82mm in its thickness, with its height at 12.71mm. The length of the three metal pins that make up the remainder of the structure are 14.27 in length, with a thickness of 1.52mm for each. Finally, the space separating each pin is 1.15mm, with the overall length and width of the entire transistor being 30.02mm and 9.66mm respectively.

The materials modelled for the semiconductor were silicon oxide. The collector pin is directly attached to the case. The gate and emitter on the other hand are connected to wire bonds. Chip areas can also be seen in Figure 4.20 (b) for each IGBT technology. The heat transfer coefficient h is defined as 5 W/m^2K over the model representing natural convection in heating unit. For higher current applications, heat sink model is built in rear side of the case through mica layer where the thermal grease boundary is defined as heat remover.

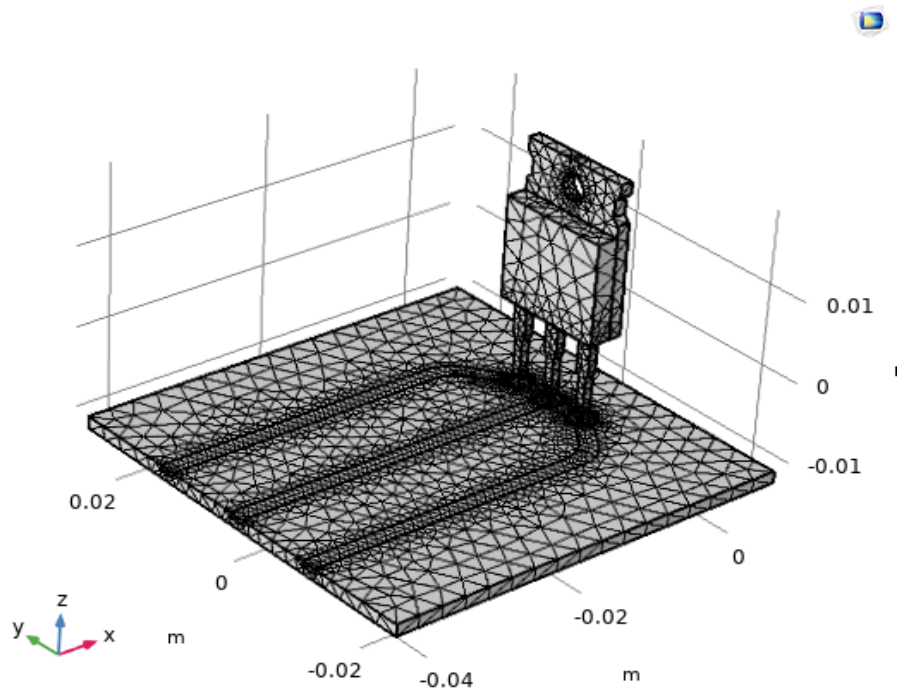

Figure 4.11 Meshing processing in COMSOL

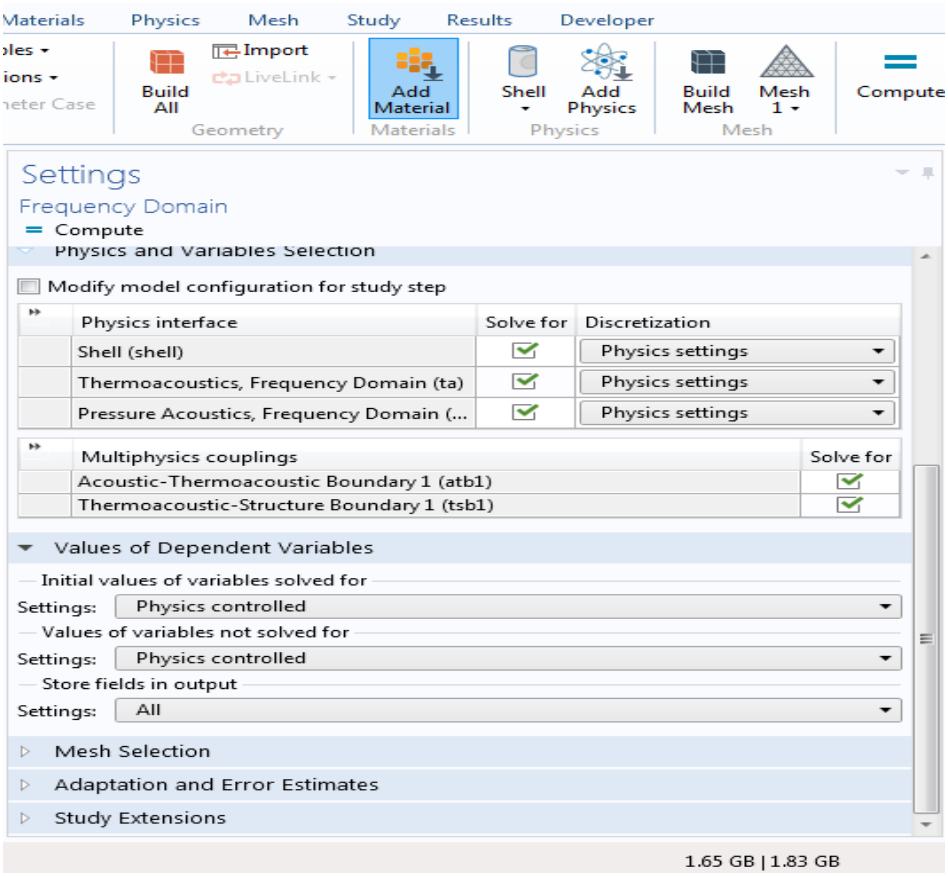

Figure 4.12 Inputting operation parameters in COMSOL

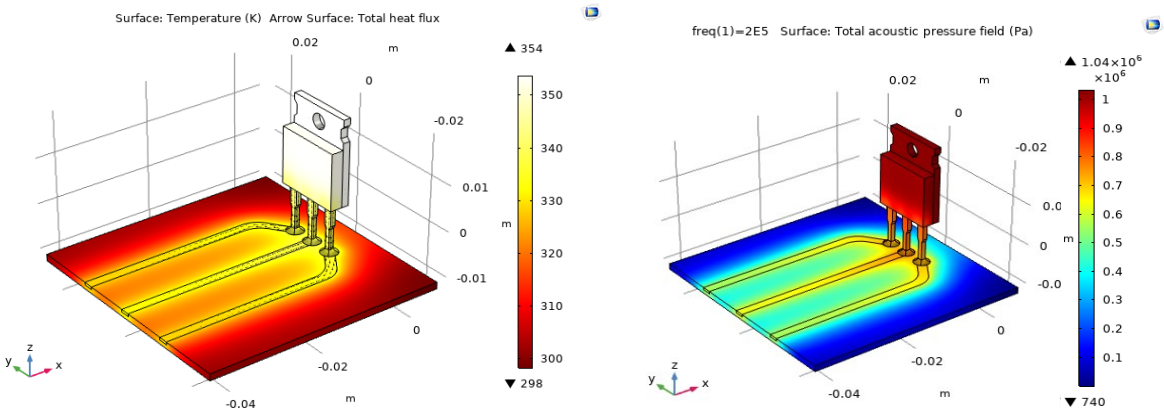

Figure 4.13 Variation of thermal and acoustic signal in COMSOL

5 Experimental Set up and Results

5.1 Introduction

The chapter begins by describing how the experimental testbed was set up to evaluate the practical characteristics of AE signals in PEDs, using an AE sensor and an appropriate data acquisition tool. Then, the results of this technical analysis are presented.

5.2 Experimental set-up

AE is a NDT that can be used to monitor IGBT modules. Compared to previous techniques which require hardware intervention to measure the electrical characteristics of PEDs, AE has the advantage of predicting their condition with minimal installation effort. Previous research has shown that AE has the ability to detect changes in the electrical characteristic in PEDs (Kärkkäinen et al., 2014a; 2014b 2015a; 2015b). An experimental testbed was set up to measure the acoustic signal emitted from an IGBT module at different junction current and switching frequencies.

A block diagram of the experimental set-up is shown in Figure 5-1. The actual experimental testbed can be seen in Figure 5-2. It consists of a pulse generator, a DC-DC converter, a transducer (see 5.2.1), an amplifier and data acquisition equipment. The function of each element is as follows: The pulse generator is used to drive the IGBT of the DC-DC converter while the transducer is set up to capture the acoustic wave generated by the IGBT of the converter. An AE sensor model NS2000m (from AV Technology) was used to gather the data and a 40 dB amplifier amplified its outputs, as shown in Figure 5-6a and b respectively.

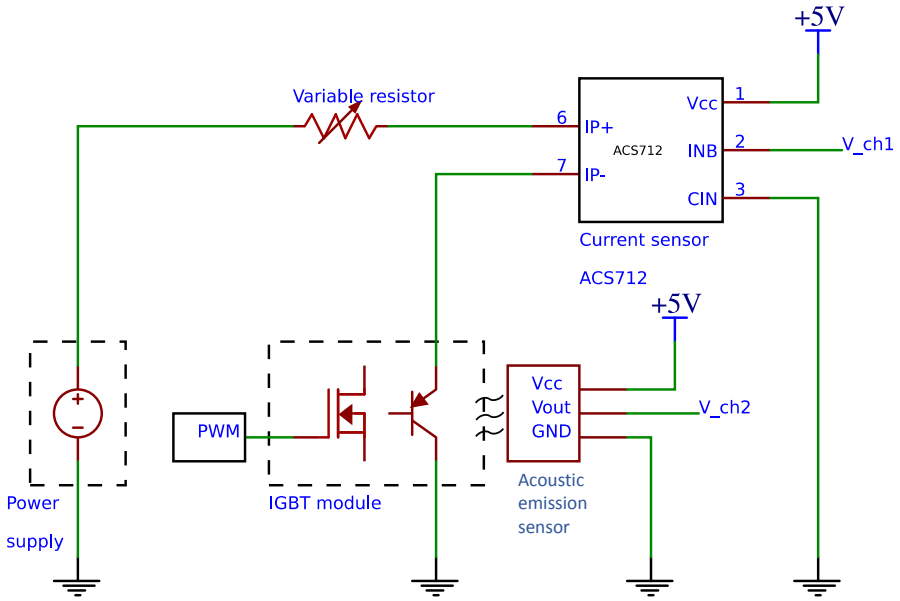

Figure 5-1: Block diagram of the experimental set-up

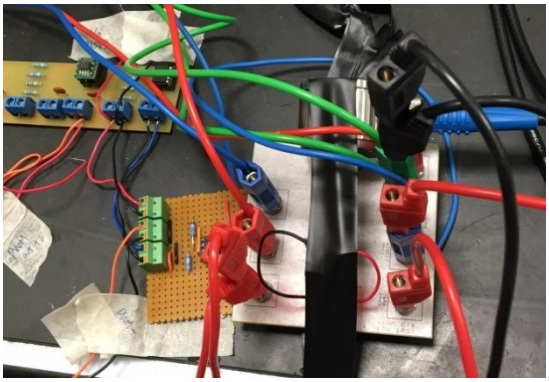

Figure 5-2: Practical experimental set-up

5.2.1 Ultrasound transducer

The transformation of an ultrasound wave from sound into a signal or vice versa is based on a principle called the piezoelectric (pressure electricity) effect, first investigated by Pierre and Jacques Curie (1880). AE sensors respond to the dynamic motion caused by an AE event. This can be achieved through transducers that convert mechanical movement into an electrical voltage signal. Thus, an ultrasound transducer constitutes an essential part of the AE technique and ultrasound testing equipment. A piezoelectric crystal, commonly made from a ceramic such as lead zirconate titanate

(PZT) acts as the transducer element in an AE sensor. Through applying an electrical current to the crystal it is apparent that the crystal appears to change shape resulting in vibrations which emit soundwaves that move outwards. However, when sound or pressure waves hit the crystal, they produce electric current (Surgeon, 2002).

A typical commercial transducer is shown in Figure 5-3 while Figure 5-4 shows a cross section of an ultrasound transducer. Transducers are selected on the basis of their operating frequency, sensitivity and environmental characteristics. The AE sensor shown in Figure 5.3 was coupled to the IGBT surface using an ultrasonic coupling gel. For each test condition, the LabVIEW codes collected 8 sets of data, averaged, to reduce random noise and to ensure repeatability.

Figure 5-3: Photograph of an ultrasound transducer

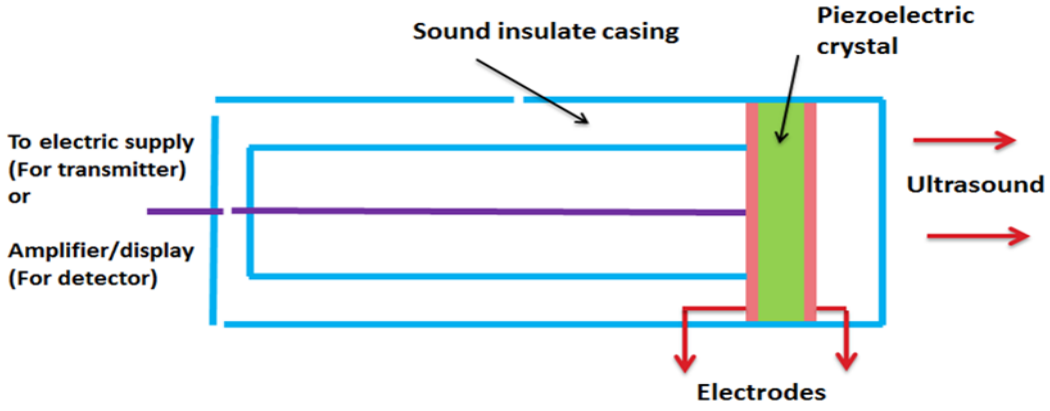

Figure 5-4: Cross-section of a piezo-electric transducer

5.3 Software layer of the experimental testbed

5.3.1 Fast Fourier Transform

The Fast Fourier Transform (FFT) is a widely used method of measurement in acoustics. It can be used to convert a complex acoustic signal down into its individual spectral components and to provide information about the frequencies of the waves that make up that signal. It has numerous applications in various types of digital signal processing, and is frequently used for quality control, fault analysis, and condition monitoring of systems or machines.

Effectively, the FFT is an optimised algorithm based on the 'divide and conquer' principle, to facilitate the calculation the Discrete Fourier Transform (DFT) of a sequence, or its inverse (IFFT). It involves dividing the signal into two smaller signals, compute the DFT of the two smaller signals and then join them again to obtain the DFT of the original signal. The order of complexity of DFT is O(n^2) while that of FFT is O(n.logn) hence, FFT is faster than DFT. A signal is sampled over a period of time and split into its frequency components. These components consist of individual sinusoidal oscillations occurring at different frequencies, each of them with its own amplitude and phase. The FFT can reveal the frequency components of a signal, by plotting the amplitudes and phases of cosines and sines against their respective frequencies (Sedjić et al., 2009). This transformation is illustrated in Figure 5-5 and shows that over the period of time measured, the signal consists of three distinct dominant frequencies.

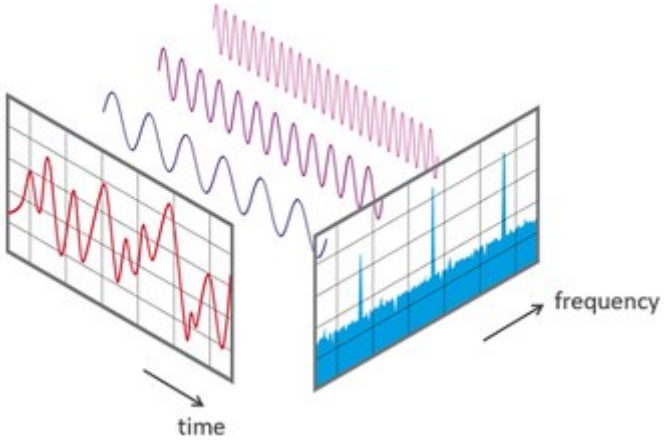

Figure 5-5 View of a signal in the time and frequency domain (source: NTI Audio)

5.3.2 Short Time Fourier Transform

A second calculation, known as the Short-Time Fourier Transform (STFT), was utilised in this research. This was used to establish the sinusoidal frequency and phase content of local sections of the acoustic signal emitted as it alters over the course of time. The procedure for calculating STFT involves dividing each length of time signal into shorter segments consisting of equal lengths. The Fourier transform is then calculated for each of these shorter segments individually. This procedure then reveals the Fourier spectrum for the separate shorter segments. These changing spectra are then usually plotted as a function of time (Sedjić et al., 2009).

5.4 Test procedure

Tests were carried out using the DC-DC boost converter shown in Figure 5-7. The driving signal was set up at 50% duty cycle, boosting the input voltage from 5 V to 9 V. The boost converter circuit and its associated printed circuit board are shown in Figure 5-6a and b respectively. For each experiment, the AE signals were recorded at different pulse frequencies ranging from 10 kHz to 300 kHz.

The two output channels of the experimental set-up, namely V_ch1 and V_ch2, were connected to a data acquisition unit, ELVIS II (National Instrument). The sampling frequency of the unit was 750 kHz, which is greater than the doubled value of the highest switching frequency to be measured. The measurement voltage range was set between -1 V and 1 V, due to the low voltage level of the AE signal. National Instrument's LabVIEW software package was used to interface with the data acquisition unit.

(a) (b)

Figure 5-6: (a) The NS2000m AE sensor (b) Pre-Amplifier

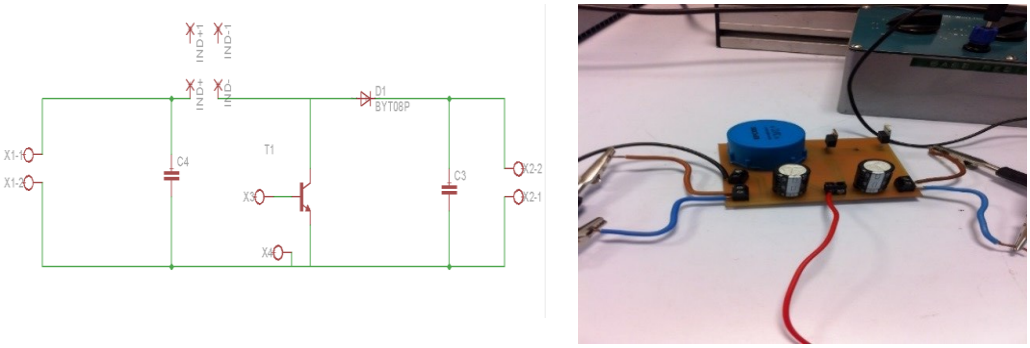

(a) (b)

Figure 5-7: The boost converter device (a) Schematic diagram (b) Photograph

5.5 Results for time and frequency domains

The experiment was carried out for two different settings: changes in switching frequency and the collector-emitter current (junction current) of the IGBT module.

5.5.1 Effect of switching frequency on AE

A set of experiments (see Figure 5-8) shows the AE peak at every rising and falling edge of the collector-emitter voltage, excited by the PWM generator with frequencies ranging from 10 kHz to 300 kHz. The transition effect is instant demonstrating that the AE signal can be applied to investigate the electrical behaviour of an IGBT. A more detailed view of transition stage data is shown in Figure 5-9. It would be useful to investigate this transition edge further by monitoring algorithm formulation.

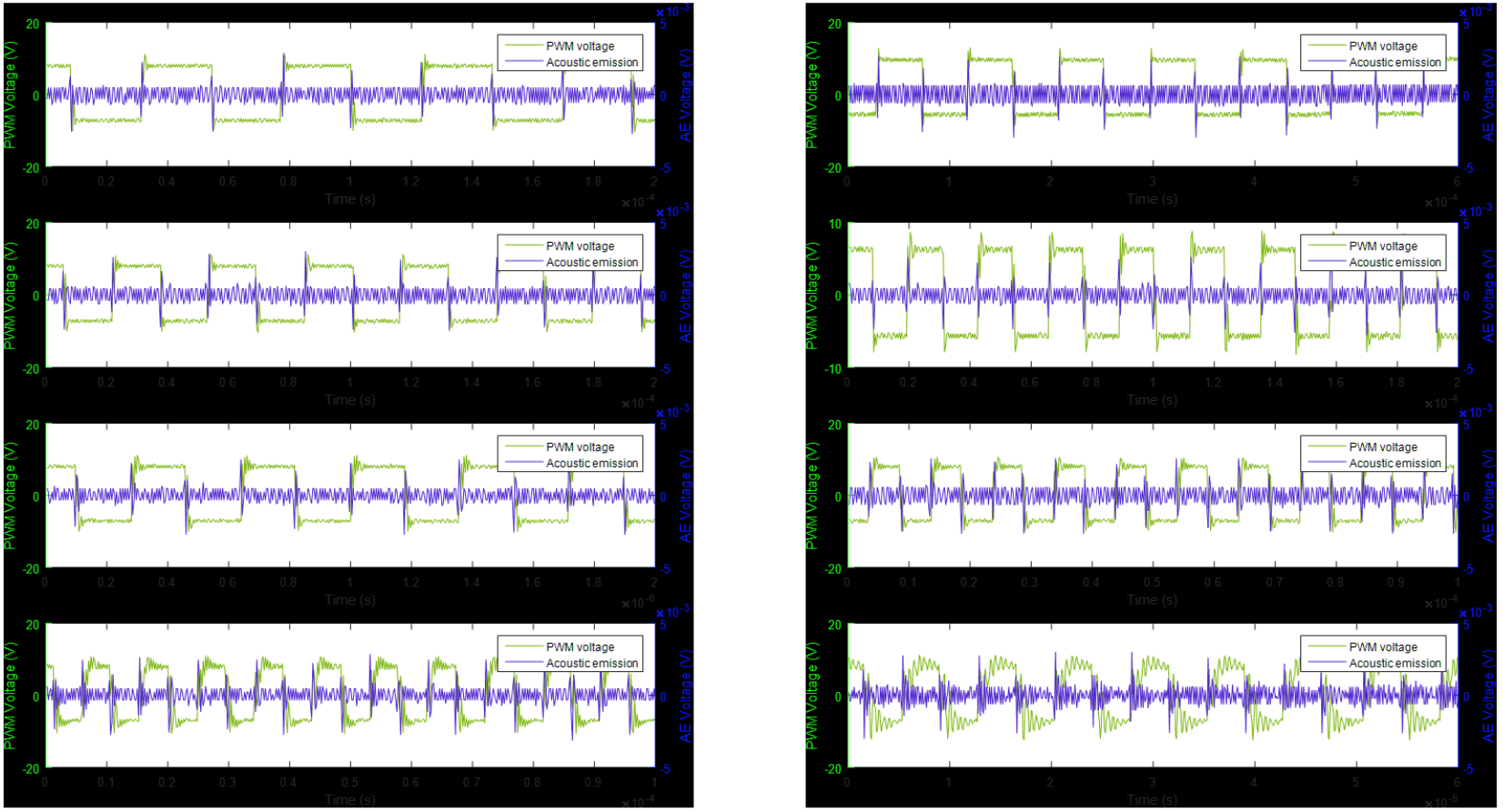

Figure 5-8: AE signal at different switching frequency of collector-emitter voltage level, excited by the PWM generator.

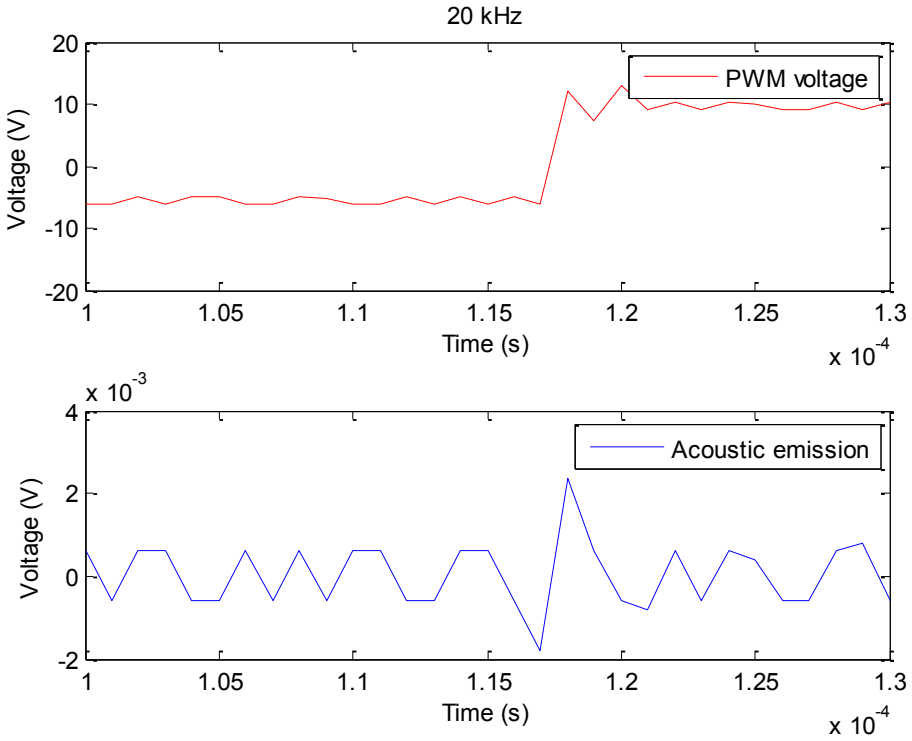

Figure 5-9: Voltage level at rising edge of collector-emitter voltage and AE signal.

5.5.2 Effect of collector-emitter current on AE

Reducing the resistive load increases the junction current across the IGBT module. Interesting results can be observed at the peak of the AE signal (illustrated in Figure 5-10) which formulates a potential mathematical model for a power loss model as depicted in 5-1 Drawing on this Foster network thermal equation, Canras et al. (cited in Batunlu and Albarbar, 2015a) suggested that the referenced value for $P_L(t)$ can be obtained by using a datasheet, simulations or experiments. They referred to the power loss model cited in previous studies, which can be formulated in a 4th order polynomial equation as depicted:

$$P_L(t) = -0.08I_c(t)^4 + 0.65I_c(t)^3 - 1.84I_c(t)^2 + 3.01I_c(t) + 0.68 \quad 5\text{-}1$$

where $P_L(t)$ is the function of transient power loss and $I_c(t)$ is the collector-emitter current across IGBT module.

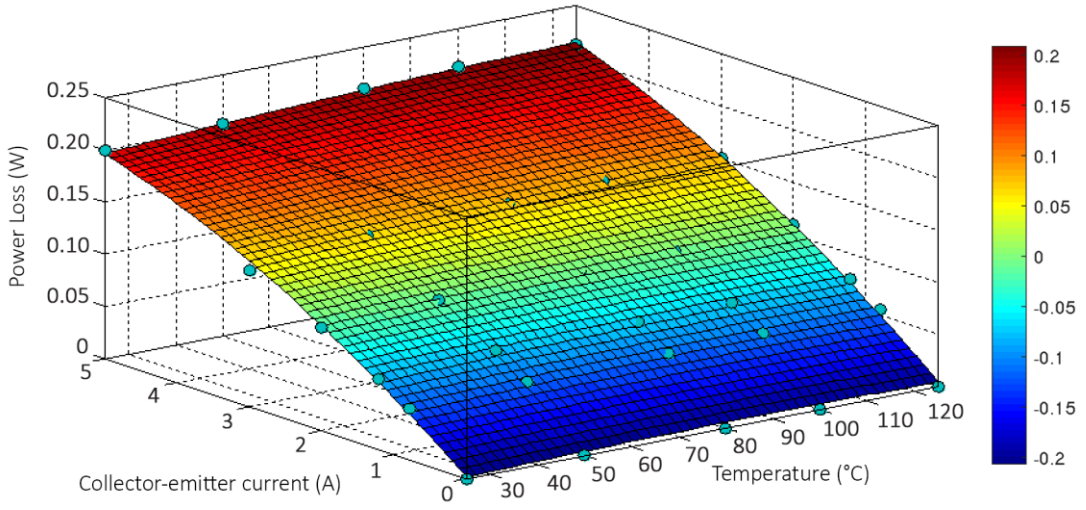

Figure 5-10: Power loss model against collector-emitter current and temperature in 3-D space

To determine the effect of collector-emitter current on AE signals, several experimental results were obtained based on different loads, which changes the collector-emitter current of the experimental testbed. Five datasets were gathered from the collector-emitter current ranging from 0.1A to 2.0A: (a) 0.1A; (b) 0.5A; (c) 1.0A; (d) 1.5A and (e) 2.0A. Figure 5-11 to Figure 5-15 show the AE signals at different collector-emitter current conditions. It can be observed that, the increase of collector-emitter current has proportional effect to the AE amplitude. However, based on Figure 5-11, Figure 5-12 and Figure 5-13, acoustic signal amplitude in (b) is lower than (a). Such phenomenon has to be revised and re-evaluated in future work.

Based on the observation, it can be used to formulate a general mathematical expression covering the electro-thermal behaviours of PEDs and AE signals, as collector-emitter current plays an important role in predicting the correct temperature characteristics of these devices.

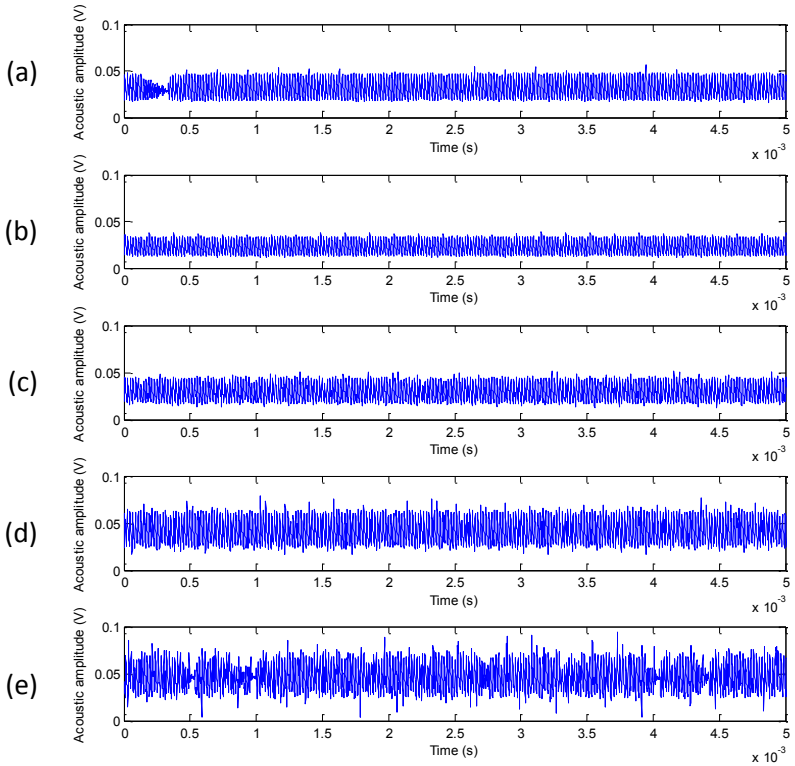

Figure 5-11: Voltage amplitude of AE signal under different collector-emitter current at 10kHz switching frequency: (a) 0.1A; (b) 0.5A; (c) 1.0A; (d) 1.5A; (e) 2.0A.

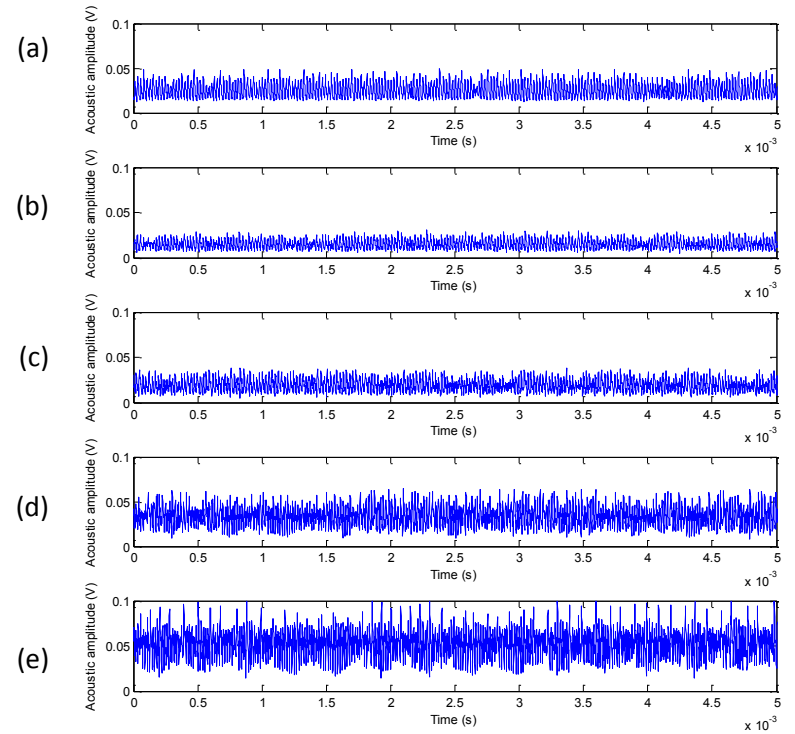

Figure 5-12: Voltage amplitude of AE signal under different collector-emitter current at 50kHz switching frequency: (a) 0.1A; (b) 0.5A; (c) 1.0A; (d) 1.5A; (e) 2.0A.

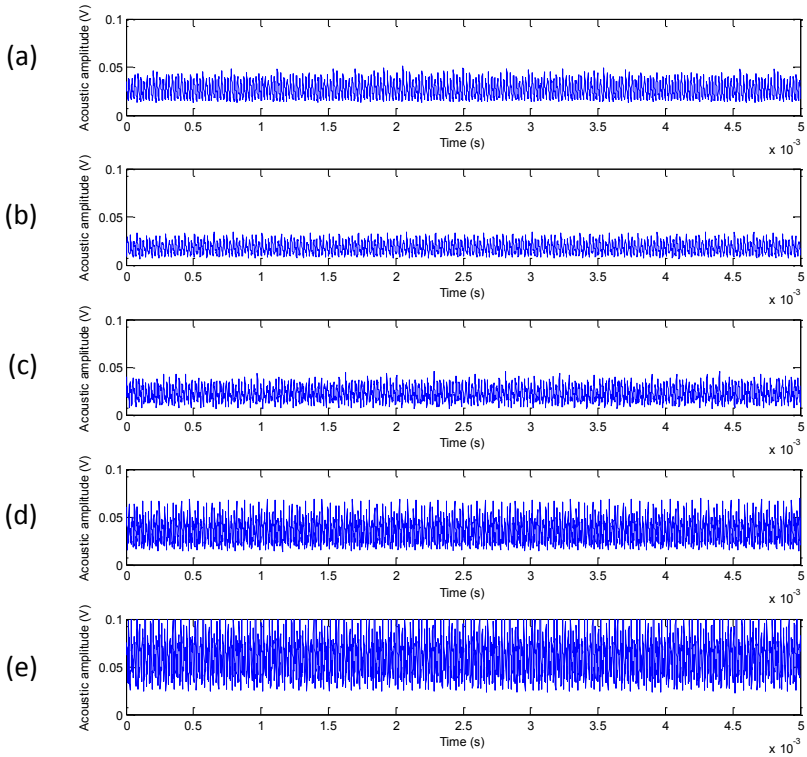

Figure 5-13: Voltage amplitude of AE signal under different collector-emitter current at 100kHz switching frequency: (a) 0.1A; (b) 0.5A; (c) 1.0A; (d) 1.5A; (e) 2.0A.

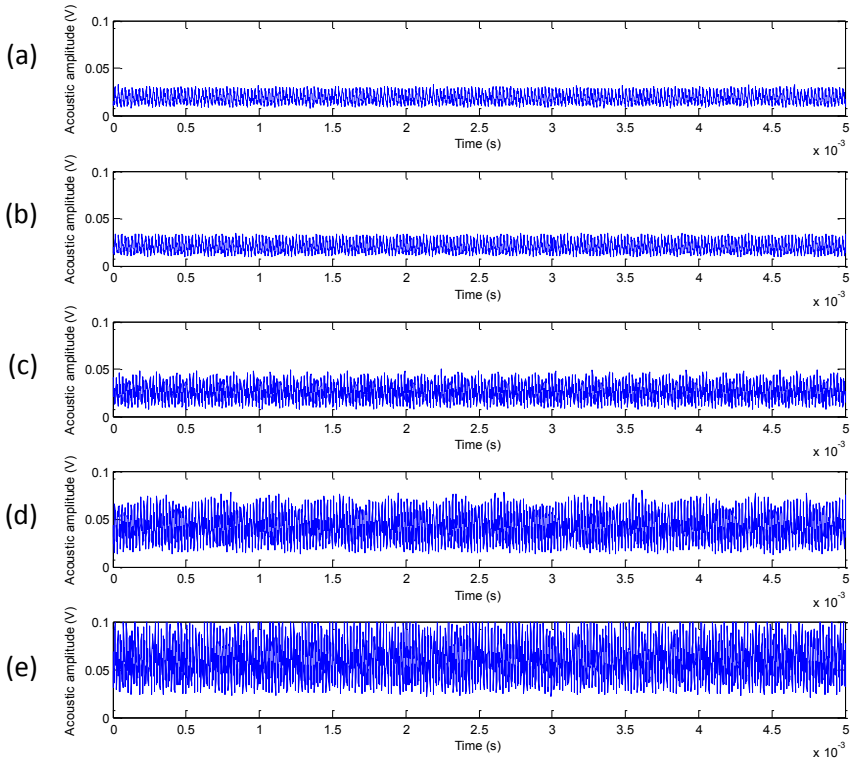

Figure 5-14: Voltage amplitude of AE signal under different collector-emitter current at 200kHz switching frequency: (a) 0.1A; (b) 0.5A; (c) 1.0A; (d) 1.5A; (e) 2.0A.

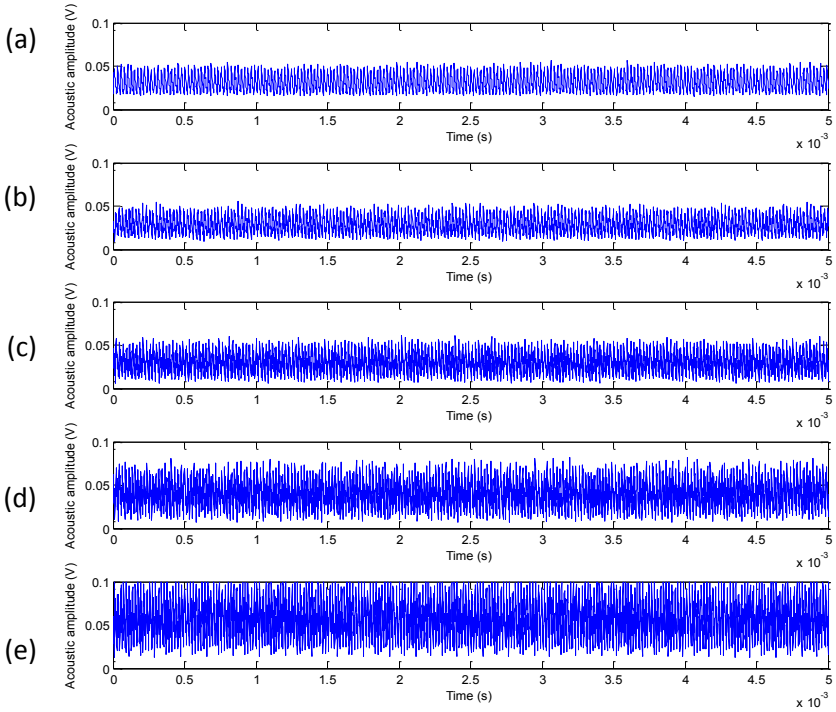

Figure 5-15: Voltage amplitude of AE signal under different collector-emitter current at 300 kHz switching frequency: (a) 0.1A; (b) 0.5A; (c) 1.0A; (d) 1.5A; (e) 2.0A.

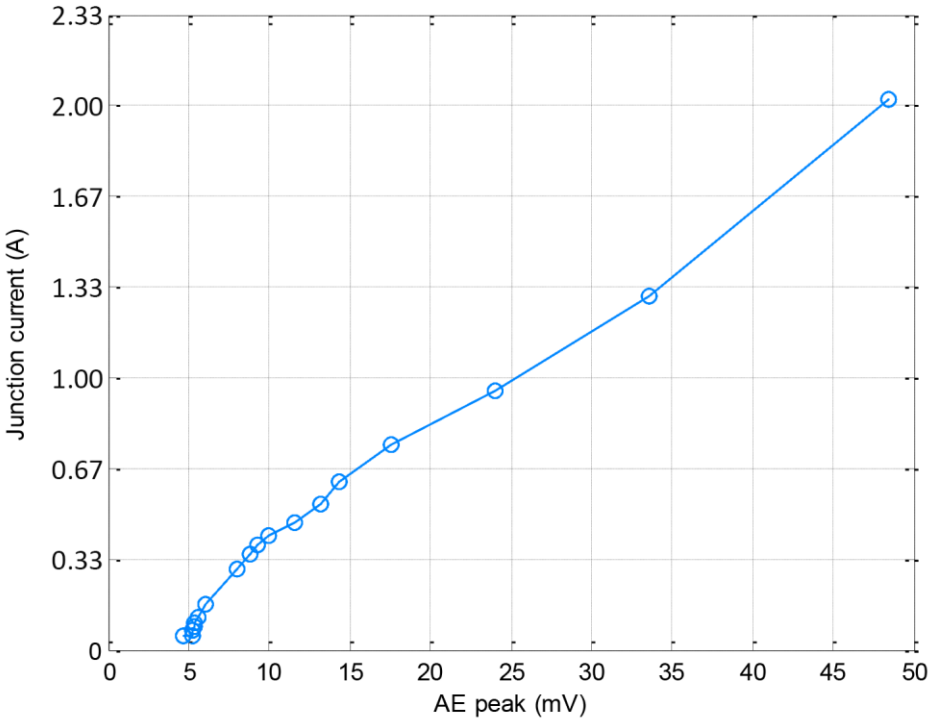

Figure 5-16: Increased AE peak when junction current is increased.

Figure 5.16 summarise the demonstrates that when the junction current increases that the amplitude of AE increases, also. The relationship between the collector-emitter current and AE voltage peak is numerically established using nth order polynomial regression method. In 4th order analysis, the following equation can be expressed as shown:

$$I_c = (-5.83 \times 10^{-7}){A_p}^4 + (7.54 \times 10^{-5}){A_p}^3 + (-3.27 \times 10^{-3}){A_p}^2 + 0.08A_p - 0.28 \quad \text{5-2}$$

where I_c represents junction current and A_p represents AE signal peak, which can be automatically obtained using threshold algorithm. 5-2 can be substituted into 5-1to determine P_L. Ultimately, electro-thermal temperature can be calculated using equation 4.1 with P_L from equation 5.1.

5.5.3 Effect of ambient electro-thermal on AE

An alternative set of experimental data was extracted to determine the thermal-behaviour of AE signals. The effect of ambient temperature on the IGBT module at different collector-emitter currents is shown below (Figure 5-17 to Figure 5-19).

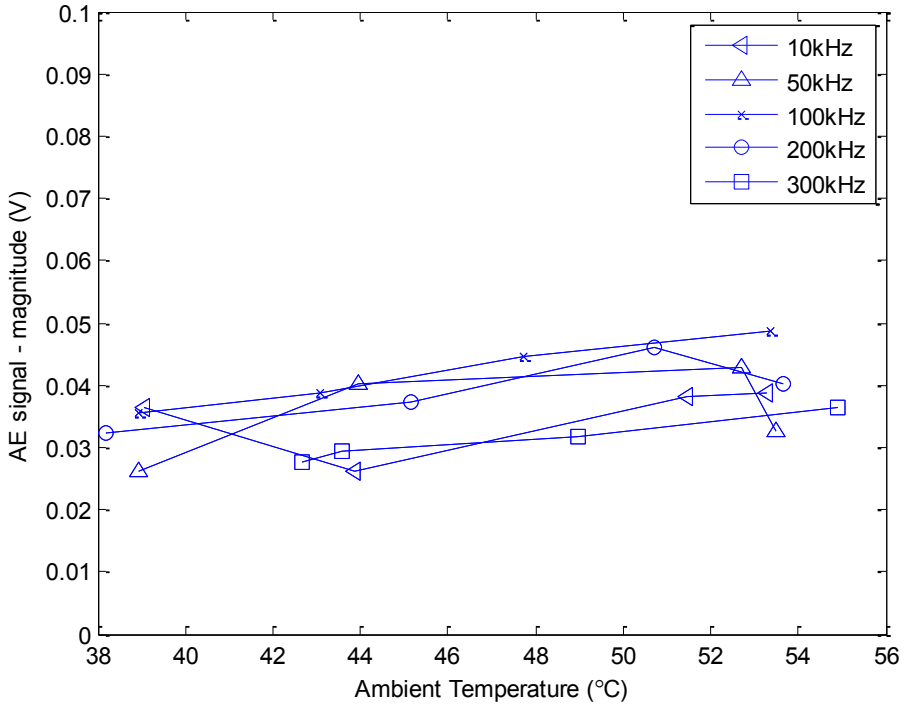

Figure 5-17: Voltage magnitude of AE signals against ambient temperature at 500mA collector-emitter current.

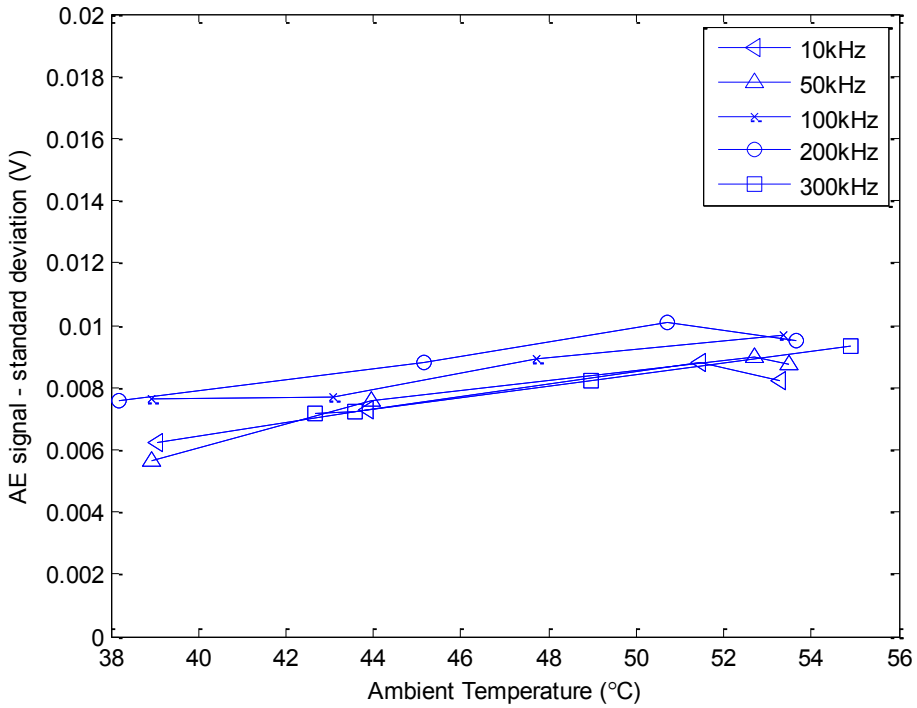

Figure 5-18: Standard deviation of AE signals against ambient temperature at 500mA collector-emitter current.

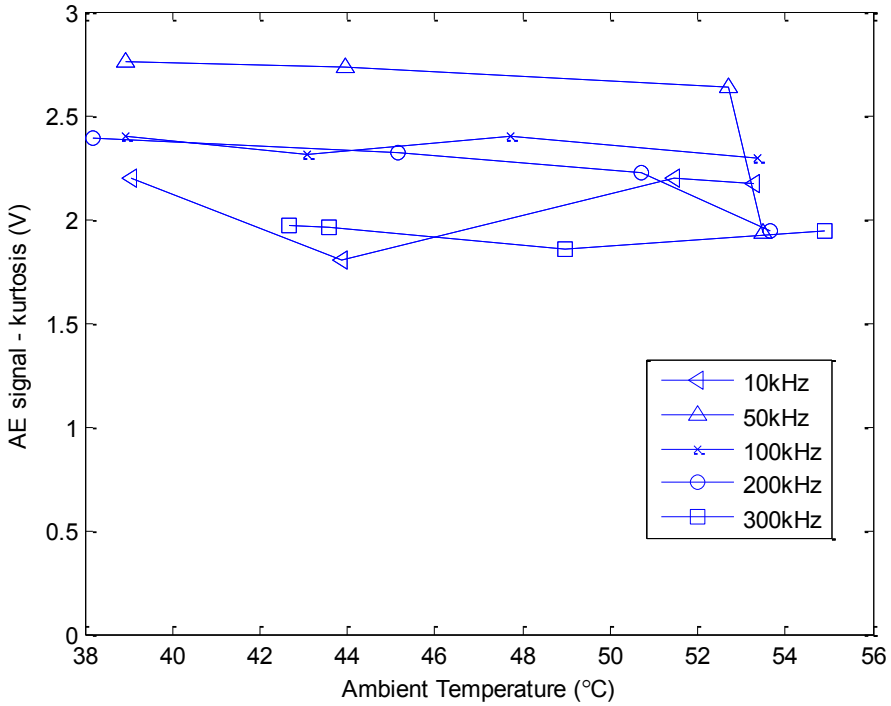

Figure 5-19: Kurtosis of AE signals against ambient temperature at 500mA collector-emitter current.

Based on figures 5.17 to 5.19 (above), three types of statistical parameters, namely, magnitude, standard deviation and kurtosis were calculated from the AE signals.

In the first one (Figure 5.17), the acoustic emission (AE) signal was measured based on different levels of ambient temperature by varying the AE signal at disparate frequencies, starting from 10Hz, going up to 50Hz, 100Hz, 200Hz, and finally 300Hz. It was noted that the output of the AE signal at various temperatures fluctuated between 200mA and 500mA. The figures also indicated that the most logical increase in AE signal occurred at 100Hz. All of the other frequencies tended to rise and then tail off as temperatures were increased. This requires further investigation as a uniform rise in AE signal was only achieved at one of the five frequencies tested. In the second diagram (figure 5.18), all of the criteria used in figure 5.17 were maintained, except

that the AE signal was now based on standard deviation instead of magnitude. The results in general showed a more logical increase in AE signal across all frequencies (from 10Hz to 3000Hz). From the frequencies tested, the best results achieved were at 200Hz. Finally, in the last diagram (figure 5.19) all criteria were repeated as per figures 5.17 and 5.18, except that the AE signal was now measured based on kurtosis. It was observed that at higher temperatures for kurtosis, the AE signal generally tended to diminish across all frequencies. In addition, it is also noted that none of the data produced using kurtosis can be relied upon due to the decrease in AE signal across the all frequencies.

Based on the calculated parameters, it can be inferred that for all three AE signal measurements, changes in ambient temperature at the levels that have been tested have not significantly affected AE signals in a positive manner. Furthemore, AE signals for each measure tested (magnitude, standard deviation and kurtosis) demonstrated a decrease in AE signal between a range of 50-55 °C . Moreover, the switching frequency of the PWM signal does not contribute weighted elements in AE signals at different ambient temperatures.

5.5.4 Comparisons of electro-thermal behaviour with measurement from temperature sensor

To validate the predicted electro-thermal values based on an AE signal, the transient model was loaded into a virtual acquisition tool called LabVIEW. Figure 5-20 the block diagram consists of an equivalent thermal model of the experimental testbed, matching its respective 3rd order thermal Foster network. The measured AE peak was loaded to the LabVIEW model and the electro-thermal temperature for that particular instance was calculated. It was then compared with a referenced temperature sensor,

LM35DZ, which continuously measures the surface temperature of the IGBT module. Their performance can be observed in Figure 5-21. The monitoring based on the AE signal is identical to the referenced sensor, which proves it is a potential candidate to investigate the behaviour of PEDs.

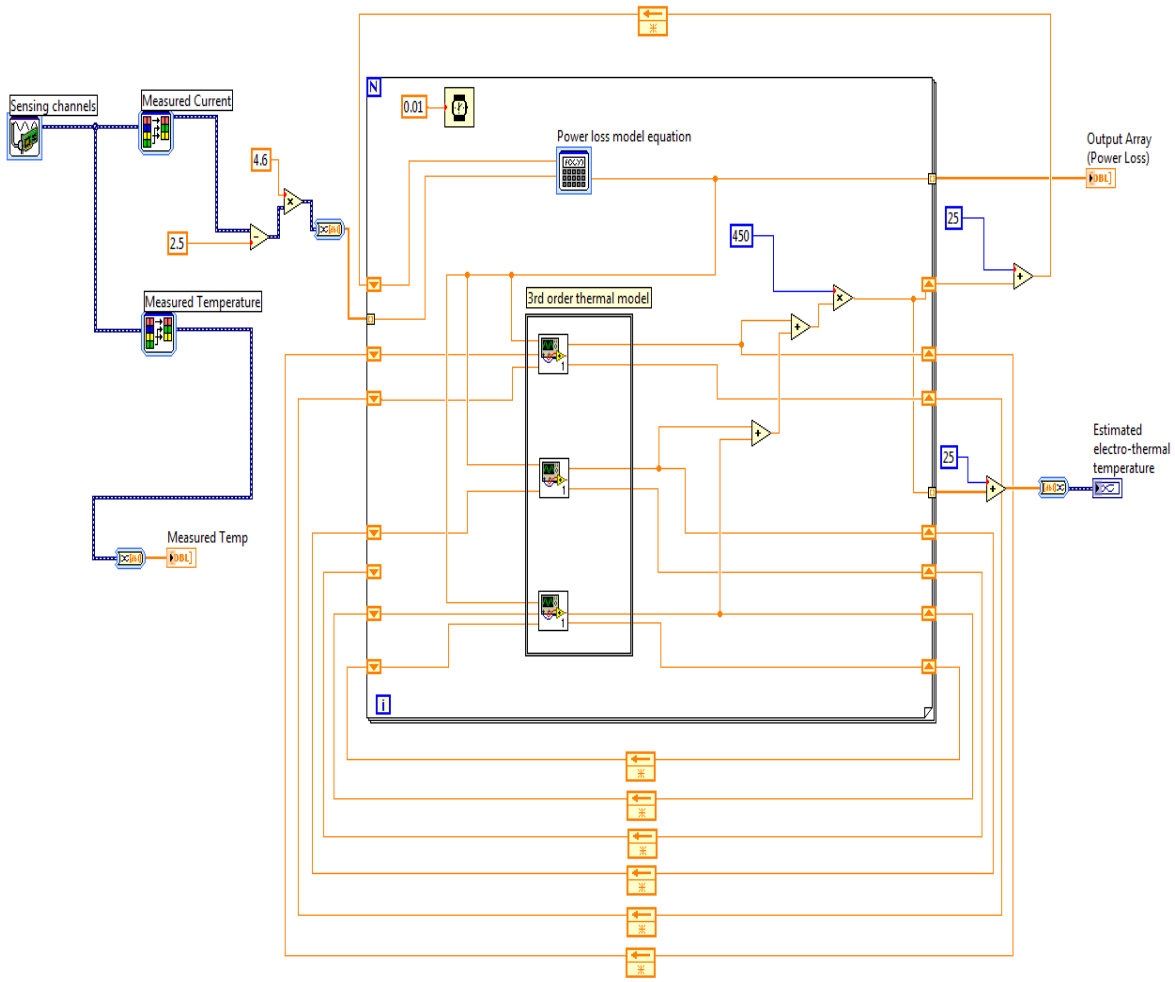

Figure 5-20 Equivalent functional block diagram of AE monitoring system for IGBT module.

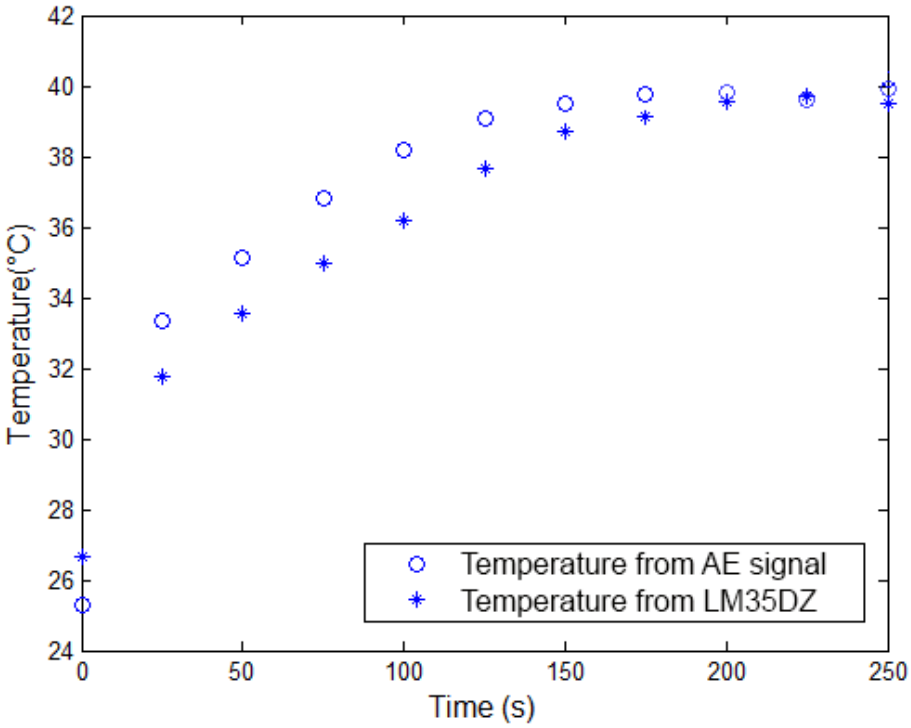

Figure 5-21: Transient electro-thermal behaviour of IGBT measured from AE signal and referenced temperature sensor LM35DZ.

5.6 Short-time Fourier transform analysis for AE signal

5.6.1 Overview

Based on the periodic characteristics of the AE signal when measuring collector-emitter current, it is believed that a power magnitude at frequency spectrum could be extracted for determining accurate current level. Figure 5-22 shows the functional block diagram for the AE signal using STFT and local maxima detection.

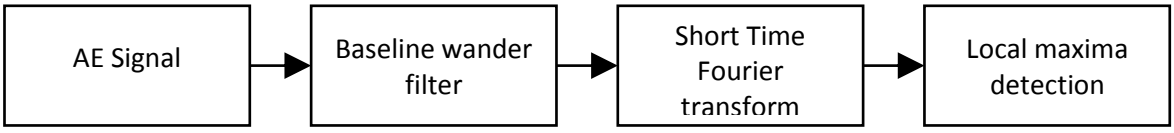

Figure 5-22 Functional block diagram for AE signal using STFT and local maxima detection

A baseline wander filter was used to eliminate low frequency components, such as DC offset. Then a 4^{th} order high pass Butterworth filter with a 1000 Hz cut-off frequency

was used. The AE signal is used to measure high frequency AE, hence it is acceptable to reduce any noise below 1000Hz. Figure 5-23 shows the frequency and phase response of the baseline wander filter.

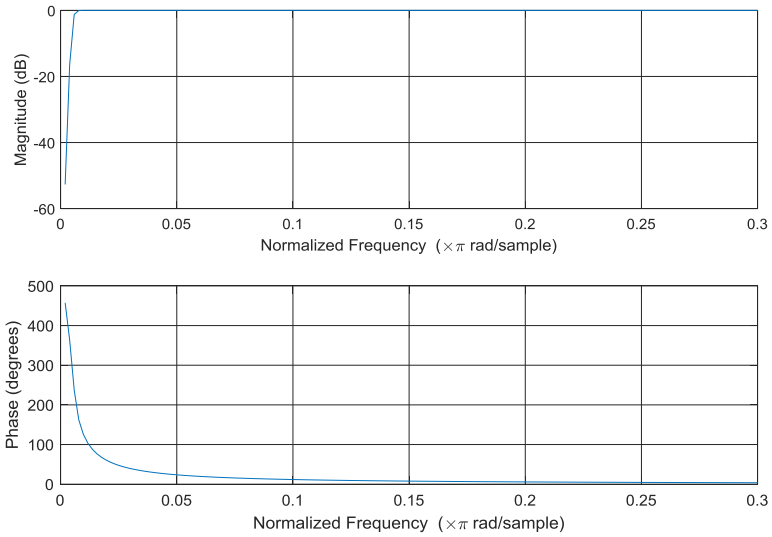

Figure 5-23 Frequency and phase response of applied 4th order high pass Butterworth filter

5.6.2 Offline fast Fourier transform analysis on AE signal

Figure 5-24 to Figure 5-28 show the power spectrum of the AE signal under different collector-emitter currents, from 10kHz to 300kHz frequency. Offline FFT processing was used to convert the time domain signal into the frequency domain signal.

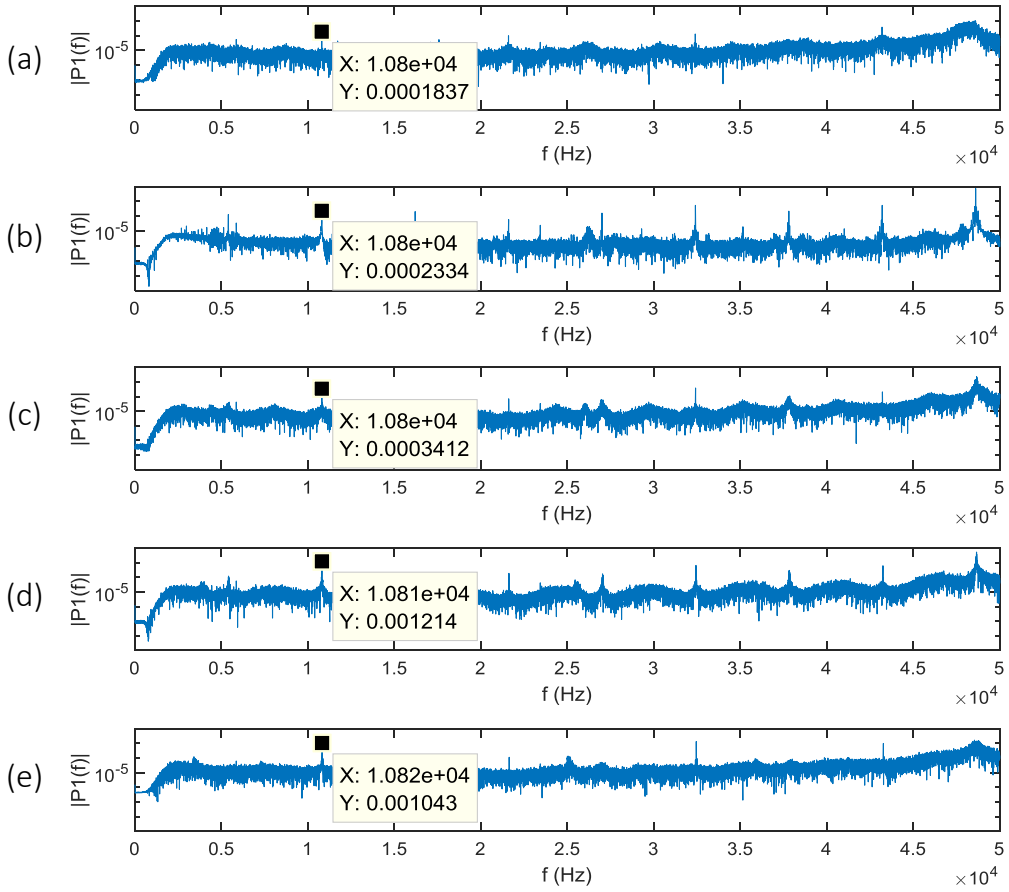

Figure 5-24 Power spectrum of AE signal under different collector-emitter current at 10kHz switching frequency: (a) 0.1A; (b) 0.5A; (c) 1.0A; (d) 1.5A; (e) 2.0A.

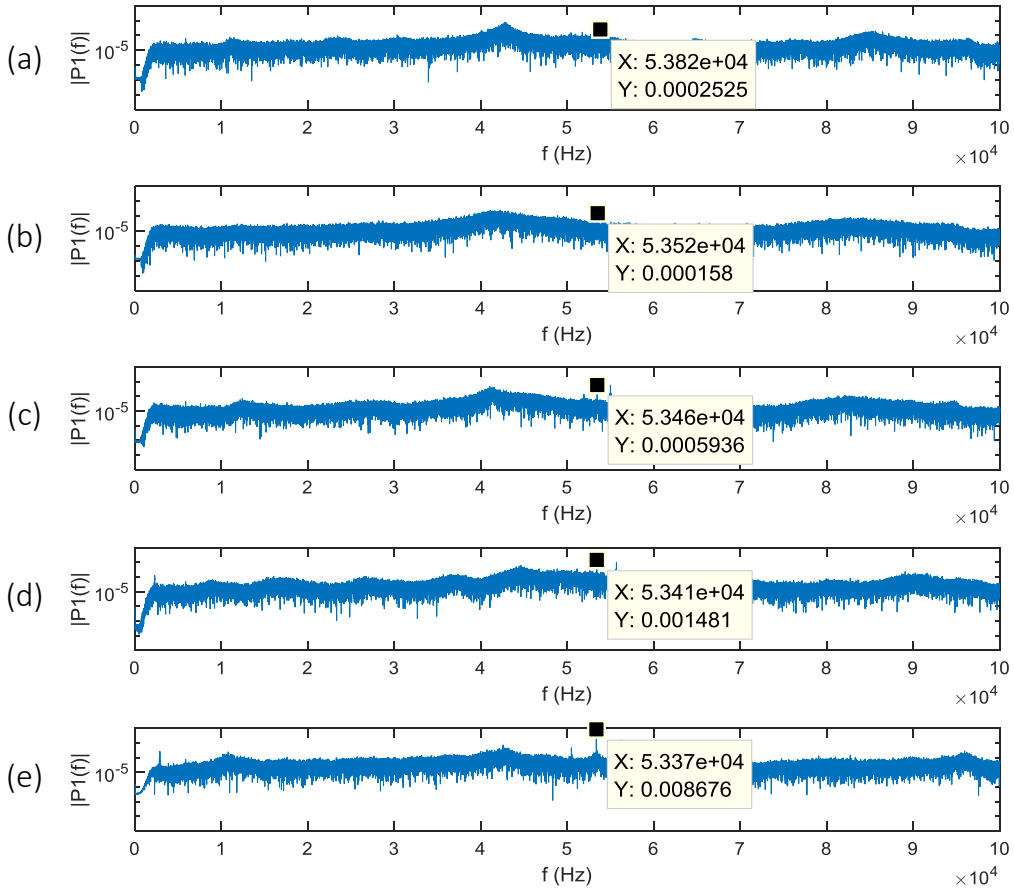

Figure 5-25 Power spectrum of AE signal under different collector-emitter current at 50kHz switching frequency: (a) 0.1A; (b) 0.5A; (c) 1.0A; (d) 1.5A; (e) 2.0A.

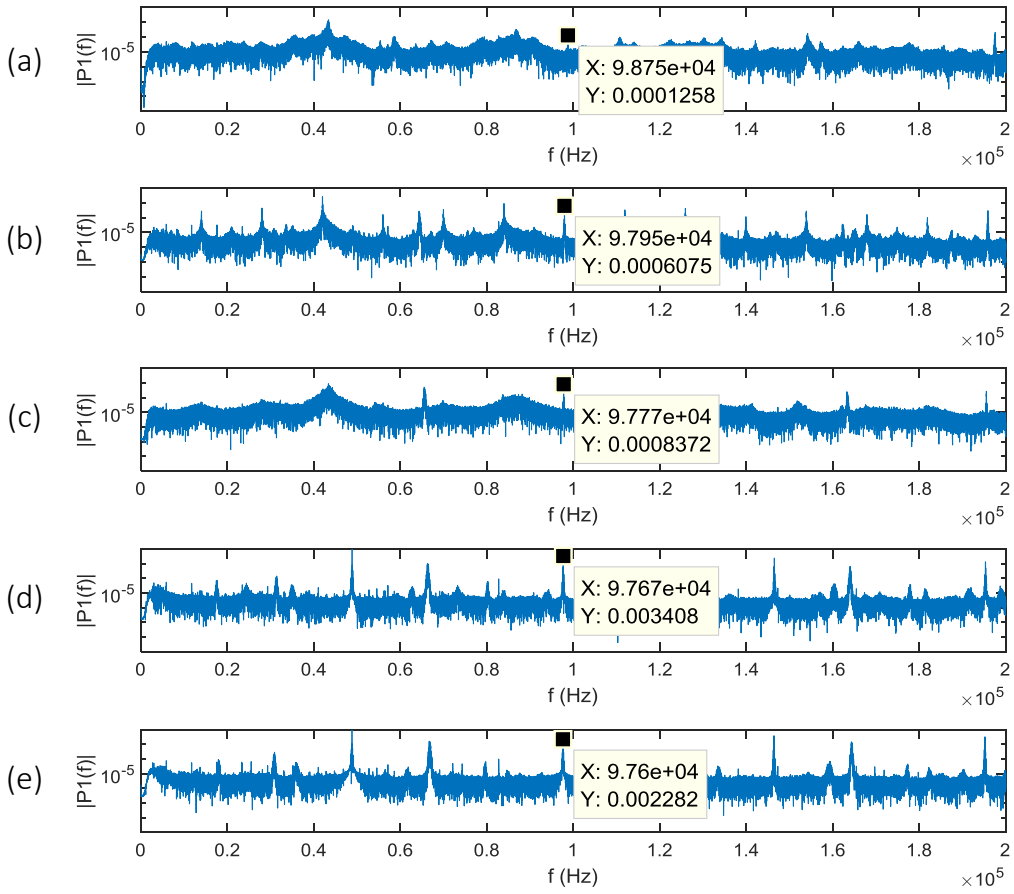

Figure 5-26 Power spectrum of AE signal under different collector-emitter current at 100kHz switching frequency: (a) 0.1A; (b) 0.5A; (c) 1.0A; (d) 1.5A; (e) 2.0A.

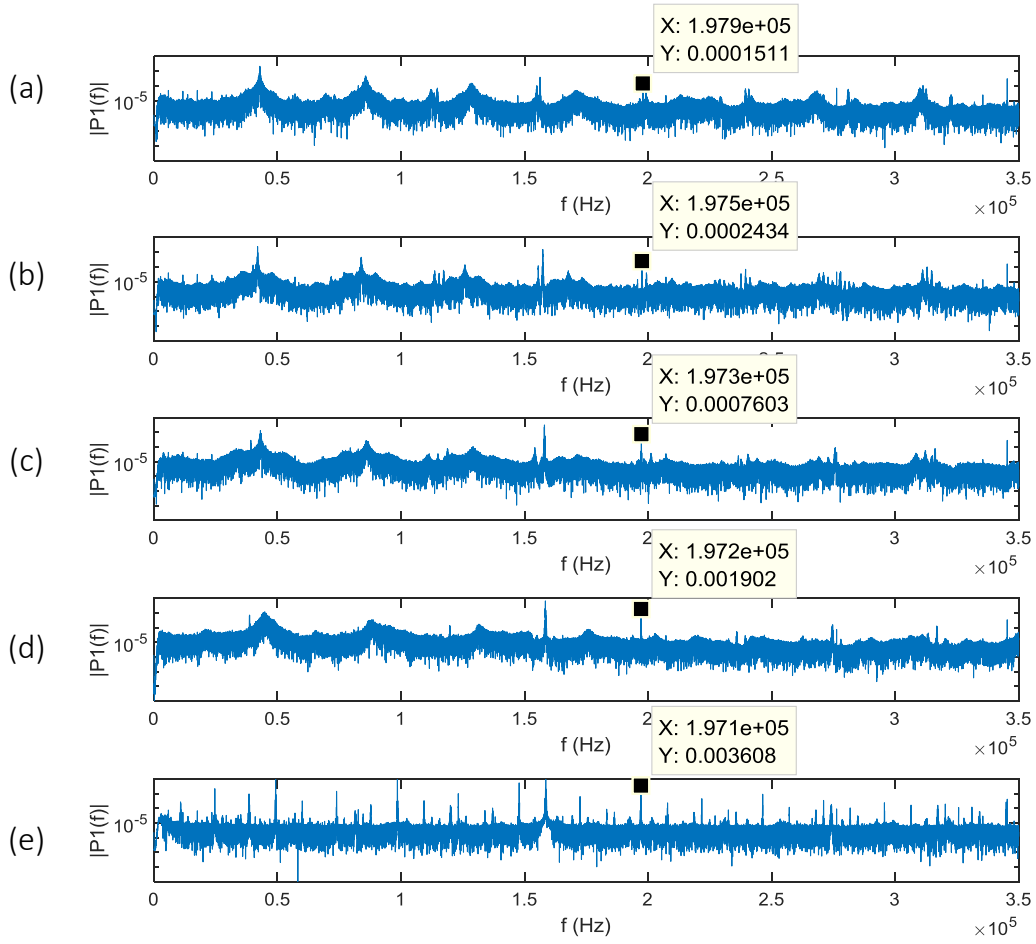

Figure 5-27 Power spectrum of AE signal under different collector-emitter current at 200kHz switching frequency: (a) 0.1A; (b) 0.5A; (c) 1.0A; (d) 1.5A; (e) 2.0A.

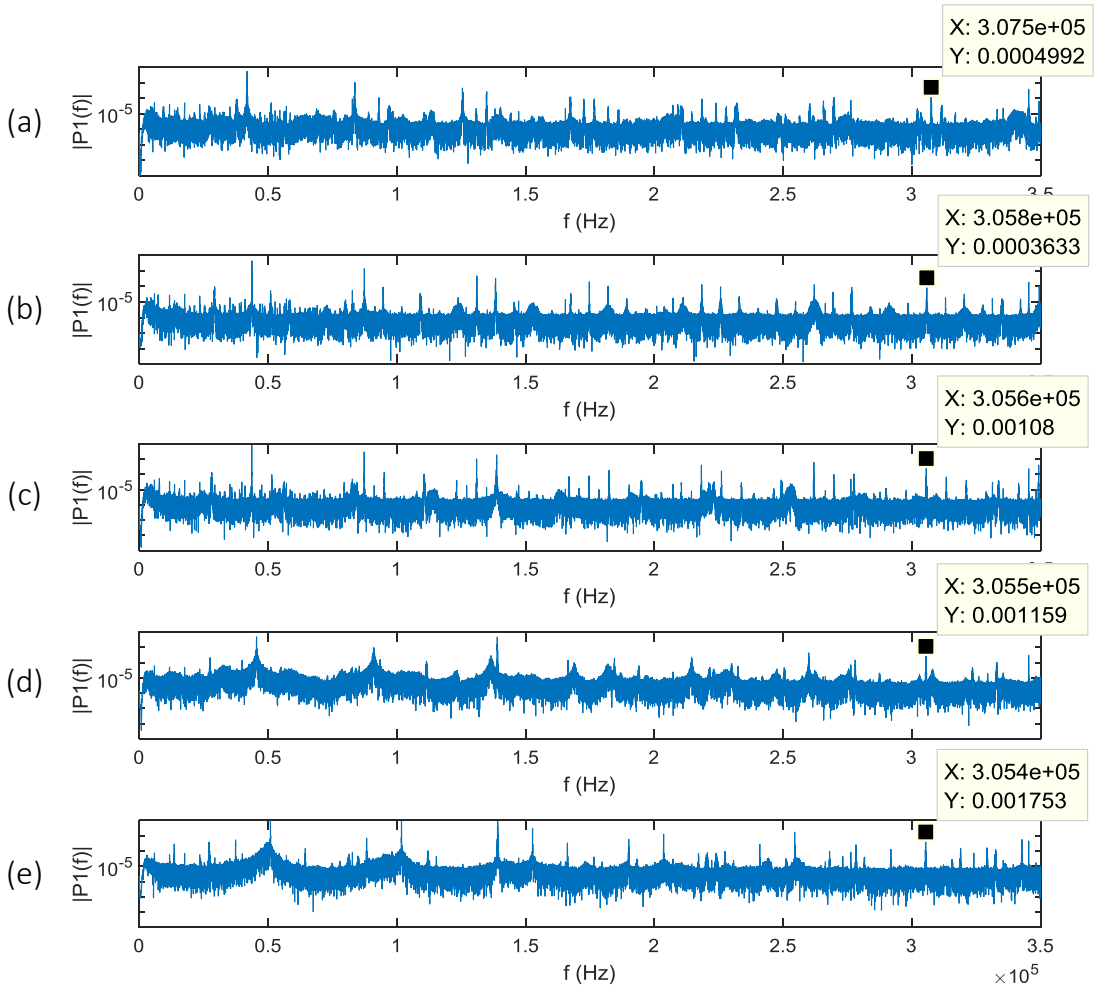

Figure 5-28 Power spectrum of AE signal under different collector-emitter current at 300kHz switching frequency: (a) 0.1A; (b) 0.5A; (c) 1.0A; (d) 1.5A; (e) 2.0A.

Figure 5-29 shows the local maxima point of the FFT spectrum. Note that the current switching frequency and current has a significant impact on and positive correlation with the FFT peak for the AE.

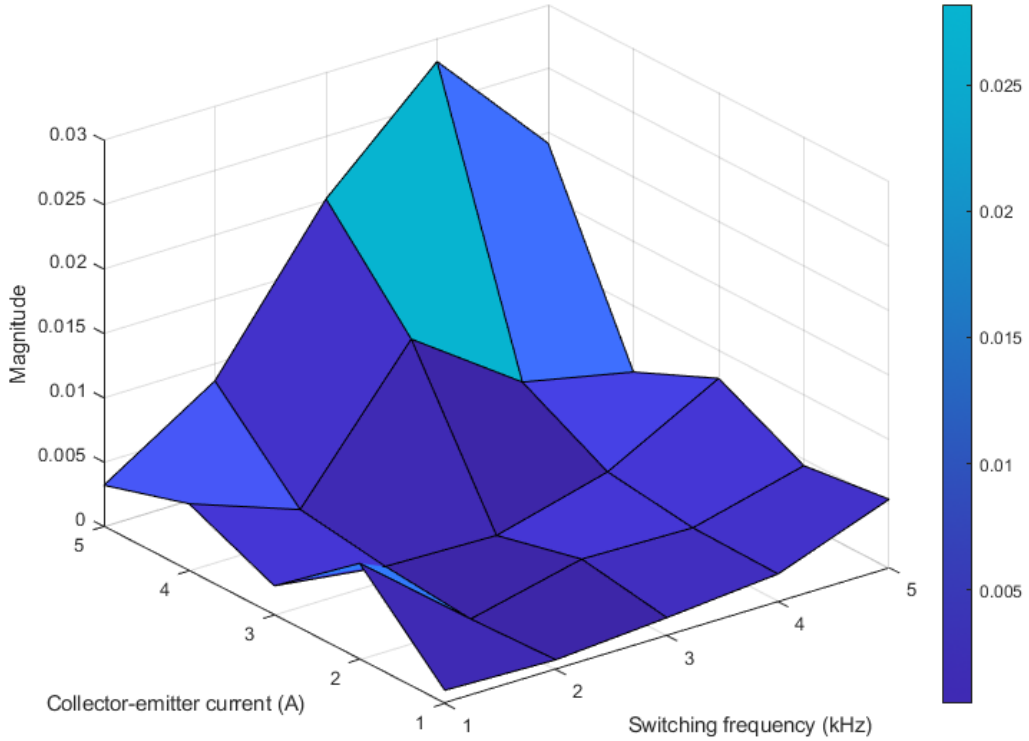

Figure 5-29 3-D mesh data of local maxima of experimental data under different conditions: Collector-emitter current and switching frequency.

5.6.3 Online short-time Fourier transform analysis on AE Signal

In order to facilitate the practical implementation of the system, an online short-time Fourier transform with autonomous local maxima detection has been integrated into the detection of electro-thermal characteristic, thus the information could be used to predict the operating lifetime of IGBT module.

Figure 5-30 illustrates the Simulink model of the integration of the STFT module with the thermal model. A filtered acoustic signal is loaded as the external source from the MATLAB workspace, with sampling frequency of 750k Hz. A 1024-point Gaussian model is used in the STFT model with 64-point overlap between the transitions of window. A local maxima detection model is added to determine the positive extrema.

A zero-order hold module was integrated to hold specific local extrema until the next cycle of STFT. These specific local extrema were then loaded into a user-defined MATLAB function, the formula for which is given in equation 5.1.

An equivalent electro-thermal model, proposed by Albarbar and Batanlu (2018) was used to identify the real-time electro-thermal characteristic of the IGBT. It should be noted that this model has a default room temperature as reference temperature. In this case study, the default temperature was set to 25°C.

Figure 5-31 to Figure 5-35 show the average STFT spectrum of the AE signal collected from collector-emitter current at different switching frequencies. Unlike FFT method in previous section, AE signals are windowed into several segments, and their respective power spectrum at different frequency is analysed. With lower number of sampled points, FFT resolution bin is reduced, hence reducing redundant noise in the frequency domain. The segmentations are then averaged to determine average STFT spectrum across the frequency range.

Based on this observation, the STFT module has produced better determination of local maxima compared to the offline FFT technique, as elaborated in the previous section.

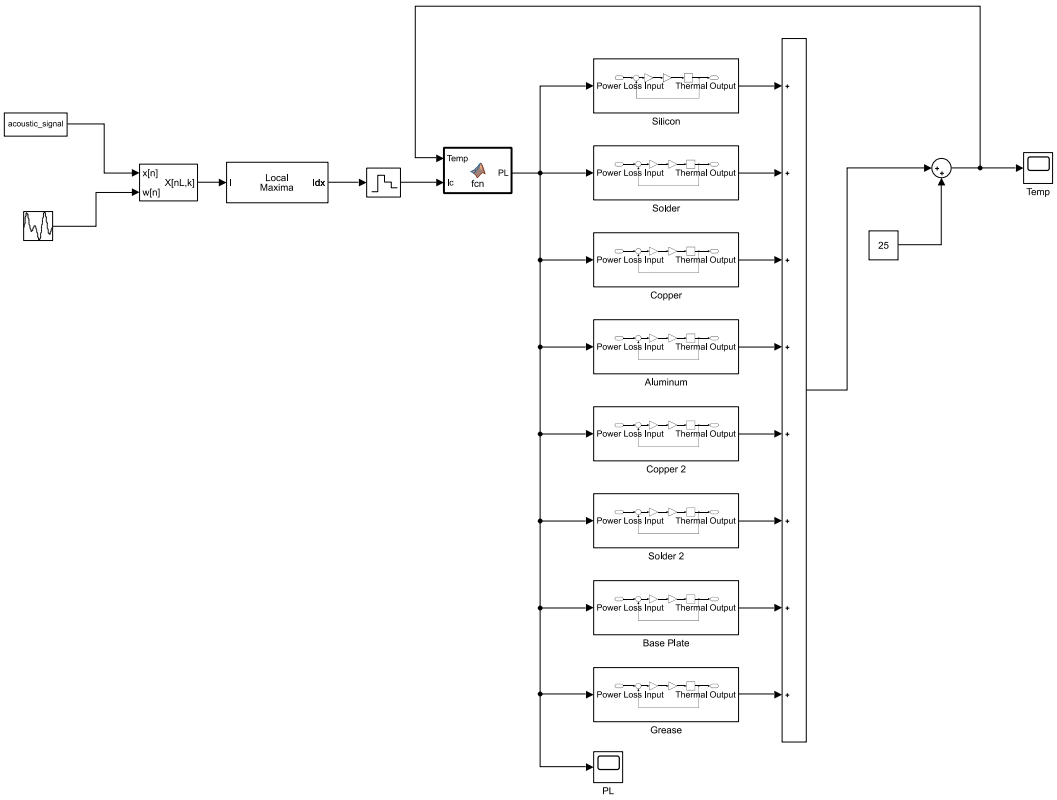

Figure 5-30 Simulink model of online STFT module with 8th order proposed thermal model.

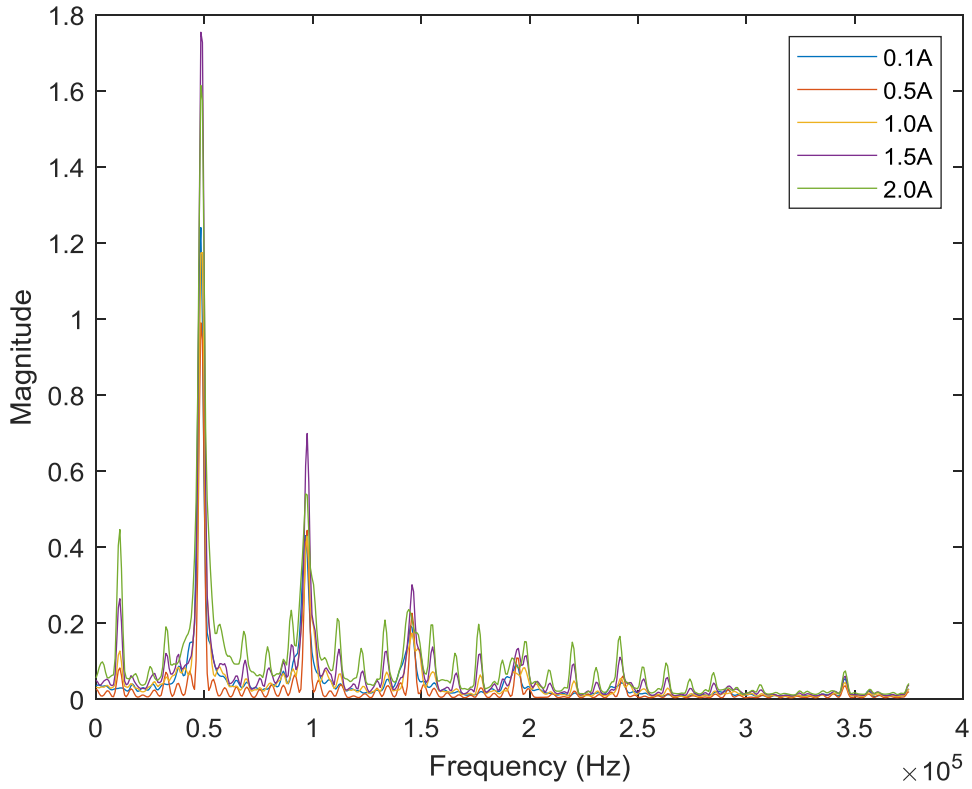

Figure 5-31 Average STFT spectrum for AE signal collected from a collector-emitter current at 10k Hz switching frequency

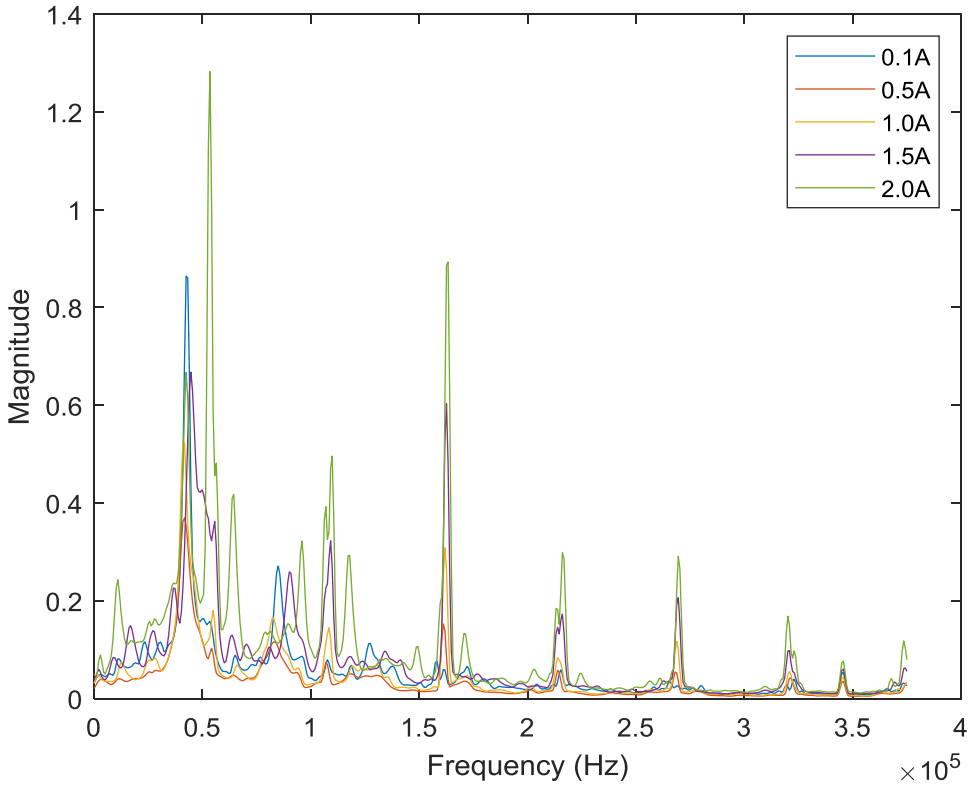

Figure 5-32 Average STFT spectrum for AE signal collected from a collector-emitter current at 50k Hz switching frequency

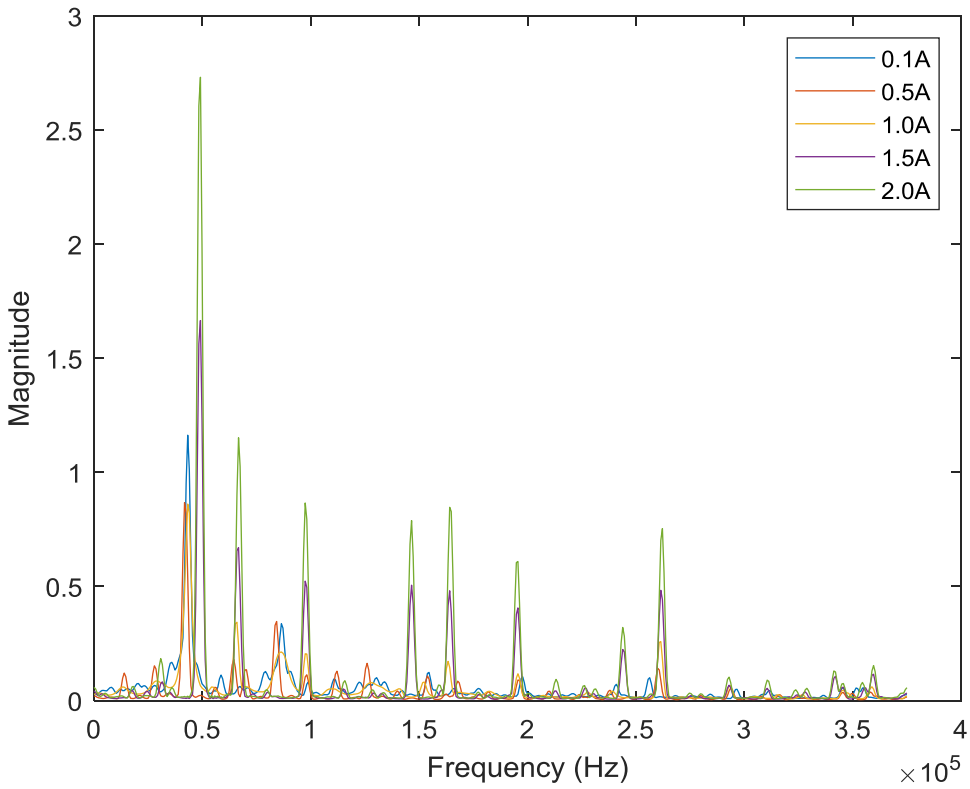

Figure 5-33 Average STFT spectrum for AE signal collected from a collector-emitter current at 100k Hz switching frequency

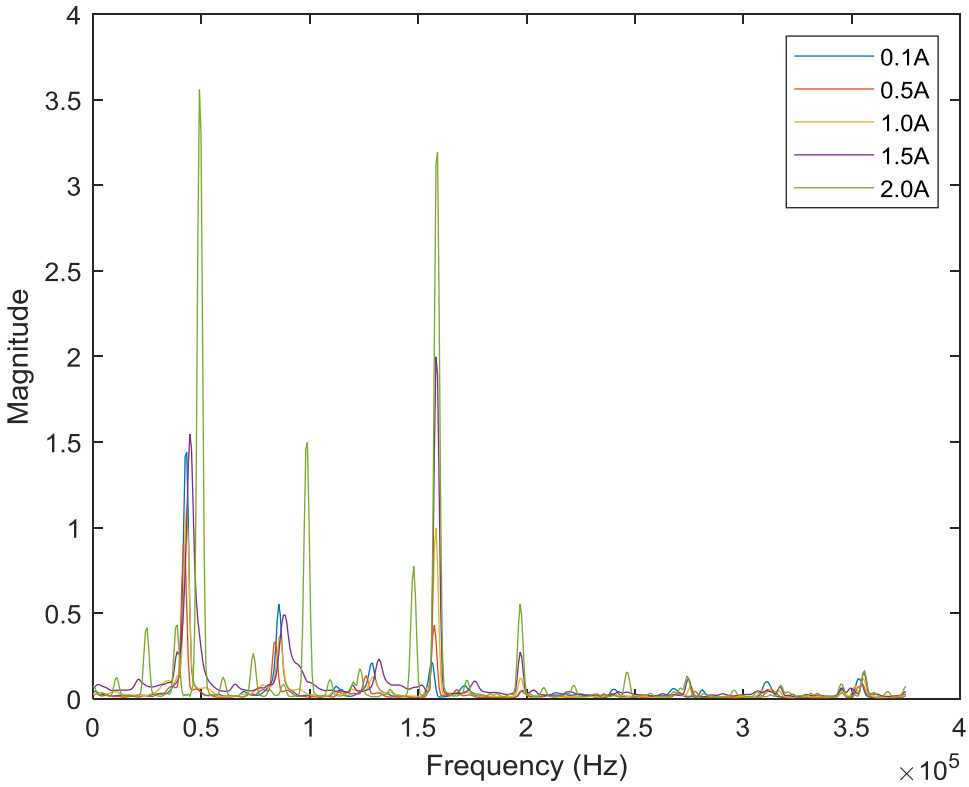

Figure 5-34 Average STFT spectrum for AE signal collected from a collector-emitter current at 200k Hz switching frequency

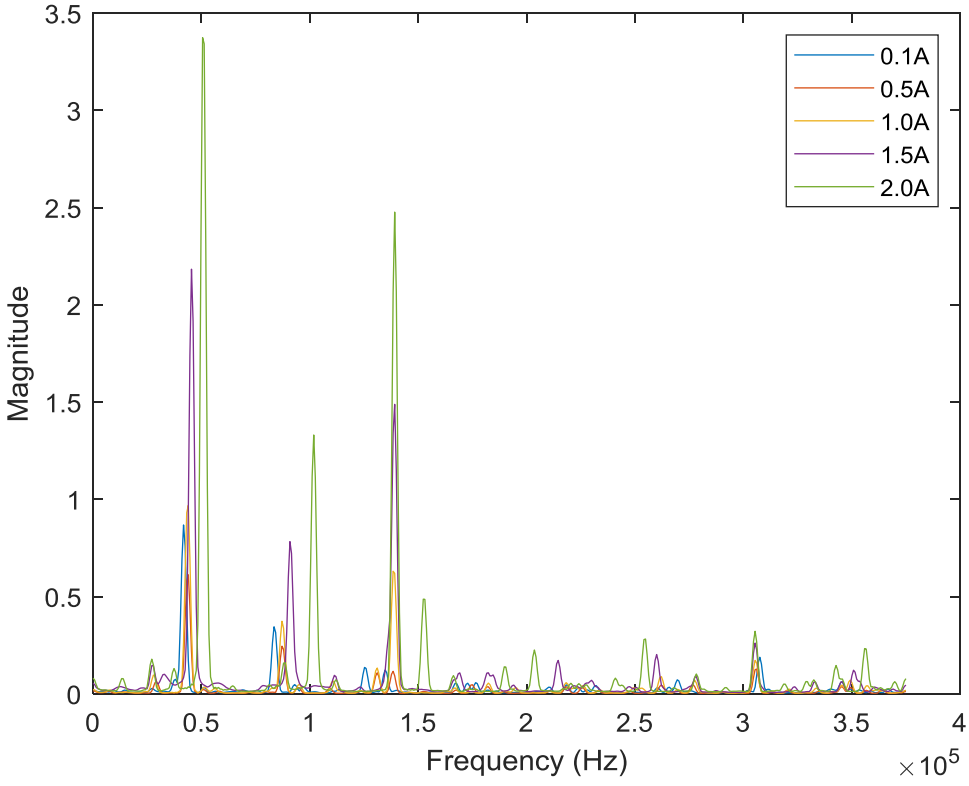

Figure 5-35 Average STFT spectrum for AE signal collected from a collector-emitter current at 300k Hz switching frequency

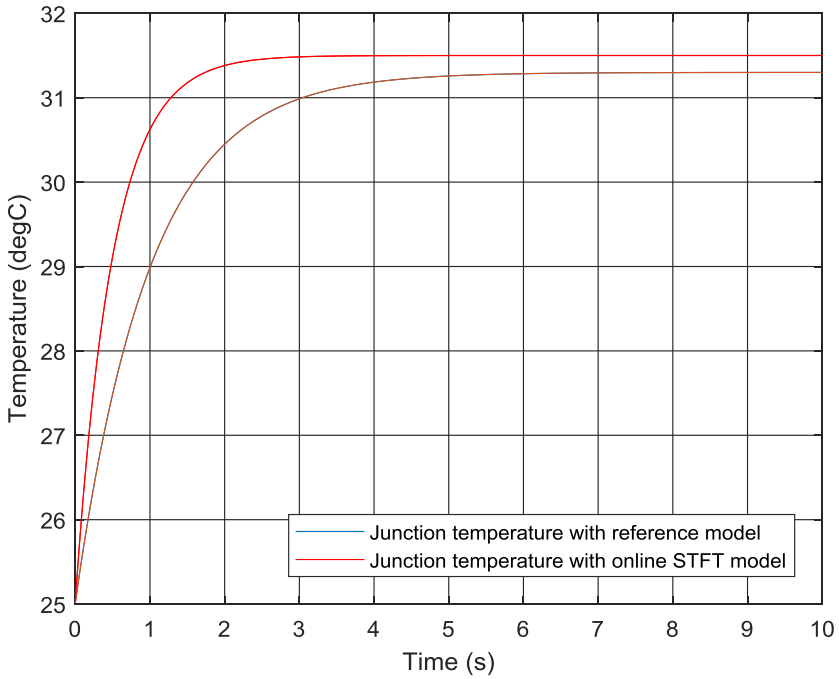

Figure 5-36 Comparison of determined temperature between reference model and proposed online STFT model.

Figure 5-36 shows the difference between the detected temperature model of the STFT model and the reference model (developed from an 8th order Foster network) under a collector-emitter current of 0.1A at 10k Hz switching frequency. This demonstrates that the STFT model that was developed has the ability to perform online monitoring as part of a NDT strategy for PEC applications.

5.7 Possible errors in measurement

Despite the relatively positive results from these experiments, it is important to recognise that there are possible errors which may have affected the quality of the actual measurement. Firstly, it is possible that the measured signal consisted of AE from other power semiconductor modules. The surrounding electromagnetic

interference can also act as a potential source of interference when collecting AE signals.

Another possible error lies in the loss of transmission between the AE source and the AE signals. Currently, the AE sensor is attached closely to the PEDs. Thus, due to the natural characteristics of AE measurement, the AE sensor picks up surrounding AE which may also affect final measurement data.

The data acquisition system, ELVIS II (National Instruments) is known to have a high signal-noise ratio when measuring low voltage. To compensate for these errors, another set of data were taken using ELVIS II in which the input channel was not connected to any measurement device. By doing this, it was able to eliminate the background noise which lies in the internal circuitry of the data acquisition system.

Precision errors may constitute another possible source of errors. ELVIS II is limited to a sampling frequency of 1MHz at 16-bit resolution. Due to the precision and high switching frequency of the AE measurement environment, it is expected that there may be some information loss during the data acquisition stage.

5.8 Summary

This chapter presented the experimental set-up used for investigating PEDs such as the IGBT using AE technique. It demonstrated the possibility of using AE signals as a tool for condition monitoring of PEDs. The AE signals that were measured are observable; they do not suffer from high attenuation, noise or other type of electrical cross talk which could cause confusion. There are many uncertainties in physical measurements, such as adjacent machines, air currents and electric power fluctuations, nearby electrical equipment, static electricity and interference from radio and radio frequency

transmissions. The accumulated signal is significantly visible and detectable even at high frequency (about 300 kHz). The AE peak at the transition instance of the PWM is an important element for predicting electro-thermal behaviour, which is validated by a referenced temperature sensor. Thus, the electro-thermal temperature can be relayed to an effective monitoring system.

In this experiment, the system consists of 3 sensors:

- Temperature sensor – LM35DZ
- Acoustic emission sensor
- Current sensor – ACS712

To ensure good quality measurement data, sensors' performance must be calibrated. LM35DZ was previously calibrated using two-point calibration method with ice-water bath and boiling water. In theory, ice water bath and boiling water has reference temperature at 0°C and 100°C. Through practical experiments, it is found that LM35DZ has great non-linearity performance, ±0.5°C, which is similar to its technical characteristics in datasheet.

Calibration of acoustic emission sensor is much complicated compared to other sensors due to its measurement complexity. To carry out accurate experiment, a technique specified by (McLaskey and Glaser, 2012), the author run a calibration tests on a thick plate with two different mechanical calibration sources: ball impact and glass capillary fracture. This methodology managed to quantify sensor aperture effects and hence, the accuracy of calibration source models is verified. An autoregressive-

moving average (ARMA) model is used to describe the performance of the sensor, thus retrieving sensor-induced distortion and extracted time-domain signals of the sensors.

Current sensor ACS712 is easily calibrated through sunt resistor being applied to the circuit, by measuring the voltage across shunt resistor, the current can be calculated through simple Ohm's Law.

6 Conclusions, Achievement and Future Work

6.1 Introduction

This final chapter of the thesis begins by considering the conclusions that can be drawn from this experimental study before reviewing the objectives of this research stated in Section 1.7.2 and evaluating its principal achievements in relation to these. It also considers the possible directions that future work in this field may follow.

6.2 Conclusions

Results showed that the AE signals that were measured are observable. Moreover, they do not suffer from high attenuation, noise or other type of electrical cross talk which would be likely to create confusion. However, there were some possible sources of error in the physical measurements, which may have been affected by adjacent machinery and electrical equipment, air currents, electric power fluctuations, static electricity and interference from radio and radio frequency transmissions. However, the accumulated signal is significantly visible and detectable even at high frequency (about 300 kHz). The AE peak at the transition instance of the PWM is an important element for predicting electro-thermal behaviour, which is validated by a referenced temperature sensor. Thus, the electro-thermal temperature can be relayed to an effective monitoring system.

Through experiments, it is found that the AE signal has positive characteristic with junction current and PWM frequency. The relationship between AE signals and junction current was formulated as explained in Chapter 5, and it successfully quantify power loss and electro-thermal characteristic. The mathematical behaviour of the relationship has good similarity towards settling electro-thermal temperature of IGBT.

This result is evaluated based on estimation from AE peaks through is then compare with referenced temperature data.

Discrepancies are assumed to be caused by thermal effect of surrounding environment and initial room temperature, as the simulation result by AE peak is heavily depend on that to estimate good result. Non-linear characteristic of temperature sensor is another factor that cause the difference between simulation and experimental data.

6.3 Contribution of this research

This research forms the basis of a valuable contribution to this field for four reasons. Firstly, it shows that AE provides a viable alternative to existing methods for troubleshooting IGBT failure. It also allows the cause of IGBT failure to be more quickly and more accurately determined than prevailing methods. Moreover, this will impact positively on repair times for faults as the remaining life and likely cause of failure could be determined using the developed AE based method presented in this thesis. Finally, it will allow the most suitable places and/or environments for effective use of AE to be determined.

6.4 Review of objectives and achievements

This research achieved its principal aim of investigating the acoustic characteristics of a power electronic converter under different loading and operating conditions.

Objective 1

To understand the working principles, topologies and roles of power electronic converters in photovoltaic (PV) solar power systems.

Achievement 1

The working principles and role of power electronic converters have been studied and understood as explained in Chapters One and Three.

Objective 2

To outline common failure modes for power electronic devices, in particular those used for PV solar power systems, condition monitoring methods used for detecting those failures.

Achievement 2

A critical survey of recent and relevant publications in this field helped to identify common failure modes as representing in chapter 2.

Objective 3

To design and model the DC-DC boost converter circuit using MATLAB and Simulink. This would provide clear understanding of their electrical behaviour and ratings.

Achievement 3

The thermo-acoustic behaviour of this model was explained, by drawing on equations relating to heat and acoustic diffusion over the converter geometry through the semiconductor layers of the electrical contacts as explained in Chapter Three.

Objective 4

To derive a realistic finite element model for describing the thermal and acoustical characteristics of semiconductor switching devices used in power electronic converts.

Achievement 4

A realistic 3-D finite element model of the various components of a PEC consisting of semiconductor devices such as IGBT, diodes input/output capacitors and an inductor was created. The outcomes of this derived model were validated using purposely implemented experimental setups. The effects of the temperature variation, load, switching frequency and duty cycle on variations in AE were tested using a sensor and employing function generators, different variable load and input power generated by a power supply to simulate a range of operating conditions. Operational, environmental and loading effects on the generated AE signals were studied in detail both in time and frequency domains, as explained in Chapter four.

Objective 5

To design and build experimental test setup for initial thermal and acoustical data collection and subsequent data analysis.

Achievement 5

A test rig and experimental setup were designed and built in this research to evaluate the practical characteristics of the thermo-acoustic behaviour of AE signals in PEDs, using an AE sensor and an appropriate data acquisition tool. The switching operation of power semiconductors was observed to obtain weighted parameters, which could be used to link the AE signals to the thermal behaviours of PEDs. Overall the

experimental results provided useful insights into the future use of AE as a NDT measurement tool as explained in Chapter five.

6.5 Future work

In conclusion, the results are promising and suggest that further research involving advanced signal processing and analysis methods such as short-time Fourier transform (STFT), wavelet transform and modal analysis will be fruitful. Principal component analysis could be used to decrease multiple statistical parameters and elicit useful information from the reduced dimensionality.

To further carry out more robust experiment, more signal processing techniques and their parameters should be used to extract useful parameters. Wavelet transform is expected to be useful to determine important characteristics from AE signals through mother wavelet analysis. Sensors should be re-calibrated wisely to ensure better repeatability and accuracy.

The gained knowledge and developed condition monitoring methodology will be applied to optimise the photovoltaic solar systems used at the sponsor of this PhD work (Royal Commission) in KSA. Exploitation of renewable energies, including solar energy, is one of the main elements in KSA 2030 Vision. Therefore, it is anticipated this work to have a very positive impact on increasing availability, life times and reducing down time of such important energy systems.

References

Adams, D. (2007) *Health Monitoring of Structural Materials and Components: Methods with Applications*. New York: Wiley.

Aggelis, D.G, Kordatos, E. Z., Matikas, T.E. (2011). 'Acoustic Emission for Fatigue Damage Characterization in Metal Plates'. *Mechanic Research Communication.* 38, 106-110.

Alawaji, S. H. (2001) 'Evaluation of solar energy research and its applications in Saudi Arabia—20 years of experience'. *Renewable and Sustainable Energy Reviews,* 5, 59–77.

Albarbar, A. and Batunlu, C. (2018) *Thermal analysis of power electronic devices used in renewable energy systems.* Berlin: Springer.

Al-Helal, I. M. and Alhamdan, A.M. (2009) 'Effect of arid environment on radiative properties of greenhouse polyethylene cover'. *Solar Energy*, 83, 790–8.

Almasoud, A. H. and Gandayh, H. M. (2015) 'Future of Solar Energy in Saudi Arabia'. *Journal of King Saud University – Engineering Sciences*, 27 (2), 153-157.

American Society of Testing and Materials (ASTM) (1982). 'Standard Definitions of Terms Relating to Acoustic Emission'. *American Society for Testing and Materials*, E610-82.

Anderson, J. and Cox, R. (2011) 'On-line condition monitoring for MOSFET and IGBT switches in digitally controlled drives'. In *Proceedings of the Energy Conversion Congress and Exposition (ECCE),* Phoenix, 17th-20th September 2011, pp. 3920 – 3927.

Assad, A-J. (2010) 'A Stand-Alone Photovoltaic System, Case Study: A Residence in Gaza'. *Journal of Applied Sciences in Environmental Sanitation*. 5(1), 81-92.

Astaw, K. S. (2007) 'Tropical area is a best place to achieve the best performance of amorphous silicon photovoltaic', TPSDP-ADB No.1792-INO, Electronic and Electrical Engineering, Loughborough University.

Baccar, D. (2015) *Development, Implementation, and Validation of an Acoustic Emission-based Structural Health Monitoring System*, unpublished Ph.D, University of Duisberg.

Baccar, D. and Söffker, D. (2013) 'Application of acoustic emission technique for online evaluation and classification of wear state'. In *Proceedings of 9th International Workshop in Structural Health Monitoring, IWSHM 2013*, 2, Stanford, CA: DEStech September 2013, pp. 1218–1225.

Bahman, A.S. (2015) *Multidisciplinary modelling tools for power electronic circuits.* Unpublished PhD, University of Aalborg DOI:10.13140/RG.2.2.10400.58882

Batunlu, C. and Albarbar, A. (2015a) 'A technique for mitigating thermal stress and extending life cycle of power electronic converters used for wind turbines'. *Electronics,* 4, 947-968.

Batunlu, C. and Albarbar, A. (2015b) 'Towards more reliable renewable power systems: thermal performance evaluation of DC/DC boost converters switching devices'. *International Journal of Power Electronics and Drive Systems*, 6(4), 876-887.

Batunlu C. and Albarbar, A. (2016) 'Real-time system for monitoring the electro-thermal behaviour of PEDs used in boost converters'. *Microelectronics Reliability*, 62, 82-90.

Baxter, M., Pullin, R., Holford, K. and Evans, S. L. (2007) 'Delta T sources location for acoustic emission, *Mechanical system and Signal Processing*'. 2, 1512-1520.

Blaabjerg, F., Chen, Z. and Kjaer, S.B. (2004a) 'Power electronics as efficient interface in dispersed power generation systems'. *IEEE transactions on power electronics*, *19*(5), 1184-1194.

Blaabjerg, F., Teodorescu, R., Chen, Z. and Liserre, M. (2004b) 'Power converters and control of renewable energy systems'. In *Proceedings of 6th International Conference on Power Electronics,* Vol. 1, pp. 1-20.

Blaabjerg, F., Iov, F., Kerekes, T., Teodorescu, R. and Ma, K. (2011) 'Power electronics-key technology for renewable energy systems'. In *Proceedings of Power Electronics, Drive Systems and Technologies Conference 2011*, pp. 445-466.

Bonkaney, A., Madougou, S. and Adamou, R. (2017) 'Impacts of cloud cover and dust on the performance of photovoltaic module in Niamey'. *Journal of Renewable Energy*, https://doi.org/10.1155/2017/9107502

Borgmann, M. (2016) 'Saudi Arabia's amazing new renewable target: 9.5GW by 2023'. *Renew Economy*. [Online] http://reneweconomy.com.au/2016/potentially-game-changing-saudi-arabian-government-restructuring-bolsters-9-5-gw-renewables-energy-target-by-2023 [Accessed on 19th August 2016].

Bose, B. K. (1992) 'Evaluation of modern power semiconductor devices and future trends of converters'. *IEEE Transactions on Industry Applications*, 28(2), 403-413.

Brown, D. W., Abbas, M., Ginart, A., Ali, I. Kalgren, P. and Vachtsevanos, G. (2012) 'Turn-off time as an early indicator of insulated gate bipolar transistor latch-up'. *IEEE Transactions on Power Electronics*, 27(2) 479–489.

Busca, C. R., Teodorescu, F., Blaabjerg, S., Munk-Nielsen, L., Helle, T. Abeyasekera, and Rodriguez, P. (2011) 'An overview of the reliability prediction related aspects of high power IGBTs in wind power applications'. *Microelectronics Reliability*, 51 (9–11), 1903–1907.

Carpinteri, A. and Bocca, P. (1991) *Damage and diagnosis of materials and structures.* Bologna: Pitagora.

Carpinteri, A., Lacidogna, G. and Pugno, N. (2007) 'Structural damage diagnosis and life-time assessment by acoustic emission monitoring'. *Engineering Fracture Mechanics*, 74(1-2), 273-289.

Carrasco, J.M., Franquelo, L.G., Bialasiewicz, J.T., Galván, E., Portillo Guisado, R.C., Prats, M.M., León, J.I. and Moreno-Alfonso, N. (2006) 'Power-electronic systems for the grid integration of renewable energy sources: A survey'. I*EEE Transactions on industrial electronics,* 53(4), 1002-1016.

Castro, M., Delgado, A., Argul, F.J., Colmenar, A., Yeves, F. and Peire, J. (2005) 'Grid-connected PV buildings: analysis of future scenarios with an example of Southern Spain'. *Solar Energy*, *79*(1), 86-95.

Chakraborty, A. (2011) 'Advancements in power electronics and drives in interface with growing renewable energy resources'. *Renewable and Sustainable Energy Reviews,* 15(4), 1816-1827.

Chen, Z. (2013) 'An overview of power electronic converter technology for renewable energy systems'. In M. Mueller and H. Polinder (eds). *Electrical Drives for Direct Drive Renewable Energy Systems.* Cambridge: Woodhead, pp. 80-105.

Chibante, R., Araujo, A. and Carvalho, A. (2003) 'A new physics based SPICE model for NPT IGBTs'. In *Proceedings of the 29th Annual Conference of the IEEE Industrial Electronics Society, 2003. IECON 2003,* vol. 2, pp. 1156–1161.

Chibante, R., Araujo, A. and Carvalho, A. (2005) 'A FEM punch-through IGBT model using an efficient parameter extraction method'. In *Proceedings of the 31st Annual Conference of IEEE Industrial Electronics Society, IECON 2005*, pp.679-684.

Chretien, J.F. and Chretien, N. (1972) 'A bibliographical survey of acoustic emission'. *Non-Destructive Testing*, 5(4), 220–224.

Clifton, D. and Tarassenko, L. (2006) 'Condition monitoring of gas-turbine engines'. Working paper, Department of Engineering Science, University of Oxford.

Costa Oliveira, R. F. do. (2004) *Health Monitoring of FRP using Acoustic Emission and Fibre Optic Techniques*. Unpublished PhD, University of Porto.

Daliento, S., Chouder, A. Guerriero, P. Massi Pavan, A., Mellit, A. Moeini, R. and Tricoli, P. (2017) 'Monitoring, diagnosis, and power forecasting for photovoltaic fields: a review', *International Journal of Photoenergy*, https://doi.org.10.1155/20171356851

Darwish, Z.A., Kazem, H.A., Sopian, K., Alghoul, M.A. and Chaichan, M.T. (2013) 'Impact of some environmental variables with dust on solar photovoltaic (PV)

performance: review and research status'. *International Journal of Energy and Environment*, *7*(4), 152-159.

Degrenne, N., Ewanchuk, J., David, E., Boldyrjew R. and Mollov, S. (2015) 'A Review of Prognostics and Health Management for Power Semiconductor Modules'. In *Proceedings of The Annual Conference of the Prognostics and Health Management Society*, San Diego, California, 19th–24th October 2015, pp. 1-11

Delfino, F. and Procopio, R. (2008) 'Photovoltaic generating units as reactive supply ancillary service providers'. *International Journal of Emerging Electric Power Systems*, 9 (4) DOI.10.2202/1553-779X.1872

Diederichs, R. (2007) 'Non-destructive testing (NDT)' *NDT Encyclopedia* [Online] http://www.ndt.net//ndtaz/ndtaz.php [Accessed on 19th April 2017]

Drews, A., De Keizer, A.C., Beyer, H.G., Lorenz, E., Betcke, J., Van Sark, W.G.J.H.M., Heydenreich, W., Wiemken, E., Stettler, S., Toggweiler, P. and Bofinger, S. (2007) 'Monitoring and remote failure detection of grid-connected PV systems based on satellite observations'. *Solar Energy*, 81(4), 548-564.

Drouillard, T. F. (1996) 'Acoustic emission: The first half century'. *Journal of Acoustic Emission,* 14 (1), 1-34.

Du, S., Wu, B., Xu, D. and Zargari, N.R. (2017) 'A transformerless bipolar multistring DC–DC converter based on series-connected modules'. *IEEE Transactions on Power Electronics*, 32(2), 1006-1017.

Dunlop, J. P. (2009) *Photovoltaic Systems*. Orlando Park, IL: American Technical Publishers.

Eade, G. (1998) 'Financial implications and cost justification'. *In* Davies, A. (ed.) *Handbook of Condition Monitoring: Techniques and Methodology*, Padstow: Chapman & Hall, pp.471-482

Elbuluk, M. and Idris, N. R. N. (2008). 'The role of power electronics in future energy systems and green industrialization'. *In* Anwari, M. (ed.) *Recent trends in renewable energy and power electronics research.* Skudai: Universiti Teknologi Malaysia, pp.1-20

Elforjani, M and Mba, D. (2008) 'Detecting the onset, propagation and location of non-artificial defects in a slow rotating thrust bearing with acoustic emission'. *Insight-Non-Destructive Testing and Condition Monitoring*, 50(5), 264–268.

Energy Information Administration (EIA). (2016) *International Energy Outlook 2016 with Projections to 2040.* [Online] http://www.eia.gov/forecasts/ieo/pdf/0484(2016).pdf [Accessed on 20th August 2016]

Energypedia. (2014) 'Charge Controllers'. [Online] Retrieved from: https://energypedia.info/wiki/Charge_Controllers [Accessed on 14th May 2017]

England, R. (2018) 'SoftBank and Saudi Arabia to build world's biggest solar farm', *Engadget* 28 March 2018 [Online] http://www.engadget.com/2018/03/28/softbank-and-saudi-arabia-to-build-worlds-biggest-solar-farm/ [Accessed on 26th June 2018]

Erel, S. (2009) 'A study of cooling effect on the operation of a polycrystalline silicon solar cell', *International Journal of Engineering Research and Development*, 1(1), 47-49.

European Solar Thermal Industry Federation (ESTIF). (2014) *UNEP Guide to Integrating Solar Thermal in Buildings: A Quick Guide for Architects and Builders*. [Online] http://www.estif.org/estif/fileadmin/content/publications/downloads/report_final_v0 [Accessed on 1st October 2016].

Evans, S. (2015) 'Fact check: how much energy does the world get from renewable?' *Carbon Brief,* 6 October 2015 [Online] https://www.carbonbrief.org/factcheck-how-much-energy-does-the-world-get-from-renewables [Accessed on 20th August 2016].

Femia, N., Petrone, G., Spagnuolo, G. and Vitelli, M. (2013) *Power Electronics and Control Techniques for Maximum Energy Harvesting in Photovoltaic Systems*. Boca Raton, FL: CRC Press.

Ferranda, R. and Leva, S. (2008) 'Energy comparison of MPPT techniques for PV Systems', *WSEAS Transactions on Power Systems,* 3, pp. 446-455.

Ferrando Chacon, J. L., Artigao Andicoberry, E. Kappatos, V., Papaelias, M. Selcuk, C. and Gan, T-H (2016) 'An experimental study on the applicability of acoustic emission for wind turbine gearbox health diagnosis'. *Journal of Low Frequency Noise, Vibration and Active Control,* 35(1), 64-76.

Fouvry, S., Liskiewicz, T. Kapsa, P. Hannel, S. and Sauger, E. (2003) 'An energy description of wear mechanisms and its applications to oscillating sliding contacts', *Wear*, 255(6), 287–298.

Gazis, P., Vokas, G. and Papathanasiou, S. (2010) 'Trends of power electronics on renewable energy systems'. *The Synergy Forum,* e-RA 5, September 2010, Piraeus, Greece. [Online] C41_ERA-5_Gazis_Vokas_Papath.pdf [Accessed on 24th May 2017]

Goel, S. Ghosh, A R. Kumar, S. and Akula, A. (2014) 'A methodical review of condition monitoring technique for electrical equipment'. In *Proceedings of National Seminar and Exhibition on Non-Destructive Evaluation, NDE 2014,* Pune, India. [Online] *www.ndt.net/article/nde-india2014/papers/CP0073_full.pdf* [Accessed on 24th April 2017]

Gorecki, K. (2013) 'The influence of mutual thermal interactions between power LEDs on their characteristics'. In *Proceedings of 19th International Workshop on Thermal Investigation of ICs and Systems*, pp. 188-193.

Gorman, M. R. (1991). 'Plate wave acoustic emission'. *Journal of the Acoustical Society of America,* 90(1) doi.org/10.1121/1.401258

Grondel, S., Delebarre, C., Assad, J., Dupuis, J-P. and Reithler, L. (2002) 'Fatigue crack monitoring of riveted strap by Lamb waves analysis and Acoustic Emission techniques'. *NDT&E International*, 35, 137-146.

Grosse, C. (2007) 'Kaiser Effect' *NDT Encyclopedia* [Online] http://www.ndt.net/ndtaz/ndtaz.php [Accessed on 24th April 2017]

Grosse, C. and Ohtsu, M. (2008) *Acoustic Emission Testing*. Berlin: Springer

Guda, H. A. and Aliyu, U. O. (2015) 'Design of a Stand-Alone Photovoltaic System for a Residence in Bauchi'. *International Journal of Engineering and Technology*, 5(1), 34-44.

Hansen, A.D., Sorensen, P., Hansen, L.H. and Bindner, H. (2000) *Models for a Stand-alone PV System*. Roskilde: Risø National Laboratory.

Haque, S. Liu, X. Lu, G.-Q. and Goings, J. (2000) 'Thermal management of power electronics modules via acoustic micrography imaging'. In *Proceedings of the 15th Annual IEEE Applied Power Electronics Conference Exposition*, 6th-10th February, New Orleans, vol. 1, pp. 299–305

Harrabin, R. (2015) 'Solar energy "could provide 4% of UK electricity by 2020"', *BBC News*, 24 March 2015. [Online] http://www.bbc.co.uk/news/science-environment-32028809 [Accessed on 21st November 2015]

Hassaine, L., OLias, E., Quintero, J. and Salas, V. (2014) 'Overview of power inverter topologies and control structures for grid connected photovoltaic systems'. *Renewable and Sustainable Energy Reviews*, 30, 796-807.

Hegazy, A.A. (2001) 'Effect of dust accumulation on solar transmittance through glass covers of plate-type collectors'. *Renewable energy, 22*(4), 525-540.

Heiple, C. R and Carpenter, S. (1987) 'Acoustic emission produced by deformation of metals and alloys- a review'. *Journal of Acoustic Emission*, 6(4), 215-237.

Hepbasli, A. and Alsuhaibani, Z. (2011) 'A key review on present status and future directions of solar energy studies and applications in Saudi Arabia', *Renewable and Sustainable Energy Reviews* 15, 5021–5050.

Hingorani, N. G. (1995) 'Future role of power electronics in power systems'. In *Proceedings of the 7th International Symposium on Power Semiconductor Devices and ICs,* 23rd-25th May, Yokohama, pp. 13-15

Hodge, B. K. (2010) *Alternative Energy Systems and Applications*, Hoboken, NJ: John Wiley & Sons.

Holford, K.M., and Carter, D. C. (1999) 'Acoustic emission source location'. *Key Engineering Materials*, 167, 162-171.

Holland, S., Kosel, T., Weaver, R. And Sachse, W. (2000). 'Determination of plate source, detector separation from one signal'. *Ultrasonic,* 38, 620-623.

Howler, B. and Fleisher, M. (2015) *Solar PV Powered Air Conditioner Analysis for an Office/Classroom in a Tropical Climate,* unpublished MSc, Dalarna University.

Huang, M., Jiang L., Liaw, P.K., Brooks, C. R., Seeley, R., and Klarstrom, D. L. (1998) 'Using Acoustic Emission in Fatigue and Fracture'. *Materials Research Journal of Materials,* 50 (11) [Online] http://www.tms.org/pubs/journals/JOM/9811/Huang/Huang-9811.html [Accessed on 21st November 2015]

Iov, F. and Blaabjerg, F. Advanced power converters for universal and flexible power management in future electricity network-converter applications in future European electricity network. UNIFLEX, School of Electrical and Electronic Engineering, University of Nottingham.

Jardine, A. K., Lin, D. and Banjevic, D. (2006) 'A review on machinery diagnostics and prognostics implementing condition-based maintenance'. *Mechanical Systems Signal Processing*, 20(7), 1483–1510.

Ji, B., Pickert, V., Cao, W. and Zahawi, B. (2013) 'In situ diagnostics and prognostics of wire bonding faults in IGBT modules for electric vehicle drives'. *IEEE Transactions on Power Electronics,* 28(12), 5568–5577.

Ji, B., Song, X., Sciberras, E., Cao, W. and Hu, Y., and Pickert, V. (2015) 'Multiobjective design optimization of IGBT power modules considering power cycling and thermal cycling'. *IEEE Transactions on Power Electronics,* 30(5), 2493-2503.

Kaldellis, J.K. and Fragos, P. (2011) 'Ash deposition impact on the energy performance of photovoltaic generators'. *Journal of Cleaner Production*, 19(4), 311-317 http://doi.org/10.16/j.clepro2010.11.008

Kalogirou, S. (2013). *Solar Energy Engineering: Processes and Systems,* 2nd edition, London: Academic Press/Elsevier.

Karatepe, E. and Hiyama, T. (2009) 'Artificial neural network-polar coordinated fuzzy controller based maximum power point tracking control under partially shaded conditions'. *IET Renewable Power Generation*, 3(2), 239-253.

Kärkkäinen, T. and Silventoinen, P. (2013) 'Considerations for active condition monitoring in power electronic converters'. In *Proceedings of the 15th European Conference on Power Electronics and Applications (EPE),* 2nd-6th September, Lille, pp. 1–5.

Kärkkäinen T. J., Talvitie, J. P., Kuisma, M., Hannonen, J. Mengotti, E. and Silventoinen, P. (2014a) 'Acoustic Emission in Power Semiconductor Modules—First Observations'. *IEEE Transactions on Power Electronics*, 29(11), pp. 6081-6087.

Kärkkäinen T. J., Talvitie, J. P., Ikonen, O., Kuisma, M. Silventoinen, P. and Mengotti, E. (2014b) 'Sounds from semiconductors – acoustic emission experiment with a power module'. In *Proceedings of 16th European Conference on Power Electronics and Applications (EPE),* 26th-28th August, Lappeenranta. pp. 1-6.

Kärkkäinen, T.J., Talvitie, J.P., Kuisma, M., Silventoinen, P. and Mengotti, E. (2015a) 'Acoustic emission caused by the failure of a power transistor'. In *Proceedings of 2015 IEEE Applied Power Electronics Conference and Exposition (APEC)*, 15th-19th March, Charlotte, USA, pp. 2481–2484. doi:10.1109/APEC.2015.7104697

Kärkkäinen T. J., Talvitie, J. P., Kuisma M. Silventoinen P. and Mengotti E. (2015b) 'Measurement Challenges in Acoustic Emission Research of Semiconductors'. *Transactions on Power Electronics, (IEEE),* 29 (11) pp. 6081–6086.

Kazem, H. A., Chaichan, M. T., Al-Shezawi, I. M., Al-Saidi, H. S., Al-Rubkhi, H. S., Al-Sinani, J. K. and Al-Waeli, A. H. A. (2012) 'Effect of Humidity on the PV Performance in Oman', *Asian Transactions on Engineering*, 2(4), 29-32.

Ketjoy, N. and Konyu, M. (2014) 'Study of dust effect on photovoltaic module for photovoltaic power plant', *Energy Procedia*, *52*, 431-437.

Kim, S.H., Cha, H., Ahmed, H.F., Choi, B. and Kim, H.G. (2017) 'Isolated double step-down DC–DC converter with improved ZVS range and no transformer saturation problem'. *IEEE Transactions on Power Electronics*, 32(3), 1792-1804.

Kjaer, S.B., Pedersen, J.K., and Blaabjerg, F. (2005) 'A review of single phase grid connected inverters for photovoltaic modules', *IEEE Transactions on Industry Applications*, 41 (5), 1292-1306.

Ko, S.H. and Chao, R.M. (2012) 'Photovoltaic dynamic MPPT on a moving vehicle', *Solar Energy*, 86(6), 1750-1760.

Kroposki, B. Pink, C. DeBlasio, R. Thomas, H. Simoes, M. and Sen, P.K. (2006) 'Benefits of power electronics for distributed energy systems'. *IEEE Power Engineering Society General Meeting*, June.

Kulkarni, N.G. and Virulkar, V.B. (2016) 'Power electronics and its application to solar photovoltaic systems in India'. *Energy and Power Engineering*, 8(2), pp.76-81.

Lamonaca, F., Carrozzini, A., Grimaldi, D. and Olivito, R.S. (2012) 'Acoustic emission monitoring of damage concrete structures by multitriggered acquisition system'. In *Proceedings of the 12th IEEE International Instrumentation and Measurement Technology Conference*, 13th-16th May, Graz, pp. 1630–1634.

Layadi, M. T., Champenois, G., Mostefai, M. and Abbes, D. (2015) *Lifetime Estimation Tool of Lead–Acid Batteries for Hybrid Power Sources Design,* Algiers: Elsevier.

Li, W. and He, X. (2011) 'Review of non-isolated high-step-up DC/DC converters in photovoltaic grid-connected applications'. *IEEE Transactions on Industrial Electronics,* 58(4), 1239-1250.

Lim, J. and Kaewkongka, T. (2007), 'Micro cracking in stainless steel pipe detection by using acoustic emission and crest factor technique'. In *Proceedings of 7th IEEE Instrumentation and Measurement Technology Conference Proceedings,* 1st-3rd May, Warsaw, pp. 1–3.

Lorenz, E. (1994). *Solar Electricity: Engineering of Photovoltaic Systems*, Mairena del Aljarafe: Progensa.

Lu, H. Bailey, C. and Yin, C. (2009) 'Design for reliability of power electronics modules', *Microelectronics Reliability*, 49 (9–11), 1250–1255.

Luque, A. and Hegedus, S. (2011) *Handbook of Photovoltaic Science and Engineering.* Hoboken, NJ: John Wiley & Sons.

Lutz, J. Schlangenotto, H. Scheuermann, U. and Doncker, D.R. (2011) *Semiconductor Power Devices - Physics, Characteristics*. Berlin Heidelberg: Springer.

Lysak, M.V. (1996) 'Development of the theory of acoustic emission by propagating cracks in terms of fracture mechanics', *Engineering Fracture Mechanics,* 55(3), 443-452.

Maammeur, H., Hamidat, A., Loukarfi, L., Missoum, M., Abdeladim, K. and Nacer, T. (2017) 'Performance investigation of grid-connected PV systems for family farms: case study of North-West of Algeria', *Renewable and Sustainable Energy Reviews*, 78, 1208-1220.

Martins, C.H.R., Aguiar, P.R., Frech, A., and Bianchi, E.C. (2014), 'Tool condition monitoring of singlepoint dresser using acoustic emission and neural networks models'. *IEEE Transactions on Instrumentation and Measurement*, 63(3), 667–679.

Mazumder, M. K, Biris, A. S., Trigwell, S., Sims, R. A., Calle, C. I. and Buhler, C. R. (2002) *Solar panel obscuration in the dusty atmosphere of Mars.* Electrostatics and Materials Physics Laboratory, University of Arkansas.

Mba, D. and Rao, R.B. (2006) Development of acoustic emission technology for condition monitoring and diagnosis of rotating machines; Bearings, pumps, gearboxes, engines and rotating structures.

Michalis, P. (1997) *Energy Production from Renewable Energy Applications.* Athens: National University of Athens.

Miguel, R.R. (2008) *Small Wind/Photovoltaic Hybrid Renewable Energy System Optimization.* Unpublished Ph.D, University of Puerto Rico.

Miller, R.K., and McIntire, P. (1987) *Acoustic Emission Testing Nondestructive Testing Handbook* Vol. 5. 2 ed. American Society for Nondestructive Testing

Miller, R.K. Hill, E.K. and Moore, P.O. (2005) *Acoustic Emission Testing*. *Nondestructive Testing Handbook*. American Society for Nondestructive Testing.

Mira, M.C., Zhang, Z., Knott, A. and Andersen, M.A. (2017) 'Analysis, design, modeling, and control of an interleaved-boost full-bridge three-port converter for hybrid renewable energy systems', *IEEE Transactions on Power Electronics*, 32(2), 1138-1155.

Miro, Z. (2014) 'Photovoltaic Systems'. [Online] http://ocw.tudelft.nl/fileadmin/ocw/courses/SolarCells/res00029/CH9_Photovoltaic_systems.pdf [Accessed on May 20th 2017].

Mohan, N.T., Undeland, M., and Robbins, W.P. (2004) *Power Electronics: Converters, Applications and Design,* 3rd edn, New York: John Wiley & Sons.

Mohanty, P. (2014) 'Role of power converters in distributed solar power generation'. *Journal of Automotive Control Engineering*, 2(1), 38-42.

Molinas, M. (2016) 'The Role of Power Electronics in Distributed Energy Systems' [Online] www.elkraft.ntnu.no/eno/Papers2008/Marta-symposium.pdf [Accessed on 10th August 2016]

Moore T. and Frank, K. A. (1995) 'Experience with non-destructive acoustic inspection of power ICs'. In *Proceedings of the 45th Electronic Component Technology Conference*, 21st-24th May, Las Vegas, pp. 305–314

Moore, L.M. and Post, H.N. (2008) 'Five years of operating experience at a large utility-scale photovoltaic generating plant'. *Progress in Photovoltaics: Research and Applications*, 16(3), 249-259.

Musallam, M., Johnson, C. M., Yin, C., Lu, H. and Bailey, C. (2008) 'Real-Time Life Expectancy Estimation in Power Modules'. *Electronics System Integration Technology Conference*, pp. 231-236.

Nahar, N, and Gupta, J. (1990) Effect of dust on transmittance of glazing materials for solar collectors under arid zone conditions of India. *Solar Wind Technologies*, 7, 237–43.

Nair, A. (2006) *Acoustic Emission Monitoring and Quantitative Evaluation of Damage in Reinforced Concrete Members and Bridges*. Unpublished Ph.D, Kerala University.

Navarro, L., Delgado, M., Urresty, J., Cusido, J., and Romeral, L. (2010), 'Condition monitoring system for characterization of electric motor ball bearings with distributed fault using fuzzy inference tools'. *In Proceedings of the 12th IEEE Instrumentation and Measurement Technology Conference*, 13th-16th May, Graz, pp. 1159–1163.

Nazarchuk, Z., Skalskyi, V. and Serhiyenko, O. (2003) *Acoustic Emission: Methodology and Application.* Berlin: Springer.

Nazeer, T., Gupta, S. and Kotwal, S.B. (2017) 'A Review of Grid Connected Photovoltaic Systems'. *International Journal of Emerging Technologies in Engineering Research,* 9 (5), 20-30.

Oh, H., Han, B., McCluskey, P., Han, C. and Youn, B. D. (2015) 'Physics-of-Failure, Condition Monitoring, and Prognostics of Insulated Gate Bipolar Transistor Modules - A Review'. *IEEE Transactions on Power Electronics*, 30 (5), 3413-2426.

Olchowik, J. M., Gulkowski, S., Cieslak, K. J., Banas, J., Jozwik, I., Szymczuk, D., Zabielski, K. and Mucha, J. (2006) 'Influence of the temperature on the efficiency of monocrystalline silicon solar cells in the South-Eastern Poland Conditions', Working paper, Materials Science Department: University of Poland, 24(4).

Omura, I. (2010) March. 'Future role of power electronics'. In *IEEE Proceedings of 6th International Conference on Integrated Power Electronics Systems*, pp. 1-9.

Pavan, A.M., Mellit, A. and De Pieri, D. (2011) The effect of soiling on energy production for large-scale photovoltaic plants. *Solar energy*, *85*(5), 1128-1136.

Physical Acoustic Corporation (PAC) (2005) *DiSP with AEwin User's Manual, Rev. 3*., Princeton, NJ: PAC.

Pollock, A. A. (1986). 'Classical wave theory in AE testing'. *Progress in Acoustic Emission* 111. The Japanese Society of NDI.

Rajesh, R. and Mabel, M.C. (2015) 'A comprehensive review of photovoltaic systems'. *Renewable and Sustainable Energy Reviews*, 51, 231-248.

Ravishankar, K. H., Aithal, R. S., Singh, P. K., Ashis, K. S. and Danak, A. R. (2008) 'Modelling of photovoltaic array and maximum power point tracker using ANN'. *JES Regular Paper*.

Renewable Energy Plus (2017) 'Photovoltaic effect' [Online] http://renewableenergyplus.com/a-key-element-in-solar-panels-efficiency/ [Accessed on 19th April 2017]

Reuben, R.L. (1998) *The role of acoustic emission in industrial condition monitoring. International Journal of COMADEM*, 1(4), 35-46.

Ribrant J. and Bertling, L. (2007) 'Survey of failures in wind power systems with focus on Swedish wind power plants during 1997-2005'. *IEEE Transactions on Energy Conversion*, 22 (1), pp. 167–173.

Rindorf, H.J. (1981). 'Acoustic emission source location in theory and in practice'. *Bruel and Kjaer Technical Review*, 2, 3-44.

Romanowicz, P. Barski, M., Muc, A. and Kedziora, P. (2014) 'Structural health monitoring (SHM) methods in machine design and operation', *Archive of Mechanical Engineering*, 61(4), 653-677.

Ruiz, F., Rey, A., Torrelo, J.M., Nieto, A., Cánovas, F.J. (2011) 'Real time test benchmark design for photovoltaic grid-connected control systems'. Electric Power Systems Research, 81, 907–914.

Salas, V., Olias, E., Barrado, A. and Lazaro, A. (2006) 'Review of the maximum power point tracking algorithms for stand-alone photovoltaic systems'. *Solar Energy Materials and Solar Cells,* 90(11), pp.1555-1578.

Sayigh, A.A.M., Al-Jandal, S. and Ahmed, H. (1985) 'Dust effect on solar flat surfaces devices in Kuwait'. In *Proceedings of the workshop on the physics of non-conventional energy sources and materials science for energy,* September. ICTP, Triest, Italy, pp. 353-367.

Scruby, C.B. (1987) 'An introduction to acoustic emission'. *Journal of Physics E: Scientific Instruments,* 30(8), 945-953. https://doi.org/10.1088/0022-3735/20/8/001

Sedjić, E. Djurović, I. and Jiang, J. (2009) 'Time-frequency feature representation using energy concentration. An overview of recent advances' *Digital Signal Processing,* 19(1), 153-183 doi.10.1016/j.dsp.2007.12.004

Shinde, S.M., Patil, K.D., Khairnar, S.S. and Gandhare, W.Z. (2009) 'The role of power electronics in renewable energy systems research and development'. In *Proceedings of International Conference on Emerging Trends in Engineering and Technology,* 2nd December 2009, pp. 726-730.

Shukri, M. (2012) *Acoustic emission for fatigue crack monitoring in nuclear piping system*. Unpublished Ph.D, Cardiff University.

Shull, P.J. (2002) *Nondestructive Evaluation: Theory, Techniques, and Applications* New York: Taylor & Francis

Smulko, J., Jozwiak, K., Olesz, M. and Hasse. L. (2011) 'Acoustic emission for detecting deterioration of capacitors under aging'. *Microelectronics Reliability,* 51(3), 621–627.

Solar professional [Online] http://solarprofessional.com/sites/default/files/articles/ajax/docs/2_SP4_5_pg76_Hernday-3_0.jpg [Accessed on 19th April 2017]

Song Y. and Wang, B. (2013) 'Survey on Reliability of Power Electronic Systems'. *IEEE Transactions on Power Electronics*, 28 (1), 591-604.

Stepinski, T., Uhl, T. and Staszewski, W. (2013) *Advanced Structural Damage Detection: From Theory to Engineering Applications*. New York: Wiley.

Stettler, S., Toggweiler, P., Wiemken, E., Heydenreich, W., de Keizer, A.C., van Sark, W.G.J.H.M., Feige, S., Schneider, M., Heilscher, G., Lorenz, E. and Drews, A. (2005) 'Failure detection routine for grid-connected PV systems as part of the PVSAT-2 project'. In *Proceedings of the 20th European Photovoltaic Solar Energy Conference & Exhibition*, June, Barcelona, Spain, pp. 2490-2493.

Stumberger G., Dezelak K., Klopcic B. and Dolinar D. (2013) 'Acoustic noise emissions caused by the transformer in a DC/DC converter for welding applications'. *Przeglad Electrothecniczny*, 89 (2) 88-91.

The Welding Institute (2017) 'Condition monitoring'. [Online] http://www.twi-global.com/condition-and-structural-health-monitoring/condition-monitoring [Accessed on 19th April 2017].

Taghvaee, M.H., Radzi, M.A.M., Moosavain, S.M., Hizam, H. and Marhaban, M.H. (2013) 'A current and future study on non-isolated DC–DC converters for photovoltaic applications'. *Renewable and Sustainable Energy Reviews*, 17, 216-227.

Tang, Y., Wang, B. Chen, M. and B. Liu. 2012. 'Simulation model and parameter extraction of Field-Stop IGBT'. *Microelectronics Reliability*, 52(12), 2920–2931.

Tensi, H.M. (2004). 'The Kaiser-effect and its scientific background'. *Journal of Acoustic Emission*, 22, 1-16.

TramStore21. (2012) *Solar Thermal Systems.* [Online] www.tramstore21.eu/ [Accessed on 11th November 2016]

Tsang, A.H.C. (1995) 'Condition-based maintenance: tools and decision making'. *Journal of Quality in Maintenance Engineering*, 1(3), 3–17.

Vallen, H. (2002) 'AE testing fundamentals, equipment, applications'. *The e-Journal of Non-destructive Testing*, 7(9), 1–7.

Wagenitz, D. Hambrecht, A. and Dieckerhoff, S. (2012) 'Lifetime evaluation of IGBT power modules applying a nonlinear saturation voltage observer'. *In Proceedings of the 7th International Conference on Integrated Power Electronics Systems,* 6th-8th March, Nuremberg. pp. 1 –5.

Walker, G. (2001) 'Evaluating MPPT converter topologies using a MATLAB PV model', *Journal of Electrical & Electronics Engineering*, 21, 49-56.

Wang, H., Zhou, D., and Blaabjerg, F. (2013) 'A Reliability Oriented Design Method for Power Electronic converters'. In *Proceedings of IEEE Applied Power Electronics Conference and Exposition,* 17th-21st March, Long Beach. pp. 2921-2928.

Wang, H. Ma, K. and Blaabjerg, F. (2012) 'Design for reliability of power electronic systems'. In *IECON 2012 - 38th Annual Conference on IEEE Industrial Electronics Society*, 2012, pp. 33–44.

Wang, W., Vinco, A. Pavlov, N., Wang, N., Hayes, M. and O'Mathuna, C. (2013) 'A rotating machine acoustic emission monitoring system powered by multisource energy harvester'. *In Proceedings of the 1st International Workshop on Energy Neutral Sensing Systems*, 14th November, Rome.

Weybourne Atmospheric Observatory (WAO). (2016) 'WAO Meteorological Data 28 January 2016'. [Online] http://weybourne.uea.ac.uk/met/wao_met_28.html [Accessed on 3rd February 2016]

Wu, R., Blaabjerg, F., Wang, H., Liserre, M. and Iannuzzo, F. (2013) 'Catastrophic Failure and Fault-Tolerant Design of IGBT Power Electronic Converters - An Overview'. In *Proceedings of 39th Annual Conference of the IEEE Industrial Electronics Society,* 10th-13th November, Vienna, pp. 507-513.

Xiang, D. Ran, L. Tavner, P. Yang S., Bryant, A. and Mawby, P. (2012) 'Condition monitoring power module solder fatigue using inverter harmonic identification'. *IEEE Transactions on Power Electronics,* 27 (1), pp. 235–247.

Zhou, S., Zhou, L. and Sun, P. (2013) 'Monitoring potential defects in an IGBT module based on dynamic changes of the gate current'. *IEEE Transactions on Power Electronics*, 28 (3) pp. 1479–148.

Zhu, P., Liu, Y., Robert, R., and Hao, X. (2011), 'Offshore wind converter reliability evaluation'. In *Proceedings of IEEE 8th International Conference on Power Electronics and ECCE Asia*, 30th May-3rd June, Jeju, pp. 966–971.

McLaskey, G. C. and Glaser, S. D. (2012) 'Acoustic Emission Sensor Calibration for Absolute Source Measurements.' *Journal of Nondestructive Evaluation*, 31(2) pp. 157–168.

Appendix A: Publications and Posters

Appendix B: MATLAB Code

```
%=========================================================
% Arrangement of Experimental Data and Spectrogram
%=========================================================
Fc = 1000;
Fs = 750e3;
gauss = gausswin(512);

%============ Filter ====================
[b,a] = butter(6,Fc/(Fs/2),'high');
freqz(b,a);

%============ STFT for signal ====================
%0.65 0.8 1.1 1.35

%===== TEST001 =======
dataOut = filter(b,a,TEST001A);
[s_TEST001A, f, t] = spectrogram(dataOut,gauss, 64, 1024, 750e3);
sm_TEST001A = mean(abs(s_TEST001A),2);
dataOut = filter(b,a,TEST001B * 0.65);
[s_TEST001B, f, t] = spectrogram(dataOut,gauss, 64, 1024, 750e3);
sm_TEST001B = mean(abs(s_TEST001B),2);
dataOut = filter(b,a,TEST001C * 0.8);
[s_TEST001C, f, t] = spectrogram(dataOut,gauss, 64, 1024, 750e3);
sm_TEST001C = mean(abs(s_TEST001C),2);
dataOut = filter(b,a,TEST001D * 1.1);
[s_TEST001D, f, t] = spectrogram(dataOut,gauss, 64, 1024, 750e3);
sm_TEST001D = mean(abs(s_TEST001D),2);
dataOut = filter(b,a,TEST001E * 1.35);
[s_TEST001E, f, t] = spectrogram(dataOut,gauss, 64, 1024, 750e3);
sm_TEST001E = mean(abs(s_TEST001E),2);

%===== TEST002 =======
```

```
dataOut = filter(b,a,TEST002A);
[s_TEST002A, f, t] = spectrogram(dataOut,gauss, 64, 1024, 750e3);
sm_TEST002A = mean(abs(s_TEST002A),2);
dataOut = filter(b,a,TEST002B * 0.65);
[s_TEST002B, f, t] = spectrogram(dataOut,gauss, 64, 1024, 750e3);
sm_TEST002B = mean(abs(s_TEST002B),2);
dataOut = filter(b,a,TEST002C * 0.8);
[s_TEST002C, f, t] = spectrogram(dataOut,gauss, 64, 1024, 750e3);
sm_TEST002C = mean(abs(s_TEST002C),2);
dataOut = filter(b,a,TEST002D * 1.1);
[s_TEST002D, f, t] = spectrogram(dataOut,gauss, 64, 1024, 750e3);
sm_TEST002D = mean(abs(s_TEST002D),2);
dataOut = filter(b,a,TEST002E * 1.35);
[s_TEST002E, f, t] = spectrogram(dataOut,gauss, 64, 1024, 750e3);
sm_TEST002E = mean(abs(s_TEST002E),2);

%===== TEST003 =======
dataOut = filter(b,a,TEST003A);
[s_TEST003A, f, t] = spectrogram(dataOut,gauss, 64, 1024, 750e3);
sm_TEST003A = mean(abs(s_TEST003A),2);
dataOut = filter(b,a,TEST003B * 0.65);
[s_TEST003B, f, t] = spectrogram(dataOut,gauss, 64, 1024, 750e3);
sm_TEST003B = mean(abs(s_TEST003B),2);
dataOut = filter(b,a,TEST003C * 0.8);
[s_TEST003C, f, t] = spectrogram(dataOut,gauss, 64, 1024, 750e3);
sm_TEST003C = mean(abs(s_TEST003C),2);
dataOut = filter(b,a,TEST003D * 1.1);
[s_TEST003D, f, t] = spectrogram(dataOut,gauss, 64, 1024, 750e3);
sm_TEST003D = mean(abs(s_TEST003D),2);
dataOut = filter(b,a,TEST003E * 1.35);
[s_TEST003E, f, t] = spectrogram(dataOut,gauss, 64, 1024, 750e3);
sm_TEST003E = mean(abs(s_TEST003E),2);

%===== TEST004 =======
dataOut = filter(b,a,TEST004A);
```

```
[s_TEST004A, f, t] = spectrogram(dataOut,gauss, 64, 1024, 750e3);
sm_TEST004A = mean(abs(s_TEST004A),2);
dataOut = filter(b,a,TEST004B * 0.65);
[s_TEST004B, f, t] = spectrogram(dataOut,gauss, 64, 1024, 750e3);
sm_TEST004B = mean(abs(s_TEST004B),2);
dataOut = filter(b,a,TEST004C * 0.8);
[s_TEST004C, f, t] = spectrogram(dataOut,gauss, 64, 1024, 750e3);
sm_TEST004C = mean(abs(s_TEST004C),2);
dataOut = filter(b,a,TEST004D * 1.1);
[s_TEST004D, f, t] = spectrogram(dataOut,gauss, 64, 1024, 750e3);
sm_TEST004D = mean(abs(s_TEST004D),2);
dataOut = filter(b,a,TEST004E * 1.35);
[s_TEST004E, f, t] = spectrogram(dataOut,gauss, 64, 1024, 750e3);
sm_TEST004E = mean(abs(s_TEST004E),2);

%===== TEST005 =======
dataOut = filter(b,a,TEST005A);
[s_TEST005A, f, t] = spectrogram(dataOut,gauss, 64, 1024, 750e3);
sm_TEST005A = mean(abs(s_TEST005A),2);
dataOut = filter(b,a,TEST005B * 0.65);
[s_TEST005B, f, t] = spectrogram(dataOut,gauss, 64, 1024, 750e3);
sm_TEST005B = mean(abs(s_TEST005B),2);
dataOut = filter(b,a,TEST005C * 0.8);
[s_TEST005C, f, t] = spectrogram(dataOut,gauss, 64, 1024, 750e3);
sm_TEST005C = mean(abs(s_TEST005C),2);
dataOut = filter(b,a,TEST005D * 1.1);
[s_TEST005D, f, t] = spectrogram(dataOut,gauss, 64, 1024, 750e3);
sm_TEST005D = mean(abs(s_TEST005D),2);
dataOut = filter(b,a,TEST005E * 1.35);
[s_TEST005E, f, t] = spectrogram(dataOut,gauss, 64, 1024, 750e3);
sm_TEST005E = mean(abs(s_TEST005E),2);

plot(f,sm_TEST001A);
hold on;
plot(f,sm_TEST001B);
```

```
plot(f,sm_TEST001C);
plot(f,sm_TEST001D);
plot(f,sm_TEST001E);
legend('0.1A','0.5A','1.0A','1.5A','2.0A');
xlabel('Frequency (Hz)');
ylabel('Magnitude');

figure;
plot(f,sm_TEST002A);
hold on;
plot(f,sm_TEST002B);
plot(f,sm_TEST002C);
plot(f,sm_TEST002D);
plot(f,sm_TEST002E);
legend('0.1A','0.5A','1.0A','1.5A','2.0A');
xlabel('Frequency (Hz)');
ylabel('Magnitude');

figure;
plot(f,sm_TEST003A);
hold on;
plot(f,sm_TEST003B);
plot(f,sm_TEST003C);
plot(f,sm_TEST003D);
plot(f,sm_TEST003E);
legend('0.1A','0.5A','1.0A','1.5A','2.0A');
xlabel('Frequency (Hz)');
ylabel('Magnitude');

figure;
plot(f,sm_TEST004A);
hold on;
plot(f,sm_TEST004B);
plot(f,sm_TEST004C);
plot(f,sm_TEST004D);
```

```
plot(f,sm_TEST004E);
legend('0.1A','0.5A','1.0A','1.5A','2.0A');
xlabel('Frequency (Hz)');
ylabel('Magnitude');

figure;
plot(f,sm_TEST005A);
hold on;
plot(f,sm_TEST005B);
plot(f,sm_TEST005C);
plot(f,sm_TEST005D);
plot(f,sm_TEST005E);
legend('0.1A','0.5A','1.0A','1.5A','2.0A');
xlabel('Frequency (Hz)');
ylabel('Magnitude');


%=========================================================
% FFT Subplot Graph
%=========================================================
[TEST005A_fft f] = accoustic_processing(TEST005A, Fs, Fc);
[TEST005B_fft f] = accoustic_processing(TEST005B*0.65, Fs, Fc);
[TEST005C_fft f] = accoustic_processing(TEST005C*0.8, Fs, Fc);
[TEST005D_fft f] = accoustic_processing(TEST005D*1.1, Fs, Fc);
[TEST005E_fft f] = accoustic_processing(TEST005E*1.35, Fs, Fc);

subplot(5,1,1)
semilogy(f, TEST005A_fft);
xlabel('f (Hz)');
ylabel('|P1(f)|');
xlim([0 40000]);
ylim([10e-10 10e-3]);

subplot(5,1,2)
semilogy(f, TEST005B_fft);
```

```
xlabel('f (Hz)');
ylabel('|P1(f)|');
xlim([0 40000]);
ylim([10e-10 10e-3]);

subplot(5,1,3)
semilogy(f, TEST005C_fft);
xlabel('f (Hz)');
ylabel('|P1(f)|');
xlim([0 40000]);
ylim([10e-10 10e-3]);

subplot(5,1,4)
semilogy(f, TEST005D_fft);
xlabel('f (Hz)');
ylabel('|P1(f)|');
xlim([0 40000]);
ylim([10e-10 10e-3]);

subplot(5,1,5)
semilogy(f, TEST005E_fft);
xlabel('f (Hz)');
ylabel('|P1(f)|');
xlim([0 40000]);
ylim([10e-10 10e-3]);

%=========================================================
% Max plane mesh
%=========================================================
max_plane = zeros(5,5);
Fs = 750000;
Fc = 2000;

max_plane(1,1) = max(accoustic_processing(TEST001A, Fs, Fc));
max_plane(2,1) = max(accoustic_processing(TEST001B*0.65, Fs, Fc));
```

```
max_plane(3,1) = max(accoustic_processing(TEST001C*0.8, Fs, Fc));
max_plane(4,1) = max(accoustic_processing(TEST001D*1.1, Fs, Fc));
max_plane(5,1) = max(accoustic_processing(TEST001E*1.35, Fs, Fc));

max_plane(1,2) = max(accoustic_processing(TEST002A, Fs, Fc));
max_plane(2,2) = max(accoustic_processing(TEST002B*0.65, Fs, Fc));
max_plane(3,2) = max(accoustic_processing(TEST002C*0.8, Fs, Fc));
max_plane(4,2) = max(accoustic_processing(TEST002D*1.1, Fs, Fc));
max_plane(5,2) = max(accoustic_processing(TEST002E*1.35, Fs, Fc));

max_plane(1,3) = max(accoustic_processing(TEST003A, Fs, Fc));
max_plane(2,3) = max(accoustic_processing(TEST003B*0.65, Fs, Fc));
max_plane(3,3) = max(accoustic_processing(TEST003C*0.8, Fs, Fc));
max_plane(4,3) = max(accoustic_processing(TEST003D*1.1, Fs, Fc));
max_plane(5,3) = max(accoustic_processing(TEST003E*1.35, Fs, Fc));

max_plane(1,4) = max(accoustic_processing(TEST004A, Fs, Fc));
max_plane(2,4) = max(accoustic_processing(TEST004B*0.65, Fs, Fc));
max_plane(3,4) = max(accoustic_processing(TEST004C*0.8, Fs, Fc));
max_plane(4,4) = max(accoustic_processing(TEST004D*1.1, Fs, Fc));
max_plane(5,4) = max(accoustic_processing(TEST004E*1.35, Fs, Fc));

max_plane(1,5) = max(accoustic_processing(TEST005A, Fs, Fc));
max_plane(2,5) = max(accoustic_processing(TEST005B*0.65, Fs, Fc));
max_plane(3,5) = max(accoustic_processing(TEST005C*0.8, Fs, Fc));
max_plane(4,5) = max(accoustic_processing(TEST005D*1.1, Fs, Fc));
max_plane(5,5) = max(accoustic_processing(TEST005E*1.35, Fs, Fc));

A = [0.1 0.5 1.0 1.5 2.0];
Switch_F = [10 50 100 200 300];

surf(A, Switch_F, max_plane);
ylabel('Collector-emitter current (A)');
xlabel('Switching frequency (kHz)');
zlabel('Magnitude');
```